THESIS

PREDICTIVE ENERGY MANAGEMENT STRATEGIES FOR HYBRID ELECTRIC

VEHICLES APPLIED DURING ACCELERATION EVENTS

Submitted by

David A. Trinko

Department of Mechanical Engineering

In partial fulfillment of the requirements

For the Degree of Master of Science

Colorado State University

Fort Collins, Colorado

Spring 2019

Master's Committee:

   Advisor: Thomas H. Bradley

   Jason C. Quinn
   Charles W. Anderson

ABSTRACT

PREDICTIVE ENERGY MANAGEMENT STRATEGIES FOR HYBRID ELECTRIC

VEHICLES APPLIED DURING ACCELERATION EVENTS

The emergence and widespread adoption of vehicles with hybrid powertrains and onboard computing capabilities have improved the feasibility of utilizing predictions of vehicle state to enable optimal energy management strategies (EMS) to improve fuel economy. Real-world implementation of optimal EMS remains challenging in part because of limits on prediction accuracy and computation speed. However, if a finite set of EMS can be pre-derived offline, instead of onboard the vehicle in real time, fuel economy improvements may be possible using hardware that is common in current production vehicles. Acceleration events (AE) are attractive targets for this kind of EMS application due to their high energy cost, probability of recurrence, and limited variability. This research aims to understand how a finite set of EMS might be derived and applied to AEs based on predictions of basic AE attributes to achieve reliable fuel economy improvements. Models of the 2010 Toyota Prius are used to simulate fuel economy for a variety of control strategies, including baseline control, optimal EMS control derived via dynamic programming, and pre-derived control applied with approximate prediction to AEs. Statistical methods are used to identify correlations between AE attributes, optimal powertrain control, and fuel economy results. Then, key AE attributes are used to define AE categorization schemes of various resolutions, in which one pre-derived EMS is applied to every AE in a category. Last, the control strategies are simulated during a variety of drive cycles to predict real-world fuel economy results. By simulating fuel economy improvement for AEs both in isolation and in the context of drive cycles, it was concluded that applying pre-derived EMS to AEs based on predictions of initial and final velocity is likely to enable reliable fuel economy benefits in low-aggression driving.

ACKNOWLEDGEMENTS

DEDICATION

This thesis is dedicated to my parents, Anthony and Susan Trinko, whose consistent love and support lay the foundation for everything I have accomplished.

TABLE OF CONTENTS

LIST OF TABLES

Chapter 1

Background

In 2016, the transportation sector was the greatest contributing sector to United States green-house gas emissions, accounting for 28% of total emissions [1]. It was also responsible for over 55% of total nitrogen oxide emissions in the United States [2]. Greenhouse gas emissions are a leading cause of climate change [3], and air pollution, including nitrogen oxide pollution, is the world's fourth leading cause of premature death [4]. Efforts are widespread and increasing to mitigate the transportation sector's harmful impacts on climate and health. Improving the fuel economy (FE) of the vehicle fleet is one of the most widely researched methods for doing so [5].

One large body of research aims to improve FE by optimizing vehicle control, most promi-nently via Eco-driving and optimal energy management strategies (Optimal EMS) [6]. Eco-driving involves reducing overall vehicle energy output by optimizing vehicle speed and implementing efficient driving behaviors. Rather than changing driving behavior, Optimal EMS improves the efficiency with which a powertrain achieves a driver's desired velocity trace, giving it a consumer acceptance advantage over Eco-driving strategies [7].

Some forms of Optimal EMS are used in current vehicles. In general, since hybrid electric vehicles (HEV) can draw power from multiple different sources at the same time, they benefit from more powertrain degrees of freedom and are ideal targets for Optimal EMS. For example, many HEV control strategies adjust engine torque and speed so that the engine always operates at its highest efficiency for the requested engine power output, which is a form of instantaneous Optimal EMS [8].

Whereas instantaneous Optimal EMS implements control in reaction to real-time changes in vehicle operation, further improvements to FE are achievable if the EMS changes from reaction-based to prediction-based. It has long been understood that knowledge of future power demands enables more globally fuel efficient EMS [9]. Vehicles are increasingly equipped with "intelli-gent" technologies that are beginning to enable this type of prediction. Location systems, cameras,

and radar, and future technologies including vehicle to vehicle communication (V2V) and vehicle to infrastructure communication (V2I), are expected to enable drastically improved prediction capabilities [10].

Two main approaches are used in the literature to derive a globally optimal FE solution with predictive Optimal EMS: dynamic programming (DP) [11] and Pontryagin's minimization principle [12]. DP is more commonly implemented because it is straightforward to apply, robust, and numerically computable [13, 14].

Most existing predictive Optimal EMS studies involve prediction of full drive cycles, which is far beyond the capabilities of current vehicle technologies [6]. One study that does not involve full cycle prediction implements a Predictive Optimal EMS in a real vehicle, but that study uses stochastic dynamic programming, which does not achieve a globally optimal solution [15, 16]. Another article studies prediction of traffic behavior over short time horizons to enable cooperative cruise control to improve FE, which is an example of a specific application of drive prediction for FE [17]. Even simpler predictions of driver behavior may be achievable using technologies that exist in current production vehicles. For example, the ending speed when accelerating might be accurately predictable using information gathered by camera or location systems. However, the means and potential to implement FE-improving control algorithms using these types of information are not well defined in literature.

Acceleration events (AEs) are of particular interest for FE improvement efforts because of their high power demand relative to most segments of a typical drive cycle [18]. Key AE attributes, such as ending speed or duration, are simpler to predict precisely than second-by-second speed or power traces. In generalized driving, AEs with approximately identical attributes repeat, potentially enabling individual predictive Optimal EMS to be derived once and applied many times. FE improvements via Optimal EMS during AEs may thus be possible on current vehicles despite hardware limitations on prediction fidelity and computation speed.

These considerations lead to a modified approach to Optimal EMS using dynamic programming (DP). The Optimal EMS matrix containing the DP exact optimal control solution can be used

as a lookup table to obtain near-optimal solutions even when used for a slightly different driving segment than the one for which the matrix was derived. This enables a vehicle controller to implement stored control matrices based on predictions of basic AE attributes, achieving a portion of the FE improvements theoretically enabled by exact AE prediction.

1.1   Research Questions

To seek understanding of the FE improvement potential for pre-computed Optimal EMS, we addressed a sequence of research questions:

1. How do differences between AEs correlate with differences between AE Optimal EMS?

2. What FE tradeoffs occur when prediction accuracy is reduced from exact velocity trace prediction to prediction of basic AE attributes?

3. How can low-accuracy-prediction enabled EMS be applied to achieve consistent FE benefits in real driving contexts?

1.2   Novel Contributions

1. Identify how key attributes of AEs influence AE Optimal EMS

2. Characterize the FE improvement potential of pre-computed Optimal EMS during AEs

3. Utilize categorization approach to apply EMS to AEs

4. Apply optimal control as a function of velocity to monotonic drive segments

1.3   Publications

Portions of the research in this thesis appear in publications that have been submitted, published, or presented. I published and presented a preliminary study of pre-computed EMS applied to AEs in drive cycles at SAE World Congress 2018 [19]. Also, material from Chapters 4 and 5 has been submitted for journal publication, authored by Dr. Zachary Asher, my advisor Dr. Thomas Bradley, and me.

Chapter 2

Prepare Simulation Tools

In Chapters 3-5, modeling and simulation techniques are used to characterize and predict the real-world performance of Predictive Optimal EMS during AEs. In this chapter, the vehicle model, control strategies, and driving data used for these investigations are described.

2.1   Develop and Validate Vehicle Model

The Toyota Prius has consistently achieved the highest FE in its class [20], so it is an ideal vehicle to model for investigations of new HEV FE improvement techniques. The 2010 model was chosen for its commercial prevalence and publicly available parameter information. A model of the 2010 Toyota Prius, derived using the Autonomie modeling software, has been shown to correlate closely with real-world performance [21]. The referenced model is not publicly available, so a model was developed and validated by modifying a 2004 Toyota Prius model included with Autonomie with 2010 Prius parameters. Table 2.1 is a list of key parameters defining the model, where m = vehicle mass; $P_{\text{ICE,max}}$ = maximum engine power; m_{fuel} is the fuel consumption model; T_{ICE} = engine torque; ω_{ICE} = engine speed; $\omega_{\text{trac,max}}$ is the maximum traction motor speed; $\omega_{\text{gen,max}}$ is the maximum generator motor speed; $Q_{\text{batt,0}}$ is the initial battery capacity; N_{sun} and N_{ring} are the number of teeth on the sun and ring gears in the planetary gearset; R_{int} is the battery's internal resistance; A_{front} is the frontal area of the vehicle; C_{rr} = coefficient of rolling resistance; r_{fd} = final drive ratio; r_{wheel} = wheel radius; C_d = drag coefficient; and V_{oc} = open circuit battery potential.

The Autonomie software produces high fidelity models that are useful for realistic modeling of a variety of vehicle signals, including power split control in a HEV, but are computationally expensive in simulation. Even if disregarding concerns about long computation times, it would be infeasible to use the Autonomie model with DP to derive the Optimal EMS, because states in Autonomie are dependent on preceding states, which is incompatible with the DP formulation (described in Section 2.2.2). Instead, the Autonomie model was used only to simulate the Baseline

Table 2.1: Significant parameters defining the 2010 Toyota Prius model

m	1380 kg	A_{front}	2.6005 m^2
$P_{\text{ICE,max}}$	73 kW	C_{rr}	0.008
m_{fuel}	$f(T_{\text{ICE}}, \omega_{\text{ICE}})$ [22]	r_{fd}	3.27
$\omega_{\text{trac,max}}$	10,000 rpm	r_{wheel}	0.317 m
$\omega_{\text{gen,max}}$	13,500 rpm	C_d	0.250
$Q_{\text{batt,0}}$	6.5 Ah	V_{oc}	201.6 V
N_{sun}	30	N_{ring}	78
R_{int}	0.373 Ω		

EMS engine control strategy, which was used as an input to a lower fidelity "power split" vehicle model for the remaining vehicle signal calculations. Details on the original development of the power split model are in a previous publication from the author's lab group [23] and reproduced briefly here.

The power split model is based on equations describing vehicle dynamics, a modeling approach that is well-defined in the literature [22,24–26]. The power required to propel the vehicle at velocity v must be provided as a sum of engine power and electric propulsion system power:

$$P_{\text{prop}} = F_{\text{prop}}v = P_{\text{elec}} + P_{\text{ICE}} \tag{2.1}$$

P_{ICE} is an input to the power split model, so the equation is rearranged to solve for P_{elec}:

$$P_{\text{elec}} = F_{\text{prop}}v - P_{\text{ICE}} \tag{2.2}$$

F_{prop} effects vehicle acceleration and counteracts the forces opposing vehicle motion:

$$F_{\text{prop}} = m\dot{v} + C_{rr}mg + \frac{1}{2}C_d\rho_{\text{air}}v^2 A_{\text{front}} \tag{2.3}$$

where $\dot{v}$ is the acceleration of the vehicle, calculated using a numerical derivative; g is acceleration due to gravity $\left(9.81 \ \frac{\text{m}}{\text{sec}^2}\right)$; and ρ_{air} is the density of air $\left(1.1985 \ \frac{\text{kg}}{\text{m}^3}\right)$. For this research, grade angle is assumed to be zero.

P_elec is served by the battery, with an efficiency penalty modeled as a function of torque and speed of the generator and traction motors:

$$\eta_\text{elec} = f(\omega_\text{gen}, T_\text{gen}, \omega_\text{trac}, T_\text{trac}) \tag{2.4}$$

as defined by efficiency maps supplied with the Autonomie model. η_elec is enforced such that energy is always lost due to inefficiencies in the electric system, whether charging or discharging:

$$P_\text{batt} = \eta_\text{elec} P_\text{elec} \text{ if } P_\text{elec} \leq 0 \tag{2.5}$$

$$P_\text{batt} = \frac{1}{\eta_\text{elec}} P_\text{elec} \text{ if } P_\text{elec} > 0 \tag{2.6}$$

where positive values of P_batt represent discharging. At timestep i, battery SOC is calculated for the next timestep $i+1$ using the following equation:

$$\text{SOC}_{i+1} = \text{SOC}_i - \frac{V_\text{oc} - \sqrt{V_\text{oc}^2 - 4P_\text{batt}R_\text{int}}}{2R_\text{int}Q_\text{batt,o}} \Delta t \tag{2.7}$$

To enable fast computation when solving the DP formulation, fuel consumption is modeled using a cubic response surface [27] representation of a publicly available Brake Specific Fuel Consumption (BSFC) map for the Generation III Prius [22]:

$$\text{BSFC} \left(\frac{\text{g}}{\text{kWh}}\right) = A_1 + A_2\omega_\text{ICE} + A_3T_\text{ICE} + A_4\omega_\text{ICE}T_\text{ICE} + A_5\omega_\text{ICE}^2 +$$
$$A_6T_\text{ICE}^2 + A_7\omega_\text{ICE}T_\text{ICE}^2 + A_8\omega_\text{ICE}^2T_\text{ICE} + A_9T_\text{ICE}^3 \tag{2.8}$$

where all A values are fitted constants. This BSFC surface has an ideal operating line [28] that represents the instantaneous optimal FE operating point (in terms of torque and speed) as a function of engine power. The fuel consumption during a timestep Δt is thus

$$m_{\text{fuel}} \left(\text{grams}\right) = \left(\text{BSFC} \times \frac{1 \text{ hour}}{3600 \text{ sec}} \right) P_{\text{ICE}} \Delta t \qquad (2.9)$$

where P_{ICE} is in kW and Δt is in seconds.

The angular speeds of powertrain components are constrained by a planetary gearset:

$$\omega_{\text{ICE}} = \omega_{\text{gen}} \frac{\rho}{1+\rho} + \omega_{\text{ring}} \frac{1}{1+\rho} \qquad (2.10)$$

where $\rho = \frac{N_{\text{sun}}}{N_{\text{ring}}}$. Speeds are also constrained by limits on the electric motors, given in Table 2.1. The ring gear speed is linearly related to vehicle speed:

$$\omega_{\text{ring}} = \frac{r_{\text{fd}}}{r_{\text{wheel}}} v \qquad (2.11)$$

2.2 Define Control Strategies

The model's powertrain is controlled by one of two different control strategies: a Baseline EMS, meant to simulate stock vehicle performance, and an Optimal EMS, derived via DP to optimize FE over a predicted driving schedule.

2.2.1 Baseline EMS

The Autonomie model is simulated over a drive cycle $v(t)$, defining the Baseline EMS $P_{\text{ICE}}(t)$, which also implicitly defines $P_{\text{elec}}(t)$ via Equation 2.2. The power split model is used to calculate the remaining outputs, including m_{fuel}, SOC, and FE. This is illustrated in Figure 2.1a.
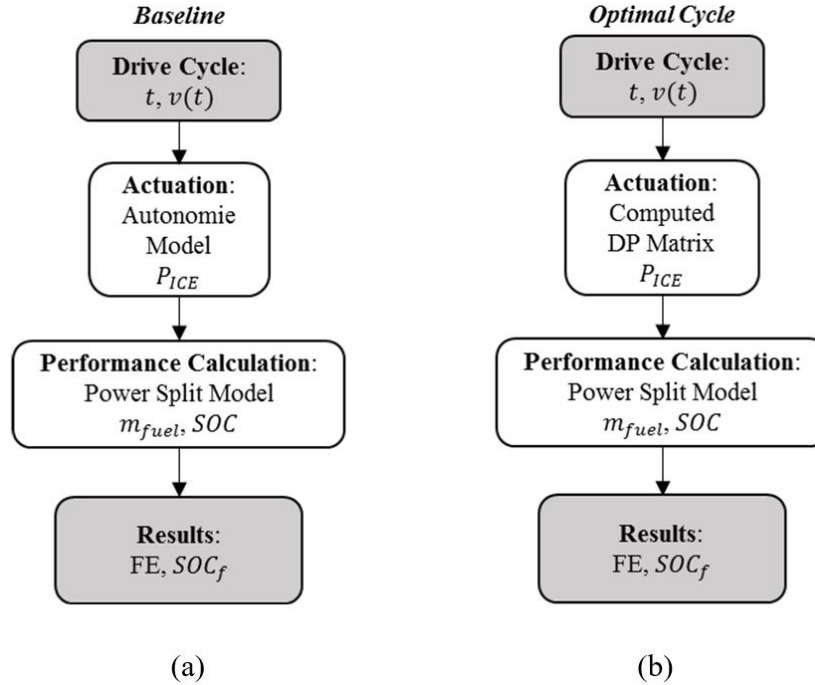
Figure 2.1: FE simulation method for (a) Baseline EMS and (b) Optimal EMS (exact schedule prediction)

To validate the Baseline EMS, the process in Figure 2.1a was used for three standard Environmental Protection Agency (EPA) FE test schedules and the FE results, corrected for change in SOC [29], were compared with experimental results for the 2010 Toyota Prius obtained by Argonne National Laboratory (Table 2.2) [30].

Table 2.2: FE results demonstrating validation of Baseline EMS model for FE investigations

EPA Drive Cycle	Simulated FE	Measured FE	% Difference
UDDS	76.4 mpg	75.6 mpg	+1.1%
US06	45.0 mpg	45.3 mpg	-0.6%
HWFET	69.1 mpg	69.9 mpg	-1.1%

Since FE differs by less than $\pm 1.2\%$ for all drive cycles, the model could be considered sufficiently validated in accordance with standard practices. However, for extra validation certainty, another validation step is used. In addition to FE, Argonne National Laboratory provides time traces of selected measurements from tests of the Generation III Prius. Simulated traces of battery

state of charge (SOC) and engine speed are qualitatively compared to experimental traces (Figure 2.2).

With battery SOC (Figures 2.2a, 2.2c and 2.2e), the simulated trace for each cycle closely follows the experimental trace for the first ~150 seconds of the cycle. The values of SOC start to diverge at later times during the cycle, but the shapes of the two curves generally resemble one another throughout the cycle. Since AE typically have much shorter durations than 150 seconds, SOC is expected to be accurately simulated for the full duration of individual AE.

Simulated and measured engine speed (Figures 2.2b, 2.2d and 2.2f) match closely for the US06 and HWFET cycles, except for a tendency for the simulated engine to shut off more frequently than the physical engine. While the global match with the UDDS cycle is not as close, shorter time windows demonstrate similarities in the two traces.

In similar studies, if validation is performed, researchers are often satisfied with just comparing simulated and measured FE. After additionally comparing traces of battery SOC and engine speed, this model is considered sufficiently validated for FE studies.
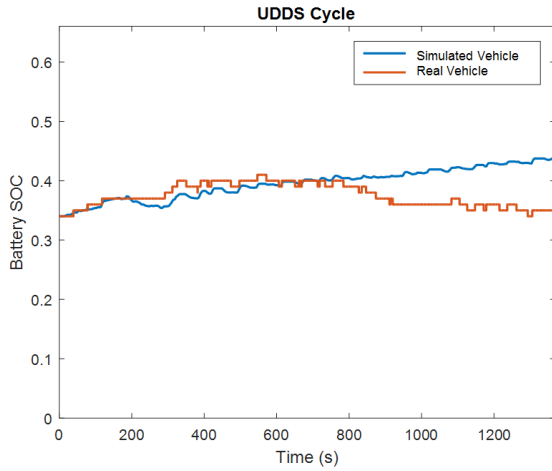
(a) Battery SOC: UDDS Cycle
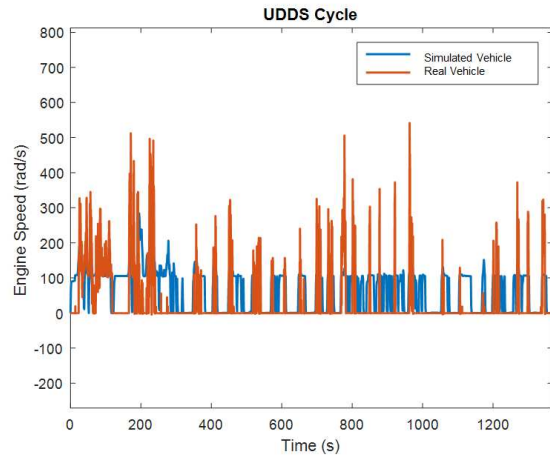
(b) Engine speed: UDDS Cycle
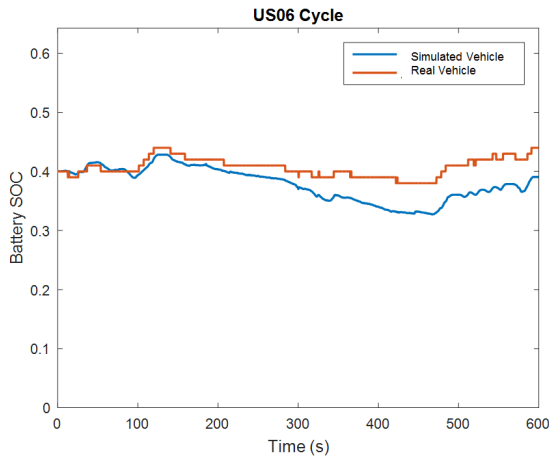
(c) Battery SOC: US06 Cycle
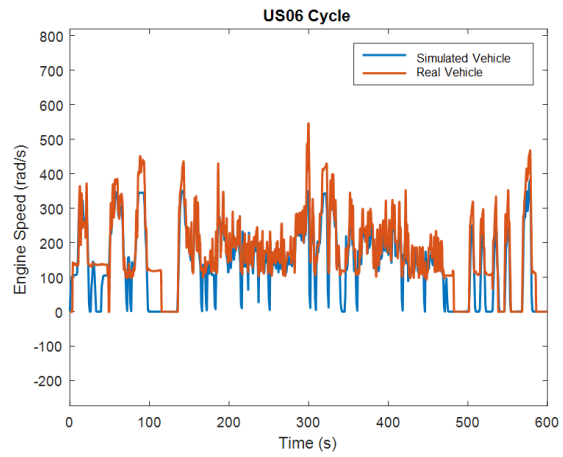
(d) Engine speed: US06 Cycle
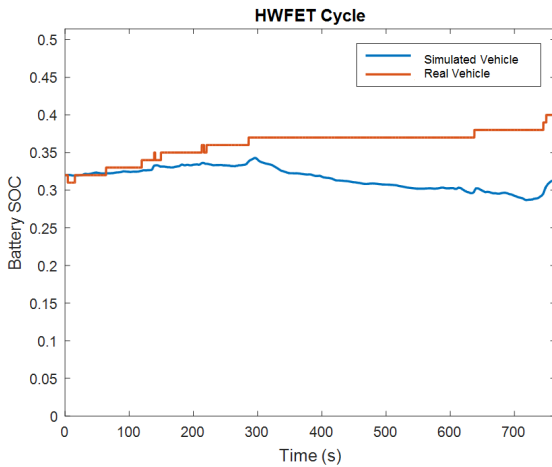
(e) Battery SOC: HWFET Cycle
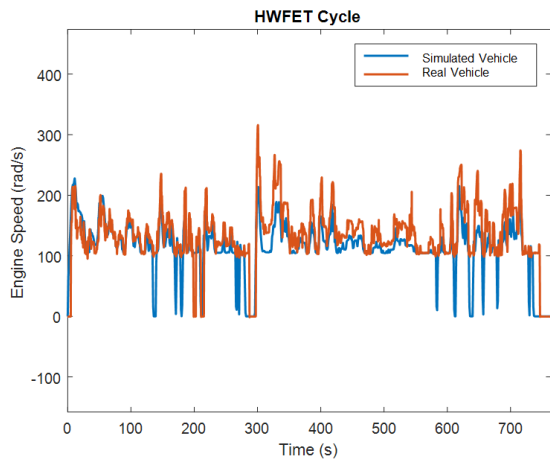
(f) Engine speed: HWFET Cycle

Figure 2.2: Validation of adjusted model using trace comparison with EPA drive cycle battery SOC and engine speed

2.2.2 Optimal EMS

The Optimal EMS is derived using deterministic DP, which uses backwards recursion to avoid solutions that are not optimal as defined by the Bellman Principle of Optimality [31, 32]. The DP scheme used for this study was detailed and validated in a previous publication [23] and will be described only briefly in this section.

In general, DP is used to compute optimal control as a function of system state by minimizing a cost function, subject to system constraints. For this study, the optimal control variable is engine power P_{ICE}, which also implicitly defines P_{elec} via Equation 2.2; the state variable is battery SOC; and the cost function is fuel consumption m_{fuel}. For the purposes of the DP scheme, vehicle velocity trace $v(t)$ is an exogenous input upon which the state variable, SOC, partially depends. The state and cost are given by the following equations:

$$\text{SOC}(k+1) = \text{SOC}(k) + f(\text{SOC}, P_{\text{ICE}}, v, k)\Delta t \tag{2.12}$$

$$\text{Cost} = \sum_{k=0}^{N-1} m_{\text{fuel}} + W\left(\text{SOC}_f - \text{SOC}(N)\right)^2 \tag{2.13}$$

where W is a penalty weight arbitrarily set at 10,000, k is the timestep index, N is the number of timesteps, and Δt is the size of a timestep. Equation 2.12 incorporates Equations 2.3-2.7 and 2.10-2.11, and Equation 2.13 incorporates Equations 2.8-2.9. The allowable state and control spaces are

$$40\ \% \leq \text{SOC}(k) \leq 80\ \% \qquad (k = 0, ...N) \tag{2.14}$$

$$0\ \text{kW} \leq P_{\text{ICE}}(k) \leq 73\ \text{kW} \qquad (k = 0, ...N - 1) \tag{2.15}$$

To summarize, the DP scheme is used to calculate engine power (discretization $\Delta P_{ICE} = 0.1$ kW) for every feasible battery SOC (discretization $\Delta \text{SOC} = 0.02\%$) for every timestep in a drive

cycle (discretization $\Delta t = 0.4$ sec) to minimize fuel consumption for a velocity trace $v(t)$ and desired SOC$_f$. In future studies, other measurements (e.g. battery temperature) and cost variables (e.g. battery life impacts) may also merit inclusion but were not included in this research.

The output of DP for a velocity trace can be visualized as a two-dimensional matrix of engine power, where row indices represent values of SOC and column indices represent timesteps (see Figure 2.3a). For any initial SOC (SOC$_i$), the DP matrix can be used as a lookup table to generate the optimal control solution $P_{\mathrm{ICE}}(t)$ achieving the driving schedule $v(t)$ that results in a desired SOC_f.

<div align="center">(a)   (b)</div>
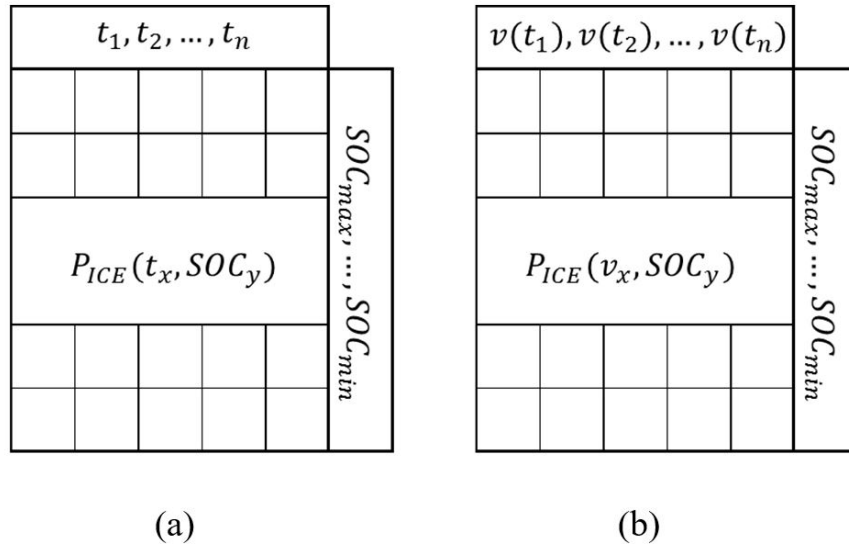
Figure 2.3: a) Illustration of matrix generated by dynamic programming algorithm; b) Illustration of matrix with conversion of time index to velocity index

Exact Drive Cycle Prediction

A DP formulation achieves an upper limit on FE improvement over the baseline strategy if prediction error is zero, i.e., if $v(t)$ is known exactly. This level of prediction fidelity may never be achieved in reality, but the results of simulations with zero prediction error serve as useful comparison points for the simulation results of more implementable EMS.

To calculate FE improvement with exact cycle prediction, the optimal control matrix is computed using $v(t)$ and SOC$_f$ from a Baseline EMS simulation. Ensuring that the baseline and

optimal solutions achieve the same SOC_f is essential for demonstrating improvement in FE; otherwise, FE could be artificially improved by utilizing more battery energy than the Baseline EMS. As illustrated in Figure 2.3a, the matrix is used as a lookup table with the time index of the drive cycle to obtain $P_{\text{ICE}}(t)$. Then, P_{ICE} is input to the power split model, which is used to calculate fuel consumption, SOC, and FE, as shown in Figure 2.1b.

Exact AE Prediction

Whereas an upper limit on FE for a drive cycle $v(t)$ is achieved by applying Optimal EMS to the entire cycle, an upper limit on FE *with only predictive control of AEs* can be achieved by simulating the Optimal EMS during AE (with exact AE prediction) and the Baseline EMS for the remainder of the drive cycle.

For this research, AEs are defined as segments of the drive cycle in which 1) vehicle speed increases monotonically, 2) the total increase in speed is greater than 9 mph, and 3) the time duration of increasing speed is greater than 4 seconds.

To calculate FE improvement for a drive cycle with exact AE prediction, the DP matrix is computed for each AE. The drive cycle is simulated where the Baseline EMS determines P_{ICE} for all but AE segments, and Optimal EMS determines P_{ICE} during AEs. This composite engine power trace $P_{\text{ICE}}(t)$ is input to the power split model to calculate fuel consumption, SOC, and FE. This is illustrated in Figure 2.4a.
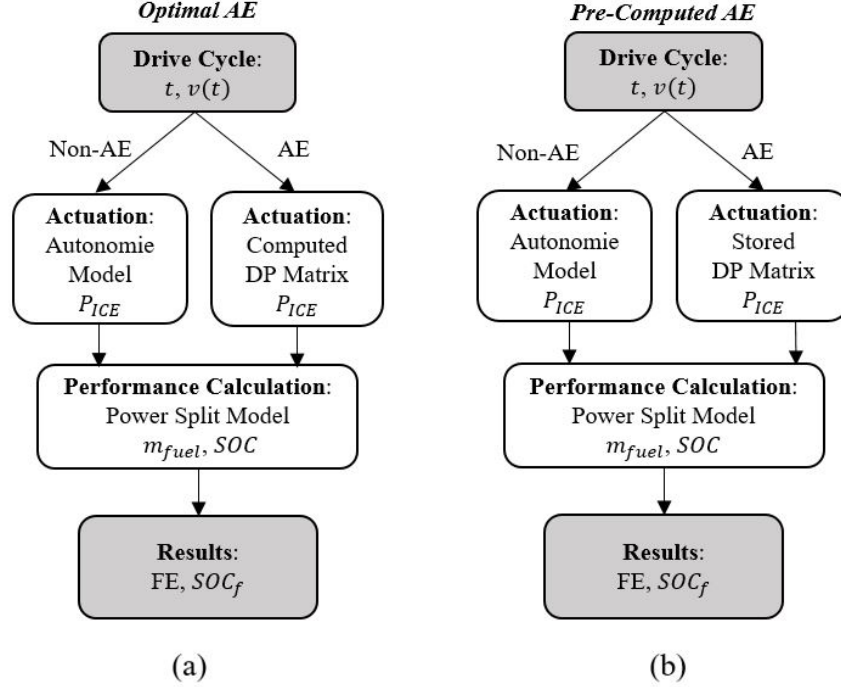
Figure 2.4: FE simulation method for (a) Optimal EMS (exact AE prediction) and (b) Pre-Computed EMS (approximate AE prediction)

Pre-Computing Optimal EMS for Approximate AE Prediction

Since the matrix generated via DP is a discrete array of optimal $P_{\text{ICE}}(k, \text{SOC})$ for timesteps $k = 0...N$, it can be used as a lookup table for a different drive cycle with the same number of timesteps. This can yield a near-optimal solution if the new drive cycle is similar to the one to which DP was applied. However, the constraint of identical durations makes this method challenging to apply in practice.

If optimal control is only applied to AEs, there is a way around the constraint of equal duration. AEs are monotonically increasing segments of $v(t)$, so they are able to be indexed using velocity. This enables the DP matrix to be converted from a mapping with respect to time and SOC ($P_{\text{ICE}}(k, \text{SOC})$) to a mapping with respect to *velocity* and SOC ($P_{\text{ICE}}(v_k, \text{SOC})$), as shown in Figure 2.3b. With this conversion, it is possible to derive a DP matrix for one AE (the "expected AE") and apply it to any other AE ("actual AE") with the same velocity range as the expected AE, regardless of any difference in duration. Whereas drivers are not constrained to repeat AEs with equal du-

rations, accelerator pedal traces, or other attributes, traffic laws encourage repetition of AEs with equal velocity ranges (for example, 0-25 mph AEs on neighborhood streets). In Chapter 3, the hypothesis that velocity range correlates with Optimal EMS attributes is investigated. In Chapter 4, different approaches to categorizing AEs to achieve similar velocity ranges are investigated.

As shown in Figure 2.4b, this strategy is simulated identically to the strategy with exact AE prediction, except that P_{ICE} is calculated using a "stored" DP matrix derived for an expected, rather than actual, AE.

2.3 Gather AE Dataset

Data used in simulations for this research come from a 384-drive-cycle dataset recorded at 10 Hz (Δt =0.1 second) from several Toyota Prius drivers. The average cycle duration is 1086 seconds, and the average speed is 28 mph. AEs in the drive cycles were identified using the logic statement:

$$[(v_j - v_{j-1}) \text{ and } (v_{j+1} - v_j) \text{ and } (v_{j+2} - v_{j+1}) \text{ and } (v_{j+3} - v_{j+2})] \leq 0.05 \text{ mph} \qquad (2.16)$$

where j is the timestep index within the drive cycle. If this inequality is true, i.e. if speed is increasing by at least $\frac{0.05mph}{0.1sec} = 0.5\frac{mph}{sec}$ for the next 3 timesteps, the section containing v_j is an AE candidate. Of sections identified as AE candidates, those with a time duration greater than 4 seconds and a speed increase greater than 9 mph are included in the AE dataset. With this process, 7,708 AEs were extracted.

To simulate AEs in isolation, the speed trace of each AE was modifed to begin and end at a steady speed. From experiments using both the Baseline and Optimal EMS, it was found that prepending 8 seconds of steady speed at the initial AE velocity and appending 12 seconds of steady speed at the final AE velocity are sufficient for the model to start and finish at a steady state. With

15

this modification, the durations of AEs in the dataset range from 22 seconds to 76 seconds, and the minimum and maximum speeds reached in the dataset are 0 mph and 50 mph.

Chapter 3

Identify Key AE Attributes

As implied in the description of the pre-computed optimal EMS strategy (end of Section 2.2.2), it is hypothesized that reliable FE improvements can be achieved if the expected AE and the actual AE have similar ranges of velocity, or similar initial and final velocities ($v_{i,expected} \approx v_{i,actual}$ and $v_{f,expected} \approx v_{f,actual}$). This is based on the expectation that AEs with similar initial and final velocities likely have similar velocity profiles, and therefore have similar optimal control profiles. Thus, the control applied to the actual AE is similar to the optimal control profile, and the resulting FE should be near-optimal.

If this hypothesis is true, then v_i and v_f must be significant attributes accounting for variance in the optimal EMS. In this chapter, these and a variety of other attributes are gathered and investigated in order to test the hypothesis underlying the proposed optimal control approach, as well as to develop an understanding of how the optimal EMS varies across the AE dataset.

3.1 Define List of AE Attributes

The baseline and optimal EMS (exact prediction) are applied in simulation to every AE in the AE dataset, and simulation outputs, including engine power, total vehicle power, fuel consumption, and SOC, are saved for each AE. Attributes based on simulation inputs and outputs, defined in addition to v_i and v_f, are computed as a post-processing step. These attributes are listed in Figure 3.1 and some are defined in Appendix B.

	Speed [kph]	Accel Pedal [%]	Acceleration [G]	Engine Power [kW]	Total Vehicle Power [kW]	Fuel Consumption [mL]	SOC [%]
Variable							
Statistic							
Maximum (during acceleration)	X	X	X	X*	X		
Minimum (during acceleration)	X	X	X	X*	X		
Range (Min → Max during acceleration)	X	X	X	X*	X		
Average (during acceleration)	X	X	X	X*	X		
Average/Peak Ratio (during acceleration)	X	X	X	X*	X		
Variance (during acceleration)	X	X	X	X*	X		
Standard Deviation (during acceleration)	X	X	X	X*	X		
Median (during acceleration)	X	X	X	X*	X		
Modality		X		X*	X		
Time from ramp-up start to velocity ramp-up		X	X	X*	X		
Time from ramp-down end to velocity stabilization		X	X	X*	X		
Time to 50% of maximum from ramp-up	X	X	X	X*	X		
Time to 75% of maximum from ramp-up	X	X	X	X*	X		
Time to 90% of maximum from ramp-up	X	X	X	X*	X		
Time above 50% of maximum is held		X	X	X*	X		
Time above 75% of maximum is held		X	X	X*	X		
Time above 90% of maximum is held		X	X	X*	X		
Time held at zero			X	X*	X		
Operation time from ramp-up to ramp-down		X	X	X*	X		
Ramp-up rate		X	X	X*	X		
Time between Maximum and Minimum		X	X	X*	X		
Dip (Start - Minimum)				X*			X*
Start (beginning of pedal ramp-up)						X*	X*
End (end of pedal ramp-down)						X*	X*
End - Start						X*	X*

Legend:
- (blank) No Calculation
- X Calculate only Baseline
- X* Calculate Baseline, Optimal, and difference

Figure 3.1: List of attributes calculated for each AE

3.2 Characterize EMS Variations

During manual examination of AE optimal control traces $P_{\text{ICE}}(t)$, two broad control "types" were identified. For some AEs, $P_{\text{ICE}}(t)$ is low or zero for an initial portion of acceleration, and high for the remainder of the acceleration. In these cases, engine power can be described as being "delayed" until partway through the AE, so this control type is named "Delayed" control. When control is not Delayed, the engine provides power throughout the AE duration, often providing more engine power than the Baseline EMS initially. This control type is named "Advanced" control. Examples are given in Figure 3.2.

(a) Delayed
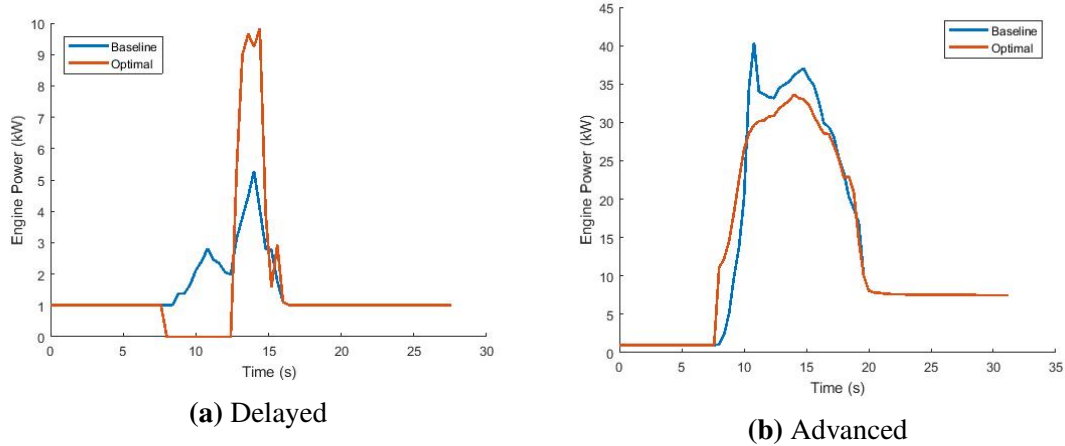
(b) Advanced

Figure 3.2: Example plots of AE with delayed control (left) and advanced control (right)

Since these two control types represent significant differences in optimal EMS, understanding which AE attributes predict Delayed or Advanced control may yield an understanding of which attributes account for the greatest variance in optimal EMS. Furthermore, the ability to predict whether Delayed or Advanced control is appropriate for a given AE may enable a simplified optimal EMS derivation technique (a path not pursued in this research).

The attributes listed in Figure 3.1 are used with filtering, PCA, and artificial neural network (ANN) methods to classify AEs into Delayed and Advanced subsets, for which the process is illustrated in Figure 3.3.
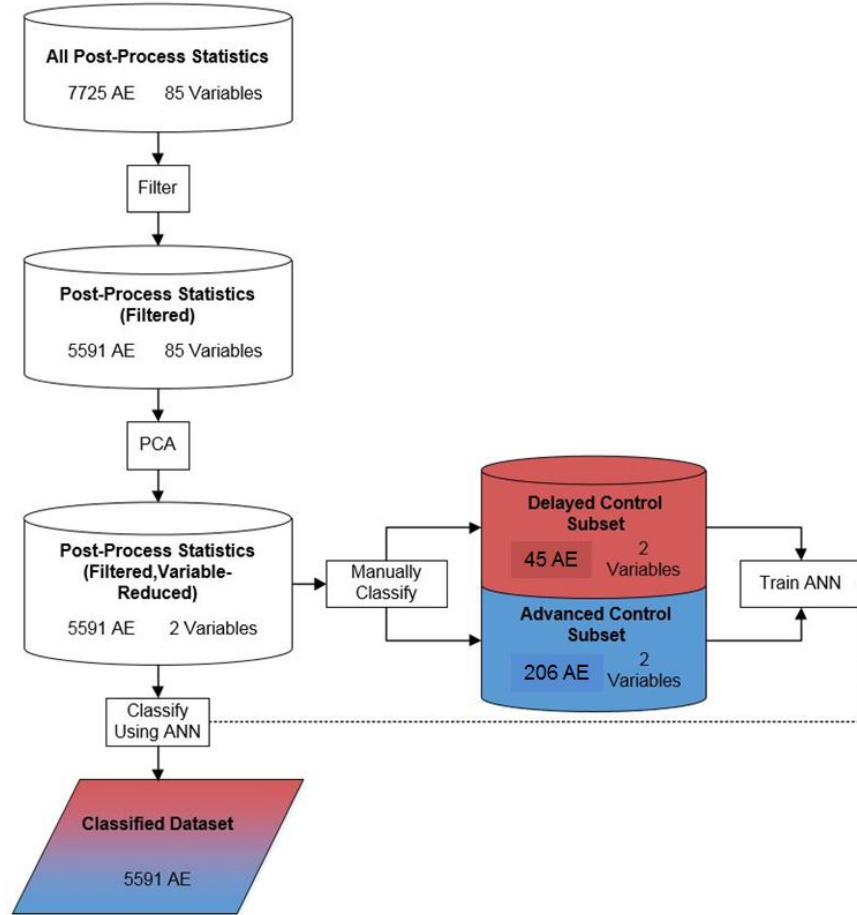
Figure 3.3: Diagram of AE dataset analysis process

3.2.1   Filter Data and Manually Classify Subset

The dataset of Section 3.1 is filtered to remove AEs unlikely to represent either control type based on the criteria in Table 3.1. If the results for an AE meet any of the criteria, the AE is removed from the analysis.

Table 3.1: Attributes and criteria used to filter AE dataset

Signal	Attribute	Criterion
Accelerator Pedal Signal	Modality	> 1
Engine Power	Modality	> 1
Fuel Consumption	Total: Optimal - Baseline	≥ 0
Battery SOC	End: Optimal - Baseline	$\neq 0$

It was observed that AEs whose control type are not clearly Delayed or Advanced often have multi-modal accelerator pedal signal and/or engine power. In these cases, the velocity curve is often not smooth, and since the accelerator pedal is being depressed and released sequentially, the AE may best be considered as multiple, immediately sequential AEs. These would complicate the control type investigation, so they are filtered out. Figure 3.4 illustrates an example of an AE with 5 accelerator pedal signal modes.
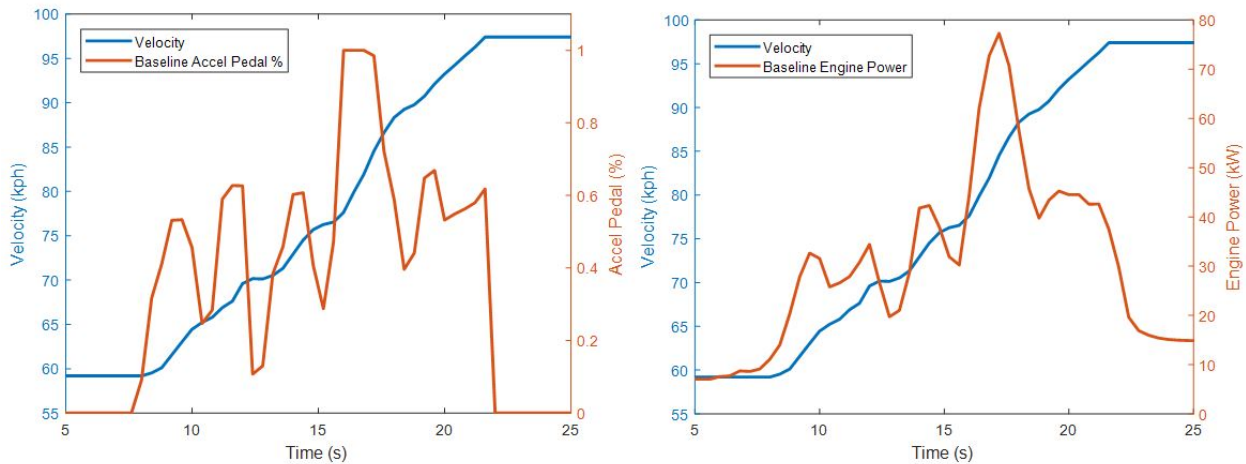
Figure 3.4: Illustration of an AE with multi-modal accelerator pedal signal and multi-modal engine power

It was also observed that for a small fraction of the dataset, optimal control results in *increased* fuel consumption and a mismatch in SOC_f, a rare consequence of discretizing the problem. These AEs are also filtered out.

Manually Classify Subset

Filtering reduces the dataset from 7725 AEs to 5591 AEs. Randomly selected AEs from the filtered dataset were manually examined for control type based on plots of baseline and optimal engine power. Figure 3.2a is a representative plot of Delayed control, and Figure 3.2b is a plot of Advanced control). Each AE was placed into one of two categories: Delayed or Advanced.

Delayed control was identified as involving engine shutoff at the beginning of acceleration before reaching a high, short-duration peak. Advanced control was identified as involving relatively

steady engine power for the full duration of the AE. Only AEs whose control type were obvious were classified. After examining approximately 450 AE, 46 examples of Delayed control and 206 examples of Advanced control were obtained.

3.2.2   Reduce Variables and Identify Key Attributes Via PCA

As dozens of attributes are calculated for each AE, the dataset has dozens of dimensions and is difficult to visualize. Principal Components Analysis (PCA) is a commonly used tool for reducing the dimensionality of this type of dataset, with the added benefit of highlighting the attributes that contribute most to variance among the samples. Prior to PCA, if attributes have significantly different ranges (e.g. if SOC were given as a fraction and power were given in watts) the data may be standardized, but for this data, ranges of attributes are all within an order of magnitude, so standardization is not performed.

Each of the principal components (PCs) is a linear combination of 106 attributes calculated from five signals (velocity, acceleration, optimal engine power, vehicle power, and battery SOC). There are 106 PCs, but the first two PCs account for 85.9% of the variance in the dataset, whereas the remainder account for a total of 14.1%, so PC1 and PC2 are analyzed. Each PC is described by 106 coefficients, one for each input attribute, where the magnitude of a coefficient is proportional to the attribute's contribution to a PC. The coefficients for the five most significant attributes defining PC1 and PC2 are given in Table 3.2. Figure 3.5 is a biplot visualizing all of the coefficients making up PC1 and PC2 3.2. From Table 3.2, all five of the highest contributors are velocity attributes. Further, from Figure 3.5, the top 5 attributes have overwhelmingly greater magnitudes than the remainder. This is striking, especially since the attributes are obviously interrelated (e.g. velocity range is the difference between maximum and minimum velocity).

Signal	Attribute	PC1 Coefficient	PC2 Coefficient
Velocity	Maximum	0.4641	0.1356
Velocity	Minimum	0.4172	-0.5007
Velocity	Range	0.0468	0.6363
Velocity	Mean	0.4560	-0.0943
Velocity	Median	0.4660	-0.0339
	Total Variance Explained	66.4%	20.9%

Table 3.2: Top 5 coefficients for PC1 and PC2
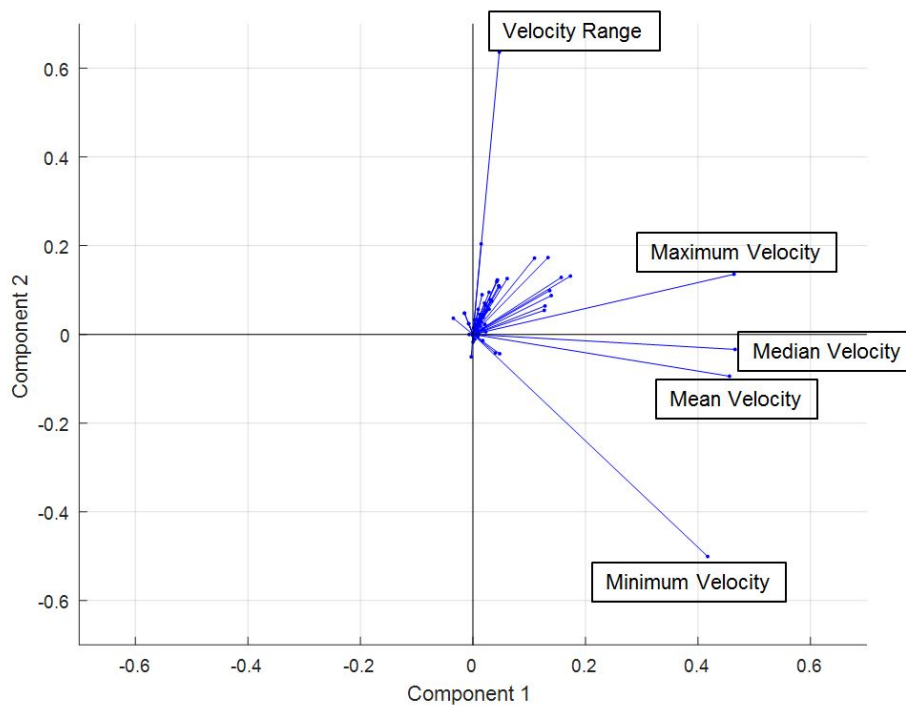
Figure 3.5: Biplot of coefficients for PC1 and PC2

3.2.3   Train Neural Network to Classify Control Type

The manually classified AE subsets (section 3.2.1) are used to train an artificial neural network for classification. The network is structured with two input units (for PC1 and PC2), two hidden layers of 10 units each, and an output layer of one unit. The output is a number between 0 and 1 that indicates a confidence level that the AE for which PC1 and PC2 are input has an Advanced optimal control profile. An output of 0 indicates high confidence classification as Delayed control,

an output of 1 indicates high confidence classification of Advanced control, and an output of 0.5 indicates a low confidence classifying as either control type.

A common technique to avoid overfitting is to reserve a portion (here, 30%) of the dataset for testing the neural network, so only 70% of the manually classified AEs are used to train the network. The trained network accurately classified 100% of the training data, and misclassified only 3 of the 75 AEs reserved for testing (96% testing accuracy).

As shown in Figure 3.6, most AEs are classified with high confidence by the ANN: over 70% are classified with greater than 99% confidence (a classification value less than 0.01 (Delayed) or 0.99 (Advanced)). The small fraction of AEs ($< 2\%$) that are weakly classified are removed: neural network outputs between 0.25 and 0.75 are considered to be undefined classifications.
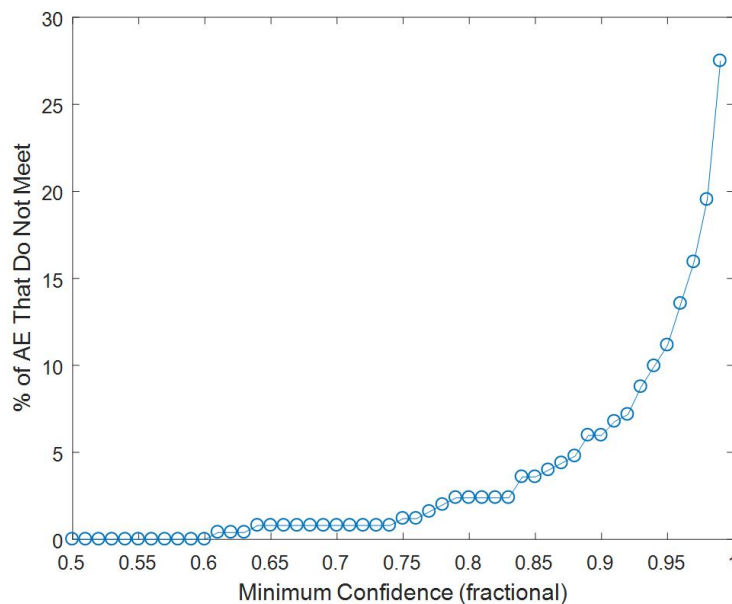
Figure 3.6: Exploration of cutoff confidence levels.

To verify the ANN classification results, AEs not in the training/testing set are randomly chosen (examples in Figure 3.7), classified, and manually examined. After examining several AE near each confidence level (100%, 75%, 25%, 0%) the ANN classification appears to agree with the manual classification.

(a) 2.4% probability of Advanced control.

(b) 25.0% probability of Advanced control.

(c) 75.0% probability of Advanced control.

(d) 100.0% probability of Advanced control.
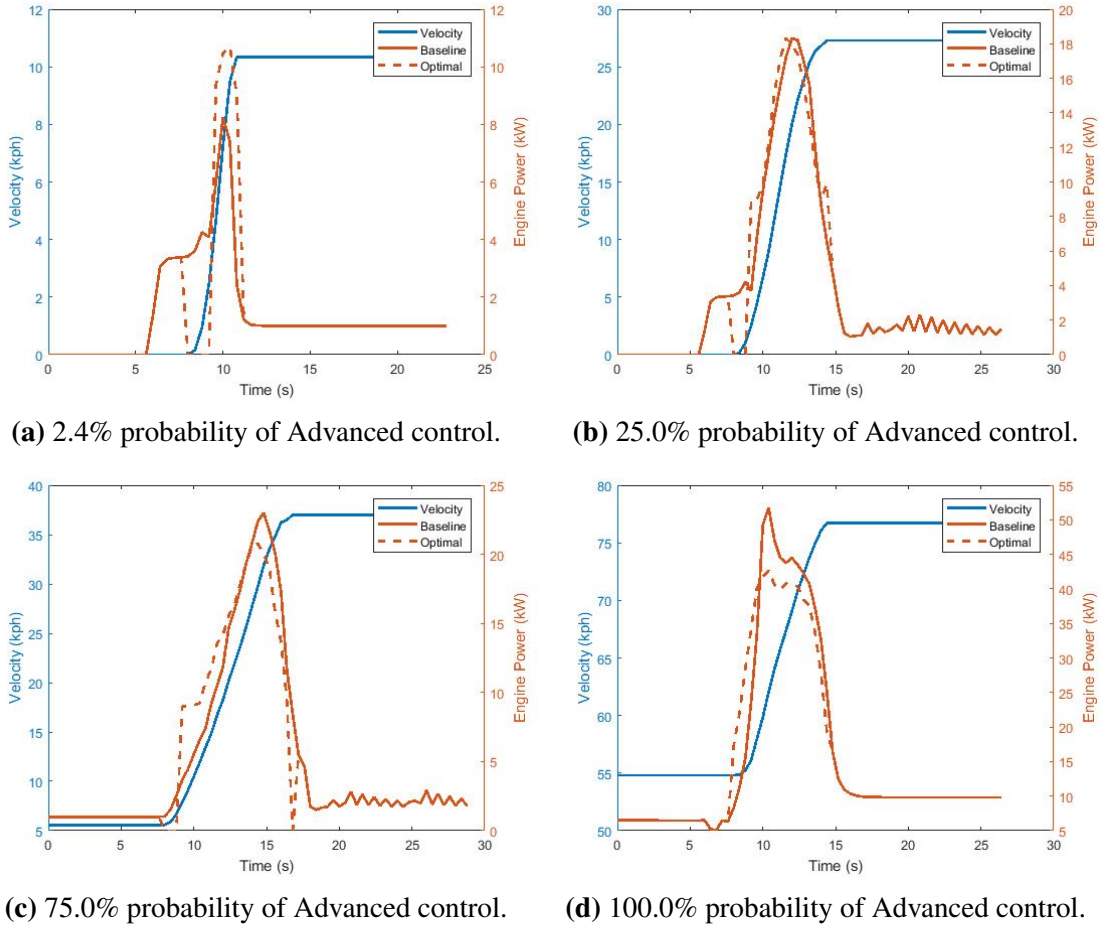
Figure 3.7: Manual verification of ANN classification

3.2.4 Classification Results and Discussion

The ANN is applied to all 5591 AEs in the filtered dataset. Figure 3.8 is a plot of PC1 and PC2 for every AE, with classification indicated by color. There is a gap in the points where examples of low-confidence classifications were removed.
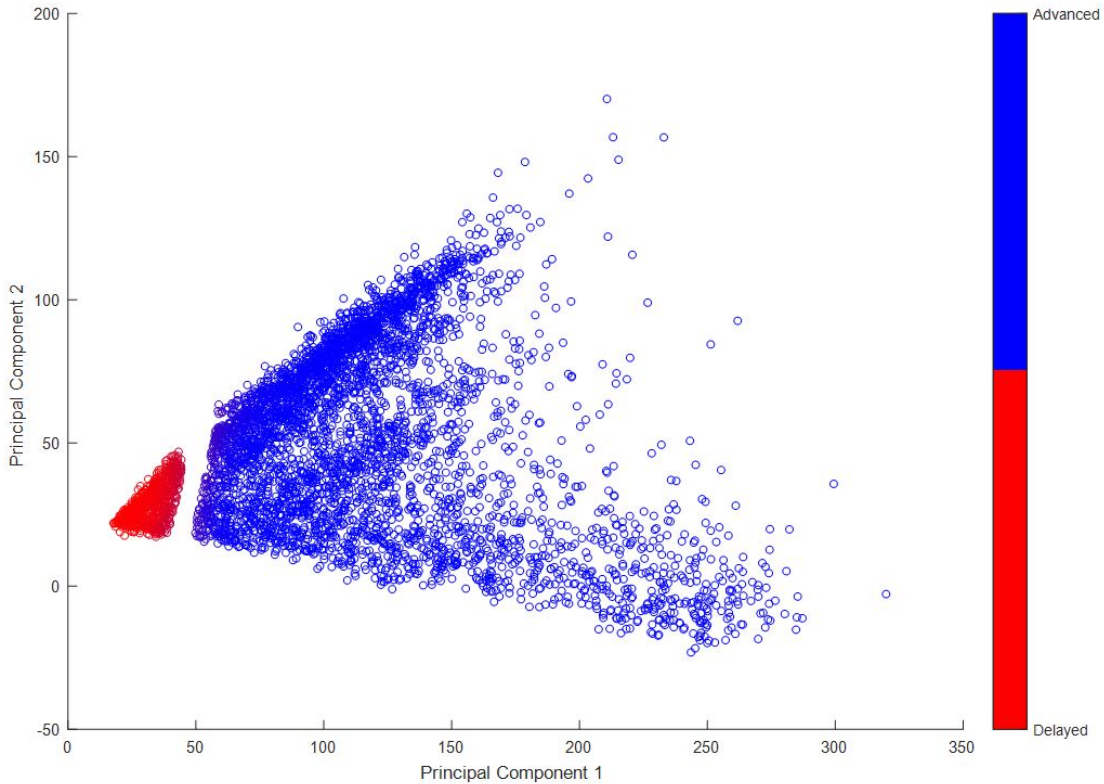
Figure 3.8: Classification of AE dataset, plotted by principal component

Figure 3.8 illustrates that a neural network is likely not the simplest way to successfully classify AE control types. A linear cutoff on the basis of PC1 and PC2 would succeed as well, or even on the basis of PC1 alone. For example, a precise criterion for Delayed control could be:

$$PC1 < 50 \tag{3.1}$$

The PCs enable a precise classification, but recall that information about the Optimal EMS was included in PCA. It is desirable to classify control type without computing the Optimal EMS first, i.e. without using attributes associated with the Optimal EMS. Given that the overwhelming majority of the information captured by PC1 and PC2 comes strictly from the velocity trace, it is expected that velocity attributes alone could be utilized to make a successful classification model.

From Figure 3.5, the five greatest constituents of PC1 and PC2 are maximum, minimum, mean, median, and range of velocity. Pairs of long, perpendicular line segments in the biplot correspond to pairs of attributes that account for significant portions of total variance in both PCs. Two nearly perpendicular pairs are chosen to investigate: range and median of velocity, and maximum and minimum velocity (or v_f and v_i). These pairs of attributes are plotted in Figures 3.9 and 3.10.
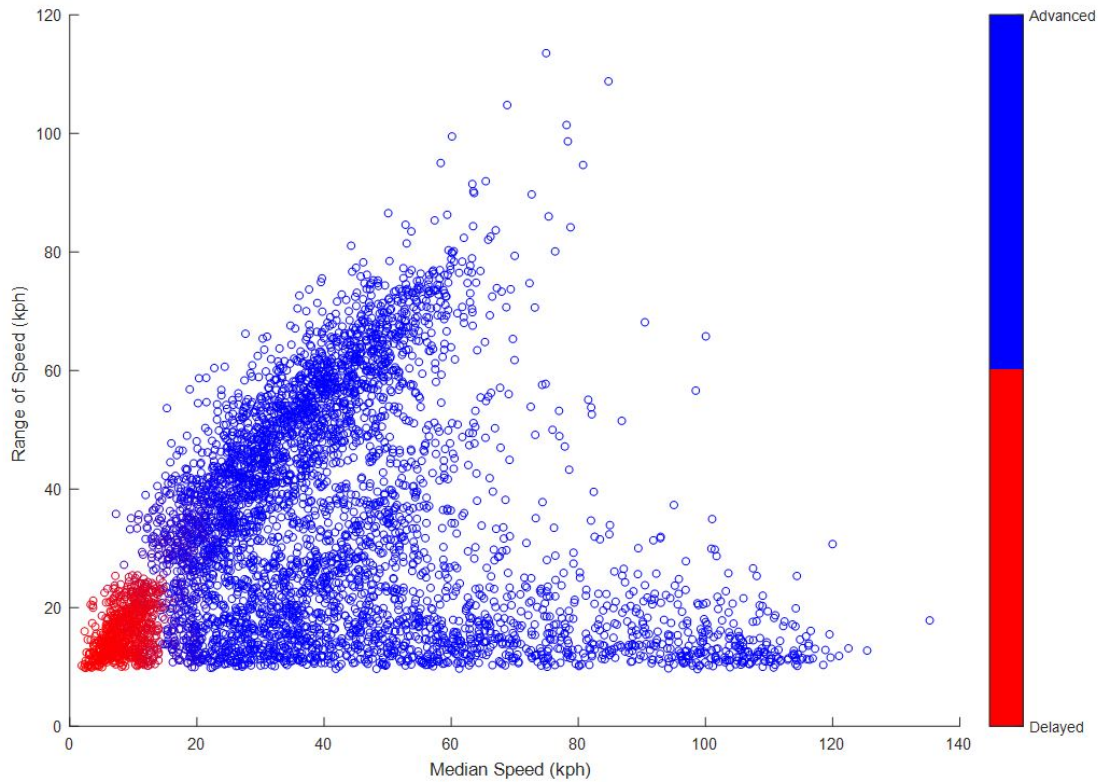
Figure 3.9: Classification of AE dataset, plotted by median and range of velocity

From Figure 3.9, control type might be classified using a linear criterion:

$$\left(v_{median} < 15 \text{ kph}\right) \text{ AND } \left[(v_f - v_i) < 30 \text{ kph}\right] \tag{3.2}$$

where control type is Delayed if the criterion is satisfied, and control type is Advanced if not.
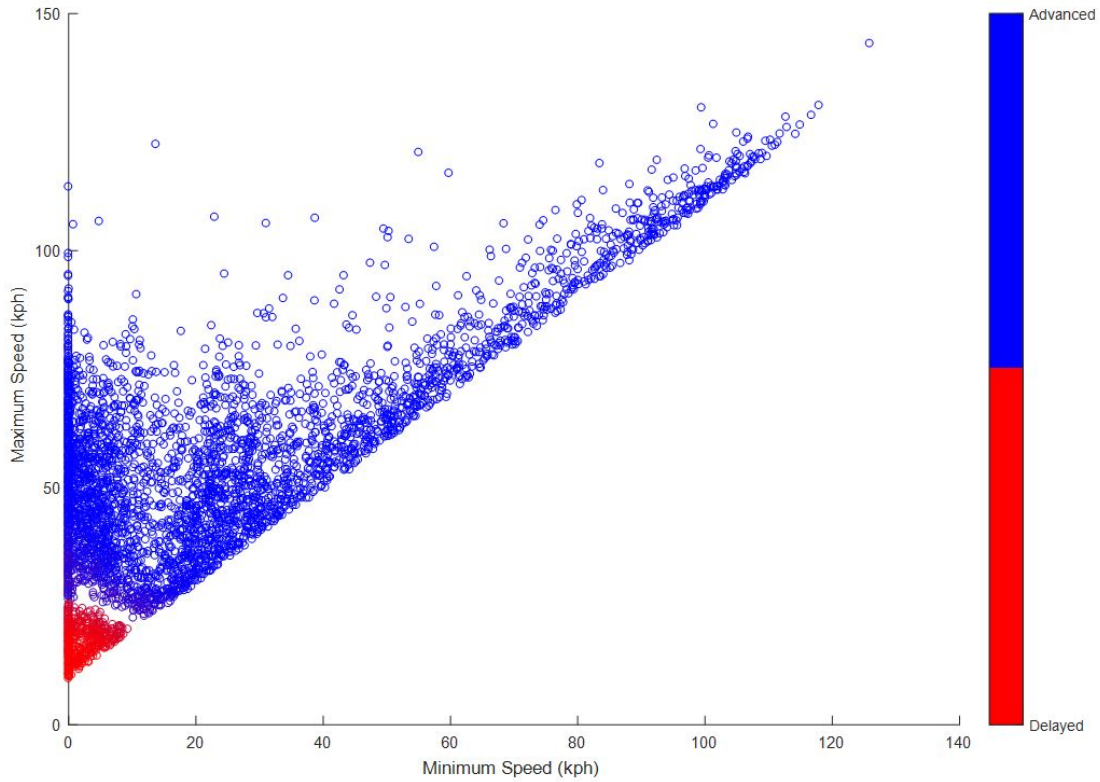
Figure 3.10: Classification of AE dataset, plotted by v_f and v_i

From Figure 3.10, v_f and v_i appear to separate the control types nearly as well as PC1 and PC2. A linear criterion based on both v_f and v_i would precisely define this separation, and even

$$v_f < 25 \text{ kph} \tag{3.3}$$

would work.

3.3 Conclusions

The experiments in this chapter primarily address Research Question #1:

1. *How do differences between AEs correlate with differences between AE Optimal EMS?*

Despite utilizing attributes associated with a variety of different signals, it was repeatedly found that attributes of the velocity trace $v(t)$ account for the majority of the variation in the dataset:

- The five PCA coefficients with the greatest magnitudes, and therefore explaining the most variance in the data, were all found to be attributes computed from $v(t)$.

- PC1 and PC2, which are primarily comprised of $v(t)$ attributes, enable precise classification (testing accuracy of 96%) between the two Optimal EMS control types observed in the dataset.

- $v(t)$ attributes, and in particular v_f and v_i, enable almost as precise classification as PC1 and PC2.

The results in this chapter support the hypothesis that AEs with similar v_f and v_i have similar Optimal EMS. This lays the foundation for experiments in the remaining chapters.

Chapter 4

Investigate AE Categorization Approaches

In Section 2.2.2, the approach is introduced of computing the Optimal EMS for an "expected" AE and applying it to an "actual" AE, enabling the Optimal EMS to be pre-computed and stored onboard the vehicle and implemented in real time. In practice, this requires some method of matching a predicted "actual" AE to a stored "expected" AE.

As concluded in Chapter 3, attributes of the velocity trace $v(t)$ are well correlated with variation of Optimal EMS attributes. In this chapter, the method of separating AEs into categories based on attributes of $v(t)$ is proposed and evaluated. In the main text, AEs are categorized in terms of initial and final velocity v_i and v_f. Categorization methods utilizing duration $t_f - t_i$ and average acceleration rate $\frac{v_f - v_i}{t_f - t_i}$ are also investigated (Appendix C).

4.1 Define Experimentation Process

To obtain measures of the magnitude and reliability of FE improvement enabled by different categorization approaches, an experimentation process is defined and repeated. AEs are split into categories; an expected AE is selected for each category and the optimal EMS for the expected AE is applied to every AE in the category; and FE results are corrected for SOC error.

4.1.1 Categorize AEs

A two-dimensional categorization scheme is used, where the AE dataset is separated into categories based on two attributes. The range of each attribute is divided into bins, and each category corresponds to some combination of bins. For example, one category might be defined as AEs with $0 \leq v_i < 1$ kph and $20 \leq v_f < 25$ kph. The three categorization schemes investigated are summarized in Table 4.1 (results for schemes 2 and 3 are in Appendix C).

Table 4.1: Summary of category schemes examined

	Attributes Used	Initial Velocity	Final Velocity
1	Number of Bins	13	14
	Expected AE Selection	Duration	
	Parameters Used	Duration	Final Velocity
2	Number of Bins	10	10
	Expected AE Selection	Final Velocity	
	Parameters Used	Average Acceleration	Final Velocity
3	Number of Bins	10	10
	Expected AE Selection	Initial Velocity	

4.1.2 Select Expected AE

For each category, one "expected" AE is selected. The Optimal EMS computed for the expected AE is the control strategy applied to all AEs in the category, so the expected AE should be a characteristic representative of the category.

The expected AE is chosen as the AE with the median value of a third attribute, additional to the two used to define the categories. For example, in a category defined as AEs with $0 \le v_i < 1$ kph and $20 \le v_f < 25$ kph, there is one AE with a duration that is shorter than exactly half of the AEs in the category, and longer than the other half. By applying the Optimal EMS for this AE to the rest in the category, the average difference between expected and actual duration is minimized. The attribute used to choose the expected AE for each categorization scheme is given in Table 4.1.

The expected Optimal EMS for each category is applied to every AE in the category, using the method introduced in Section 2.2.2, and the results are saved.

4.1.3 Correct FE for SOC Error

When applying Optimal EMS with exact prediction, the change in battery SOC during the AE is constrained to perfectly match the baseline change in SOC. When expected control is applied to an actual AE, this is no longer the case, as illustrated in Figure 4.1.
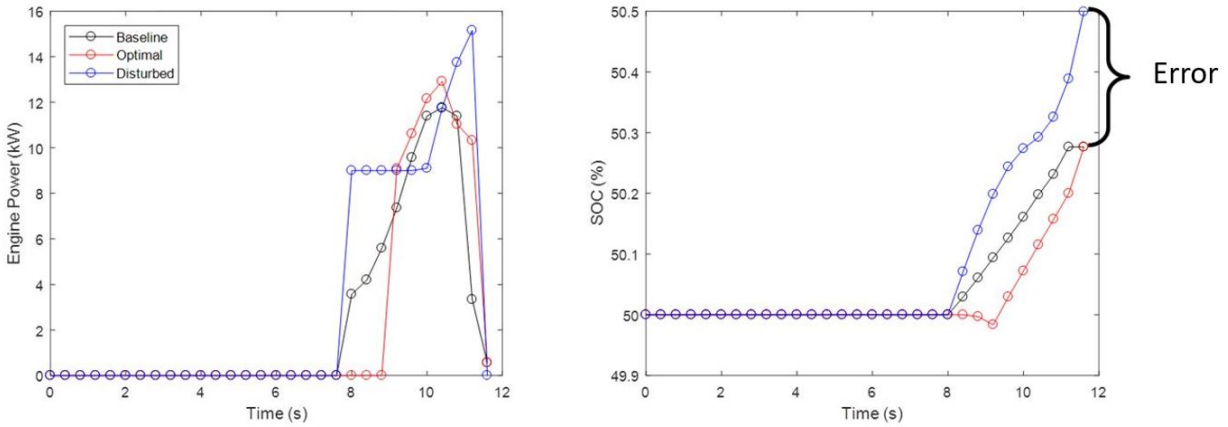
Figure 4.1: Example of AE with SOC_f mismatch

FE improvement relative to baseline must be adjusted to account for SOC_f deficits or excesses relative to baseline SOC_f, since the battery is charged by burning fuel. A commonly used method is to convert SOC_f differences into equivalent amounts of fuel by assuming a nominal energy conversion efficiency, but that would be insufficient here because the Optimal EMS inherently takes advantage of the variability in engine efficiency. Instead, the fuel equivalency method is applied individually to each category, based on the assumption that the engine's average efficiency within a category has less variability than it does in general.

In individual categories, a linear relationship between SOC_f error and FE improvement is observed. As shown in Figure 4.2, the slope of a linear fit of SOC_f error and FE improvement can be used to obtain the SOC_f-corrected FE improvement for each AE.
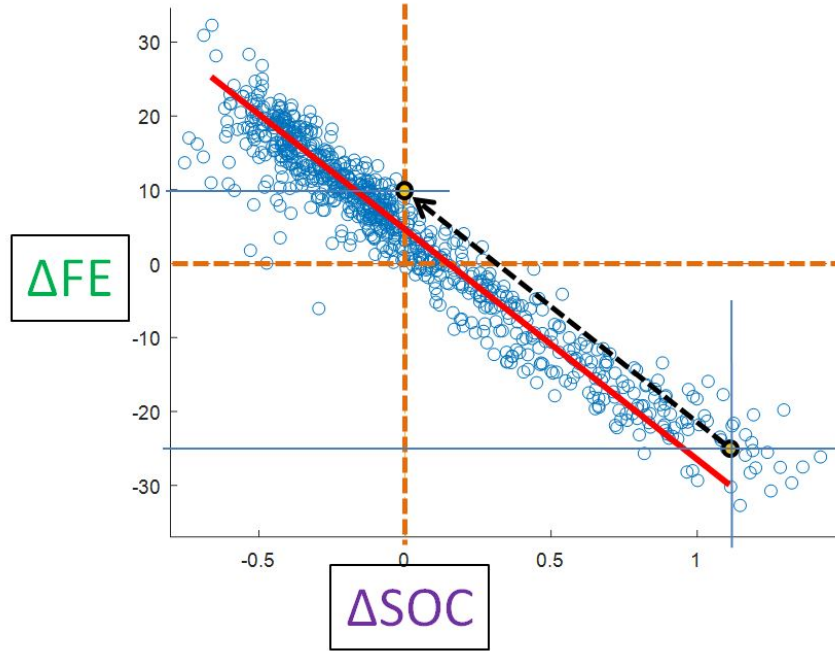
Figure 4.2: Illustration of FE correction method for SOC_f

This FE correction method is described by the following equations:

$$\Delta\text{FE} = \frac{\text{FE}_{optimal} - \text{FE}_{baseline}}{\text{FE}_{baseline}} \times 100\% \tag{4.1}$$

$$\Delta\text{SOC}_f = \text{SOC}_{f,optimal} - \text{SOC}_{f,baseline} \tag{4.2}$$

$$\Delta\text{FE}_{corrected} = \Delta\text{FE} - m\Delta\text{SOC}_f \tag{4.3}$$

where m is the slope of the fit line, obtained via least squares linear regression, of ΔFE versus ΔSOC for the category. As an example, Figure 4.3 shows the lines of best fit calculated for all categories in an example 5×5 categorization scheme.
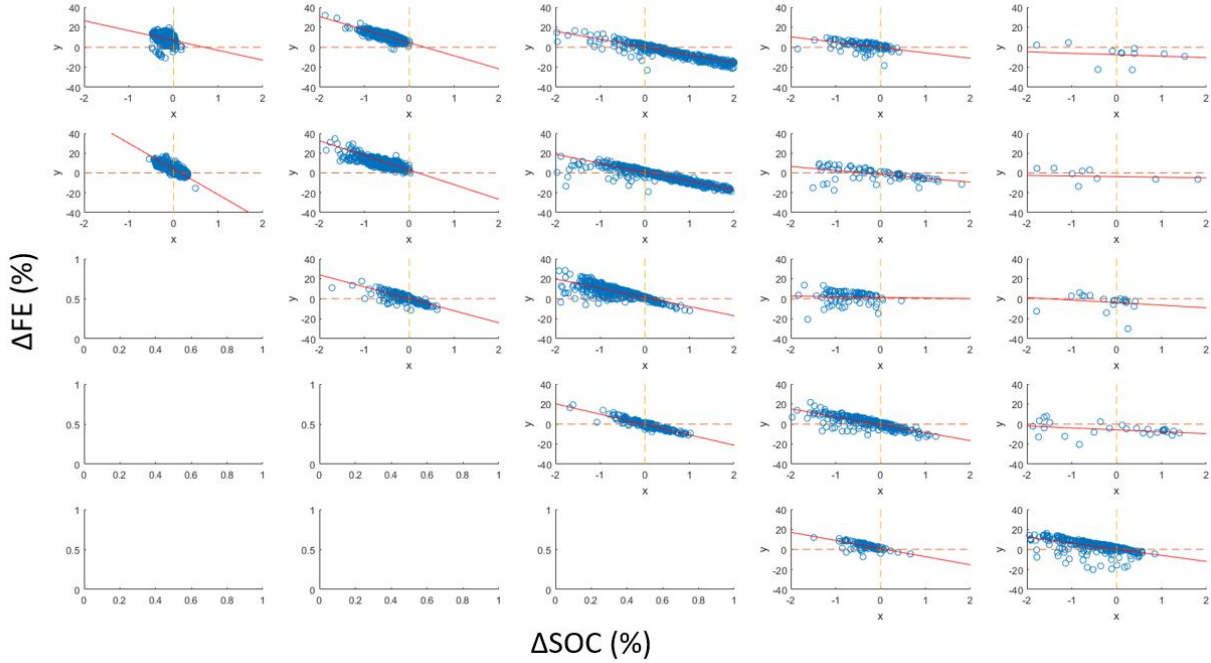
Figure 4.3: FE correction fit lines for an example 5×5 categorization scheme

Once corrected for errors in SOC_f, the FE improvement results for applying Optimal EMS for

an expected AE to an actual AE can be used to identify areas of greatest and least benefit in a given

categorization scheme. In the next section, results for categorization schemes based on v_f and v_i

are evaluated.

4.2   Categorize Using Initial and Final Velocity

Table 4.2: Summary of velocity category scheme

Attributes Used	Start Velocity	End Velocity
Number of Bins	13	14
Expected AE Selection	Duration	

Categories are defined using initial velocity and final velocity (referred to here as the "velocity"

category scheme). Category bins are 5 kph wide, with the exception of a 0-1 kph initial velocity

bin representing AEs that begin at 0 kph, and a 0-15 kph final velocity bin because none of the AEs

34

have a final velocity less than 10 kph. The scheme constrains initial velocity and final velocity to 60 and 80 kph, respectively. There are 13 bins of initial velocity and 14 bins of final velocity, for a total of $13 \times 14 = 182$ categories. Since initial velocity is always less than final velocity, 64 of these categories are empty. As illustrated in Figure 4.4, the dataset overwhelmingly consists of AEs that begin at zero speed.
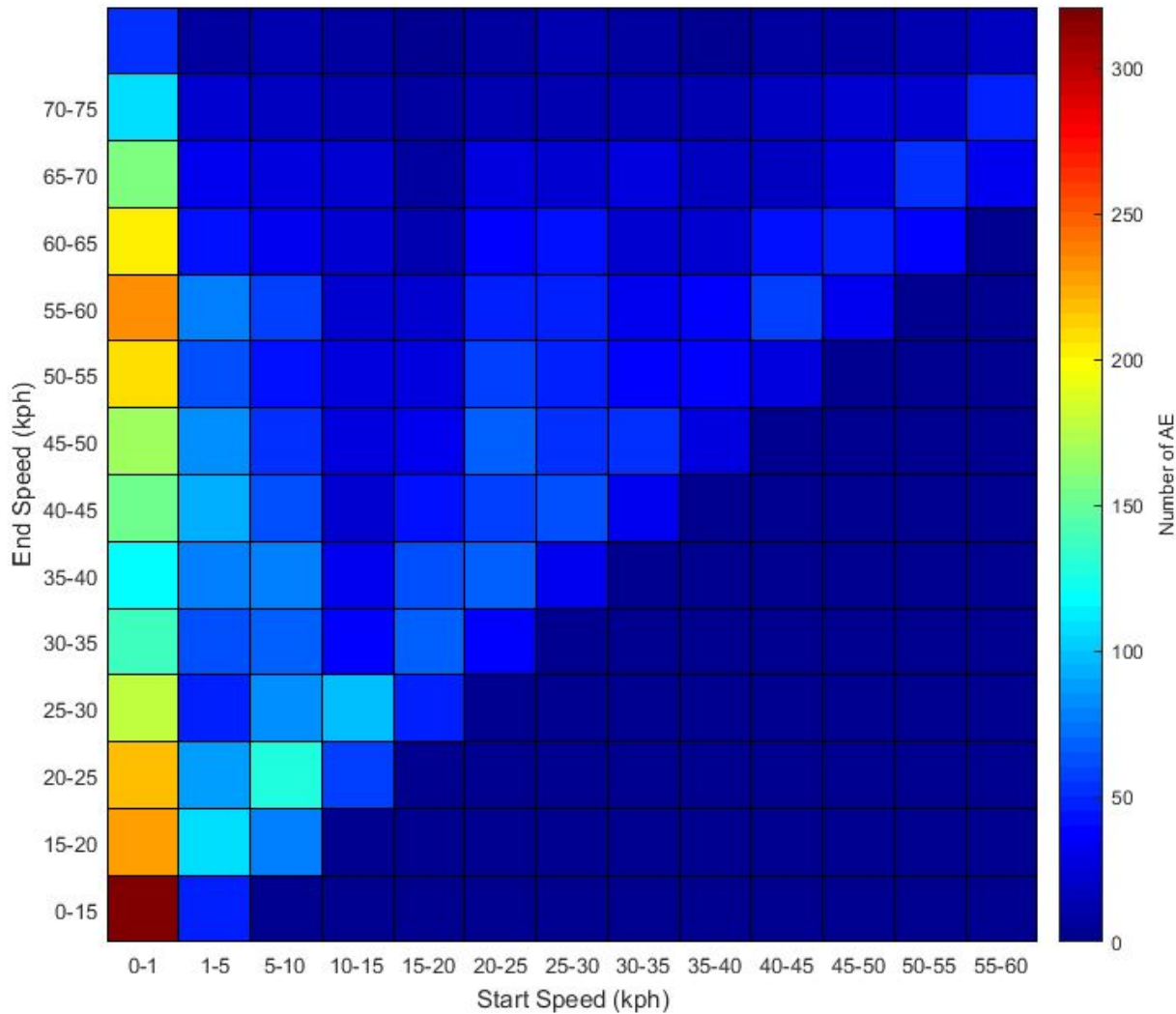
Figure 4.4: Population of velocity categories

35
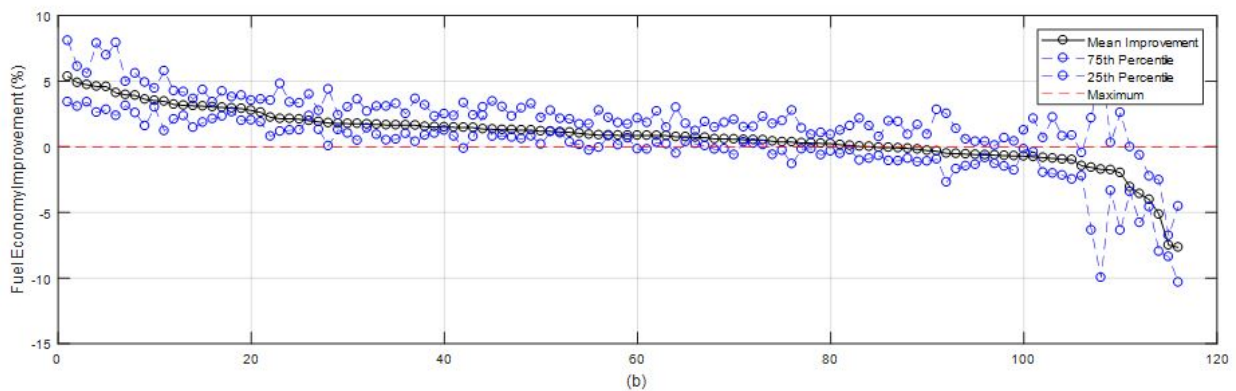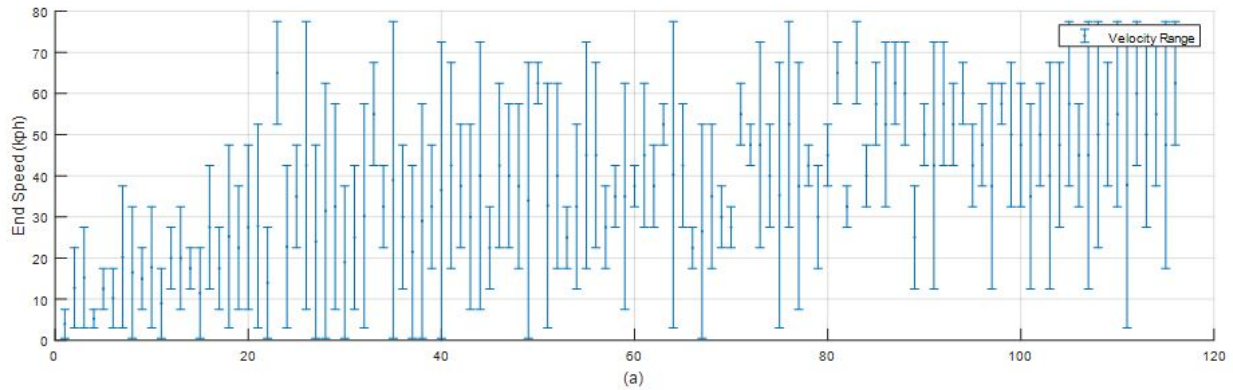
Figure 4.5: FE improvement results by velocity category in order of decreasing mean FE improvement

FE improvement results are shown in Figure 4.5. Every point along the horizontal axis corresponds to a single category, sorted by decreasing mean FE improvement (points in (a) and (b) correspond vertically between the two plots). The initial and final velocity defining each category are given in Figure 4.5a. The 25th, 50th (mean), and 75th percentiles of FE improvement are given in Figure 4.5b.

For some categories, the mean FE improvement is negative, with a greater likelihood for categories with greater initial and final velocities. For these categories, the differences between the 25th and 75th percentiles of FE improvement also tend to be greater than for the other categories, indicating greater variability in FE improvement. As shown in Figure 4.4, the high-velocity categories are sparsely populated, which may account for the greater variability in these categories.

36
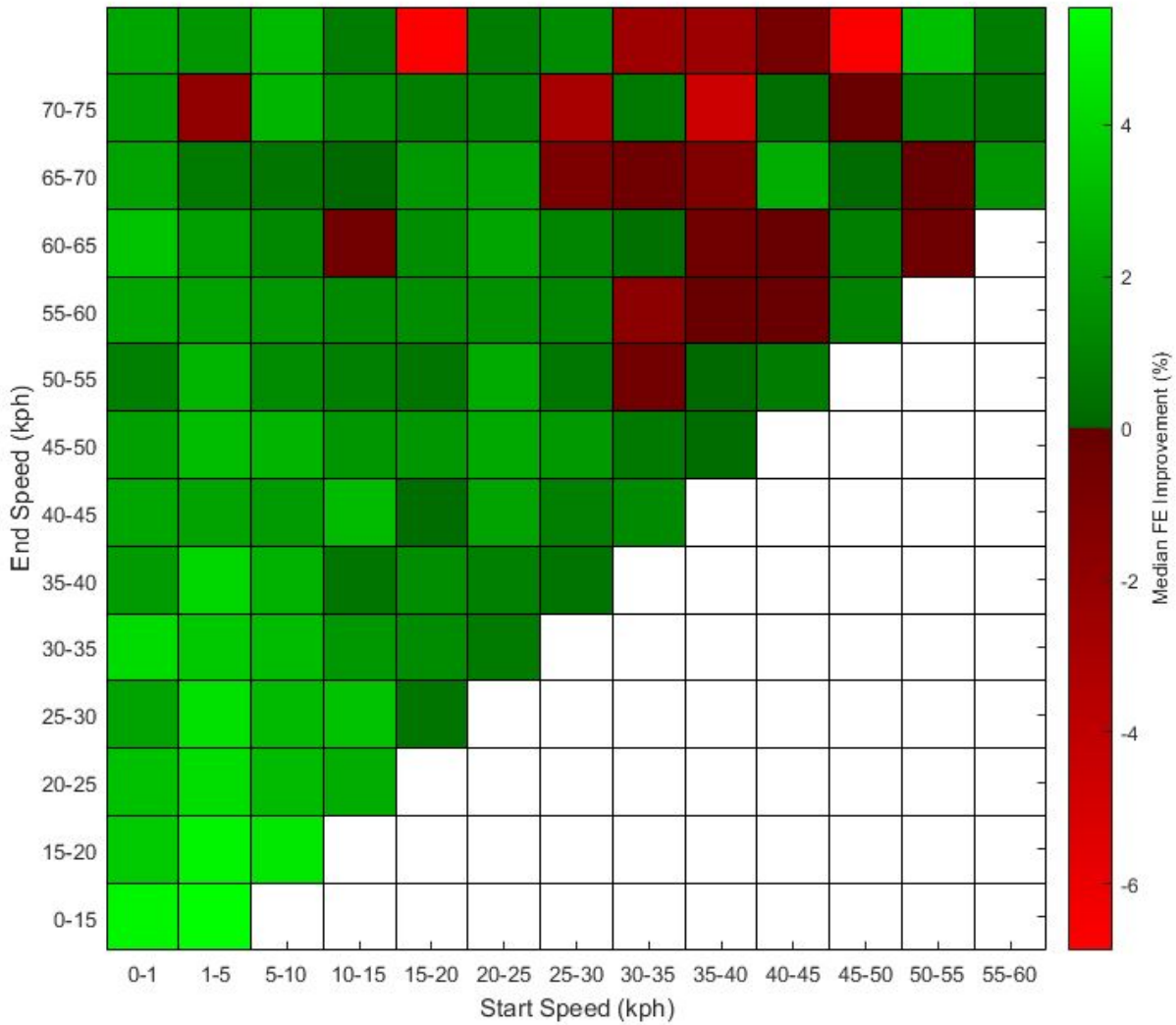
Figure 4.6: Median FE improvement results organized by velocity category

Figure 4.6 is another visualization of FE improvement per category, showing the median FE improvement for each category analogously to Figure 4.4. Matching what is apparent in Figure 4.5, the greatest FE improvements are achieved in lower-velocity, more populated categories.

4.2.1 Investigate Control Type Mismatch

In some instances where FE was reduced relative to the Baseline EMS, it was observed that Delayed control was being applied to an AE for which the Optimal EMS is Advanced control, or vice versa. The ANN classification of control type from Chapter 3 was used to investigate whether

this explains FE loss in general. The control type of the expected AE for each category is shown in Figure 4.7, and the control types of the actual AEs are shown in Figure 4.8.
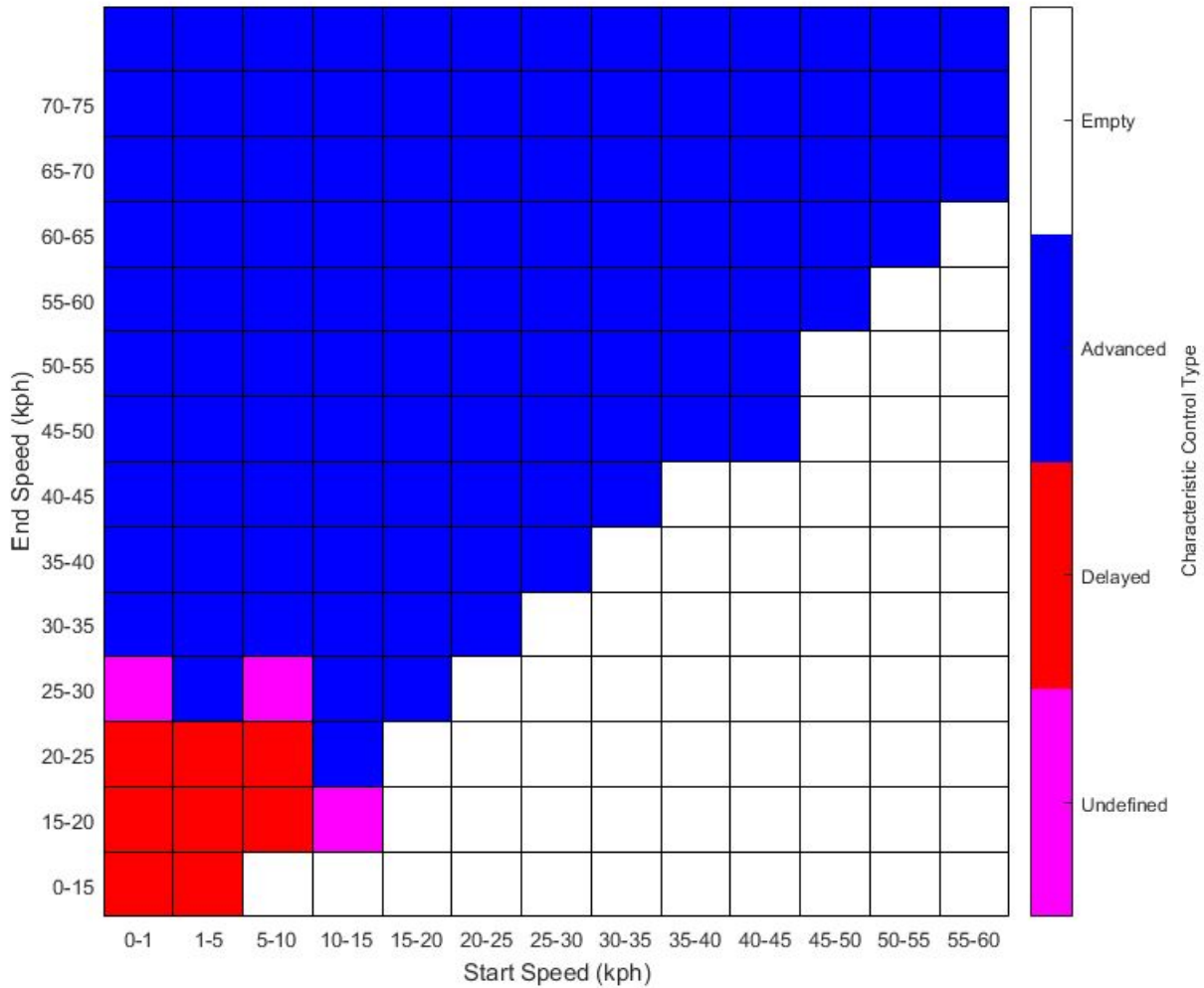
Figure 4.7: Expected AE control type organized by velocity category
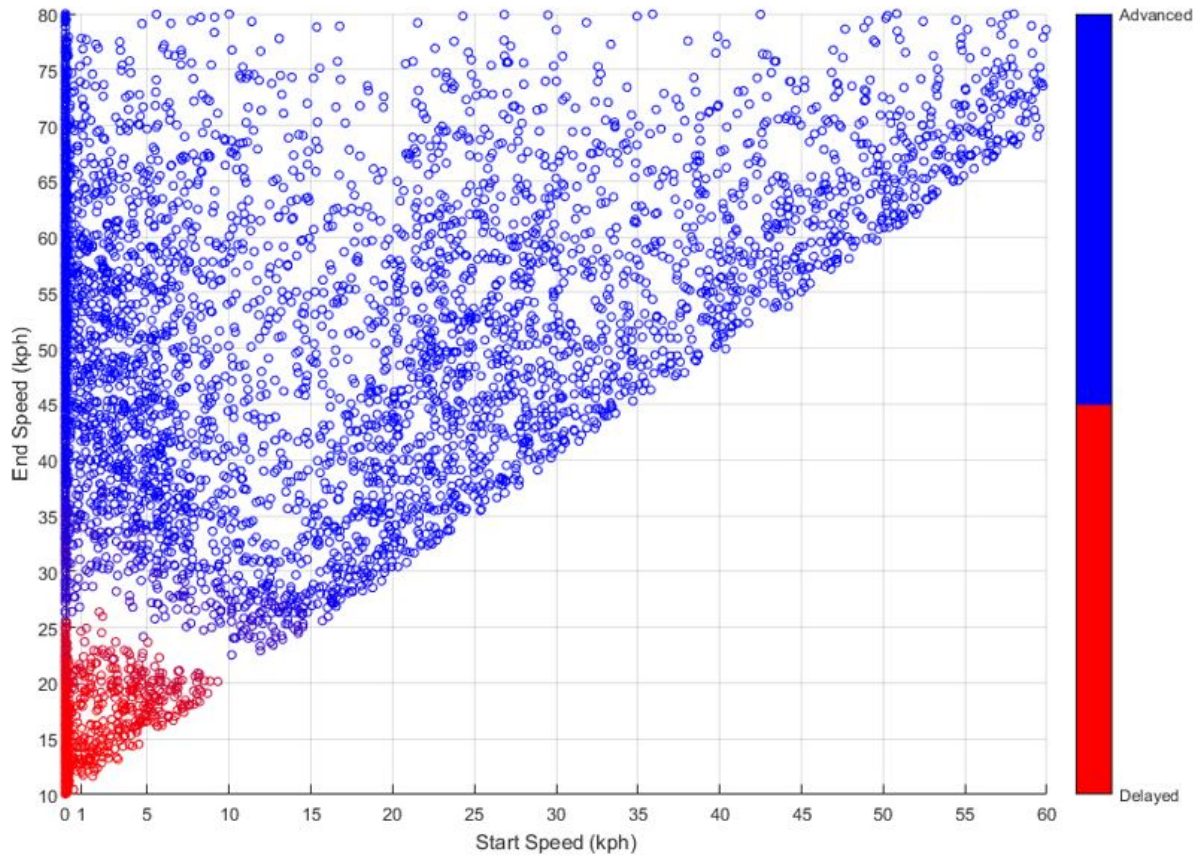
Figure 4.8: Actual AE control types on grid corresponding to velocity categories
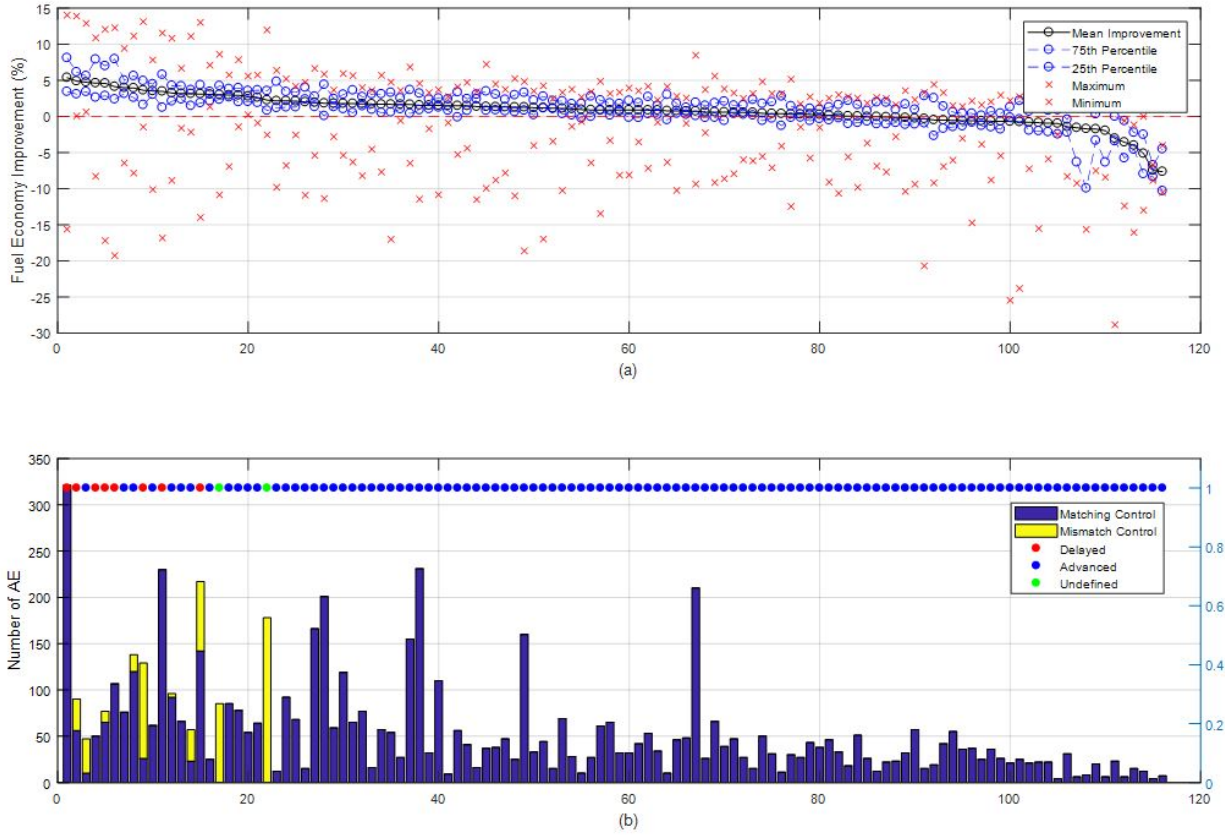
Figure 4.9: Control type mismatch and FE improvement for velocity categories

Figure 4.9a replicates Figure 4.5b, additionally depicting maximum and minimum FE improvement for each category. Again, horizontal axis points correspond vertically between the plots. Figure 4.9b is a stacked bar graph showing the number of AEs in each category, with blue bar segments representing AEs whose optimal control type matches the applied control type, and yellow segments representing AEs whose optimal control type does not match the type applied. The dot above each bar indicates the applied control type for the category.

Since Delayed control is applied to low-velocity AEs, there is further evidence that the greatest FE improvements are achieved for low-velocity AEs: all of the red dots are on the left end of the plot. There is also more evidence that the worst-performing categories are the least populated: all of the categories toward the right end of the plot contain fewer than 50 AEs, whereas all but two of the 20 best-performing categories have more than 50 AEs. Since every case of control type

mismatch cases occurs in one of the 23 best-performing categories, there is no evidence in Figure 4.9 to support the hypothesis that control type mismatch is a primary cause of FE reduction.

4.2.2 Investigate Prediction Error

Prediction error, or the difference between expected and actual $v(t)$, is hypothesized to be the primary cause of FE reduction. Prediction error in v_f and v_i are constrained by the categorization, whereas error in AE duration is not, so in this section prediction error refers specifically to duration prediction error. Figure 4.10 plots duration prediction error against FE improvement and SOC_f error.
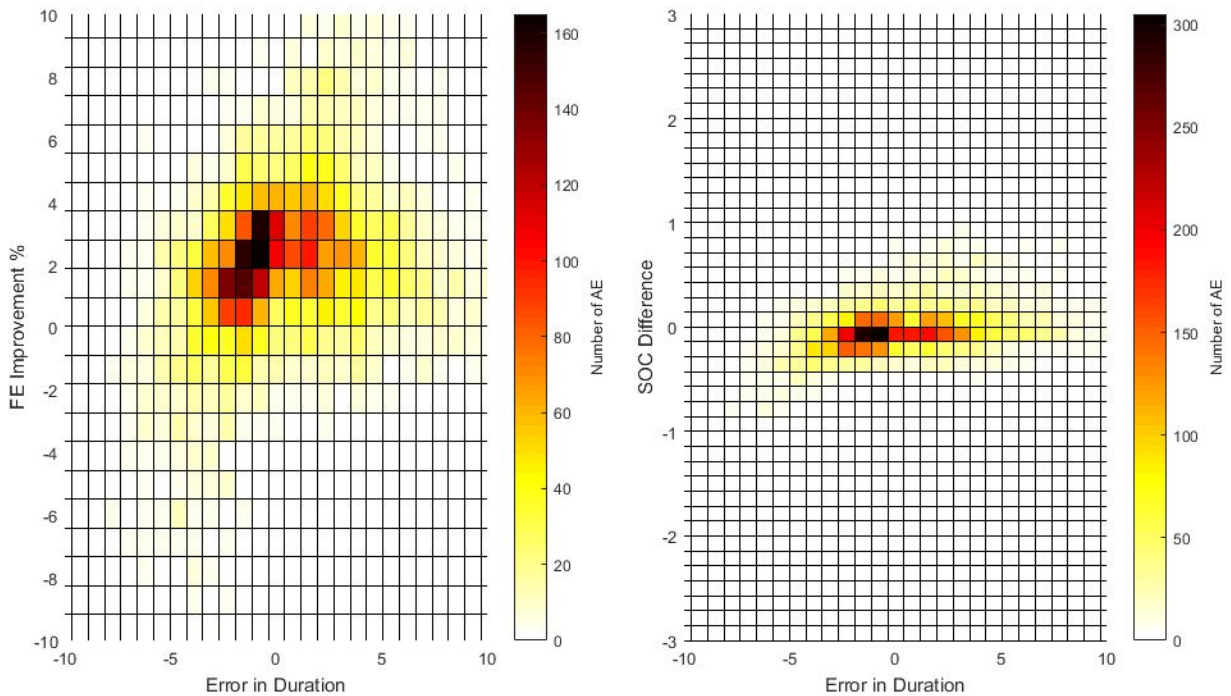
Figure 4.10: Duration prediction error, FE improvement, and SOC_f error for velocity categories

Here, the prediction error is defined as the actual duration minus the expected duration, so, for example, a duration error of -5 seconds means the actual AE is 5 seconds shorter than the expected AE, or, the AE duration was overestimated by 5 seconds. FE reductions occur more commonly as prediction error increases in the negative direction, whereas positive duration errors do not seem

to cause significant FE reductions. Negative prediction error also associates with greater SOC errors. Overall, there is evidence to suggest that *overestimating* the actual AE duration has a more detrimental effect than *underestimating* actual AE duration.

4.2.3   Adjust Category Sizes

Since AEs in well-populated categories tend to have greater FE improvement on average, categorizing more coarsely to increase average category population could improve FE results. However, prediction error, in terms of duration and in terms of v_f and v_i, increases with coarser categorizations, which may be detrimental to FE results. In this section, the FE improvement results for coarser and finer categorizations are obtained and analyzed, as summarized in Table 4.3.

Table 4.3: Finer and coarser categorizations by velocity

Attributes Used	Initial Velocity	Final Velocity
Number of Bins	1-200	1-200
Expected AE Selection	Duration	

Figure 4.11 is a representation of the different schemes that were simulated. Figure 4.11a shows the bin counts for v_f and v_i that define each scheme, Figure 4.11b shows the mean, 25th, and 75th percentiles of FE improvement for each scheme (inclusive of all categories), and Figure 4.11c shows the frequency of matching and mismatched control type. Schemes are sorted by decreasing final velocity bin counts from left to right.
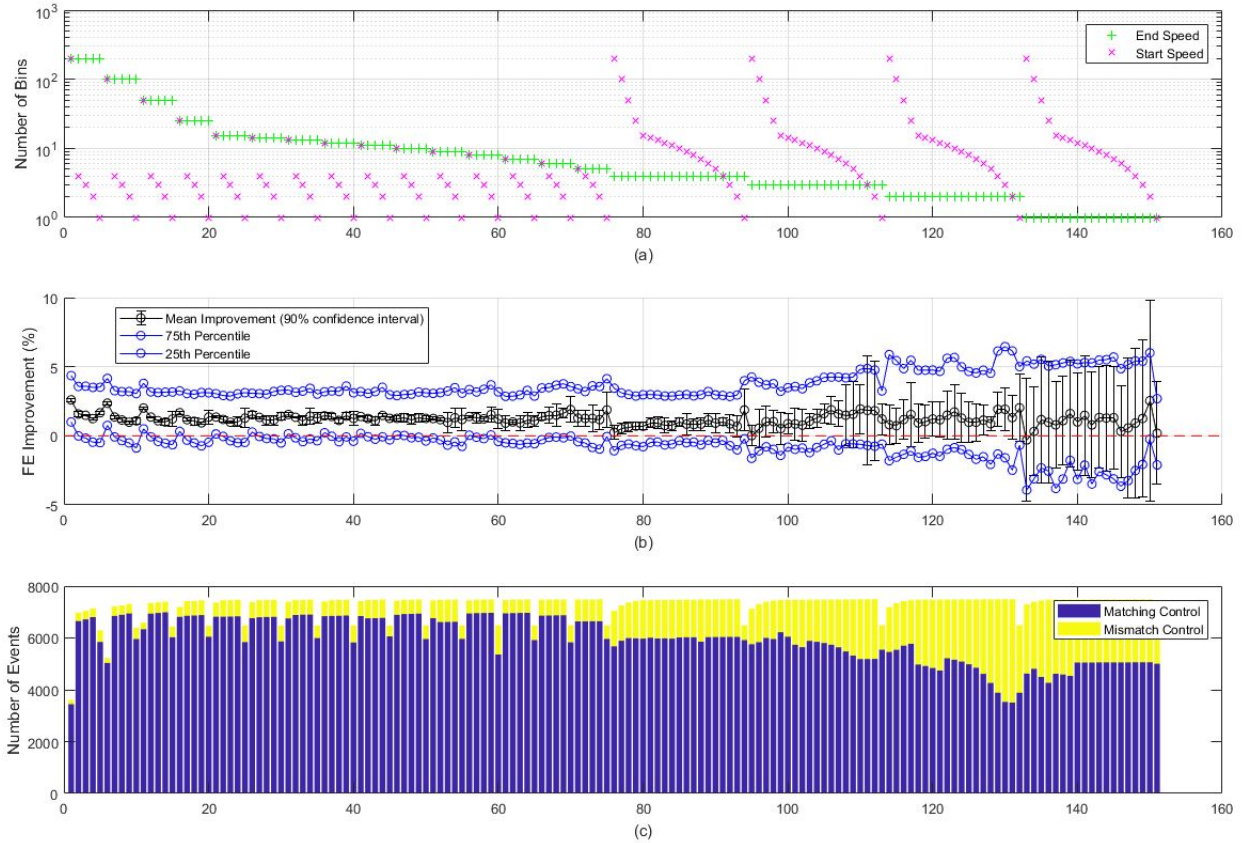
Figure 4.11: FE results for finer and coarser velocity categorizations

With more categories, mean FE improvement is greater, likely because finer categorization resolutions admit smaller prediction errors. But, with extremely fine categorization schemes such as the 200×200 categorization, categories are so sparsely populated that many are occupied by one or fewer AEs. Categories with just one AE have one expected AE and zero actual AEs, so FE improvement results cannot be obtained. This is why the total number of AEs in the fine categorizations, as shown in Figure 4.11c, is significantly less than the size of the dataset (7725 AEs). This suggests that the results are limited by the AE dataset: with an infinite AE dataset, an infinitely fine categorization would be expected to approach the FE achievable with exact prediction.

Bin counts for initial velocity and final velocity do not have symmetric effects. For example, with 1 v_i bin and 200 v_f bins, the mean FE improvement is approximately 2% with a tight confidence interval on the mean, and the range between the 25th and 75th percentile is about 4%. In

43

the opposite scheme, with 200 v_i bins and 1 v_f bin, the mean FE improvement is negative with an extremely wide confidence interval, and the range between the 25th and 75th percentiles is nearly 10%. This trend holds with different categorizations, suggesting that constraining error in v_f is more important than constraining error in v_i for achieving reliable FE improvement.

In application, the size of the AE dataset and the number of expected AEs that can be stored onboard a vehicle are limited. The results in Figure 4.11 suggest that FE improvement is nearly equivalent for any scheme with 10 or more v_f bins, such as the 13×12 categorization scheme investigated earlier in the section.

4.3 Categorize Using Other Attributes

As discussed in the previous section, the primary goal of a categorization scheme is to constrain prediction error in order to match the expected and actual $v(t)$ as closely as possible. It is possible that constraining error in attributes other than v_i may enable greater or more reliable FE improvements. To investigate this, two other categorization schemes, utilizing duration $t_f - t_i$ and average acceleration rate $\frac{v_f - v_i}{t_f - t_i}$ in combination with v_f, are studied (details in Appendix C).

The major conclusions of Section 4.2 are supported by the results in Appendix C. The most reliable FE improvements are achieved in categories containing AEs with low speeds, long durations, and low acceleration rates, irrespective of control type mismatch (Figures C.6 and C.14). Averaged over all categories, the FE improvement for the best categorization schemes is between 1 and 2% regardless of the categorization attributes. Categorizing based on duration enables slightly greater FE improvements on average (Figure C.8), but categorizing based on acceleration rate enables a slightly smaller range of FE improvements (Figure C.16. An upper limit on average FE improvement appears to be achieved for 10×10 (or even slightly coarser) schemes, regardless of categorization attributes.

4.4 Conclusions

In this chapter, the FE results of applying Optimal EMS control via a variety of categorization methods were analyzed. This chapter primarily addresses Research Question #2:

2. *What FE tradeoffs occur when prediction accuracy is reduced from exact velocity trace prediction to prediction of basic AE attributes?*

Prediction accuracy was varied by adjusting the attributes and resolutions with which categories are defined, and the FE results were compared with baseline FE results. Key conclusions are listed below.

4.4.1 AE Factors Influencing FE Results

- The greatest and most reliable FE improvements are achieved for low speed, long duration, and low acceleration rate AEs, regardless of category scheme. FE reductions tend to occur during high-aggression AEs, which are characterized by high speeds, short durations, and high acceleration rates.

- FE improvements are more reliably achieved when the actual AE duration is equal to or longer than the expected AE duration.

- On average, categories for which the Expected AE Optimal EMS is of the Delayed control type achieve greater FE improvements than those with Advanced control type, regardless of category scheme.

- Mismatch of control type between the expected and actual AE does not correlate with losses to FE.

4.4.2 Categorization Factors Influencing FE Results

- Prediction error of final velocity must be constrained via categorization to achieve consistent FE improvements.

- Constraints on initial velocity error, duration, and average acceleration are less impactful than constraints on final velocity error, but constraining one *in addition* to final velocity error can improve FE results.

- Average FE improvement increases with increasing categorization resolution, but reaches a reasonable upper limit when each attribute is divided into 10 bins.

- The poorest average FE improvement occurs in sparsely populated categories.

The results in this chapter suggest that a 13×14 categorization scheme based on v_f and v_i approaches a reasonable upper limit on average FE improvement. In the next chapter, Expected AE Optimal EMS utilizing this categorization scheme is applied to drive cycles.

Chapter 5

Implement Optimal EMS in Drive Cycles

In Chapter 4, Optimal EMS were applied to AEs in isolation. In this chapter, the categorization method of Chapter 4 is applied to AEs in the context of drive cycles.

The four control strategies introduced in Chapter 2 are applied to seven drive cycles of various types, as shown in Tables 5.1a and b. The Baseline EMS achieves the FE upon which FE improvement is defined, utilizing no prediction. The Approximate AE Optimal EMS applies an expected Optimal EMS from the corresponding category based on simulated predictions of v_f and v_i. (The Approximate AE Optimal EMS is also referred to as the Disturbed AE Optimal EMS, referring to prediction error as a "disturbance" to the system.) The Optimal AE and Optimal Cycle control strategies utilize the exact velocity trace $v(t)$ to derive and implement Optimal EMS during AEs and throughout the drive cycle, respectively.

Table 5.1: Drive cycles and control strategies investigated in Chapter 5

Cycle Type	Cycle Name
City	NYCC
	Denver Downtown
	Fort Collins Downtown
Highway	HWFET
	Denver Highway
	Fort Collins Highway
Aggressive	US06

(a)

Prediction Type	Control Used	
	During AE	Not During AE
None	Baseline	Baseline
Approximate/ Disturbed AE	Expected Optimal	Baseline
Exact AE	Exact Optimal	Baseline
Exact Cycle	Exact Optimal	Exact Optimal

(b)

The overall FE results for all seven cycles are shown in Table 5.2. Results for one cycle of each driving type (city, highway, and aggressive) is analyzed in detail in the main text, and results for the remaining cycles are in Appendix D.

Table 5.2: Results for all drive cycles and control strategies

Drive Cycle	Baseline FE (mpg)	Approximate AE FE (mpg)	Optimal AE FE (mpg)	Optimal Cycle FE (mpg)
US06	40.60	40.13	40.82	42.19
		-1.16%	0.54%	3.91%
HWFET	61.08	61.39	61.60	64.15
		0.50%	0.84%	5.01%
NYCC	37.90	39.38	39.81	42.10
		3.92%	5.06%	11.10%
Denver Downtown	65.94	67.56	68.33	75.90
		2.46%	3.63%	15.12%
Denver Highway	71.22	72.68	72.90	77.17
		2.05%	2.37%	8.36%
Fort Collins Downtown	62.19	63.53	64.19	66.54
		2.16%	3.22%	6.99%
Fort Collins Highway	50.52	50.65	50.90	53.84
		0.26%	0.75%	6.58%

5.1 Evaluate Individual AEs in Cycles

As a measure of the effect an individual AE's control has on a drive cycle's overall FE, dFC, the net fuel consumption increase or reduction caused by the disturbed EMS is calculated:

$$d\text{FC} = \left(\text{FC}_{f,\text{Disturbed}} - \text{FC}_{f,\text{Baseline}}\right) - \left(\text{FC}_{i,\text{Disturbed}} - \text{FC}_{i,\text{Baseline}}\right) \tag{5.1}$$

Just as in Chapter 4, Disturbed EMS may result in a different SOC_f than Baseline EMS. To correct for this, the dFC metric is adjusted using a linear fit (Figure 5.1) on dFC versus dSOC for all cycle AE (Figure 5.1), where dSOC is defined as:

$$d\text{SOC} = \left(\text{SOC}_{f,\text{Disturbed}} - \text{SOC}_{f,\text{Baseline}}\right) - \left(\text{SOC}_{i,\text{Disturbed}} - \text{SOC}_{i,\text{Baseline}}\right) \tag{5.2}$$

Then,

$$dFC_{\text{corrected}} = dFC - m \, dSOC \tag{5.3}$$

where m is the slope of the fitline (3.406 $\frac{\text{mL}}{\%\text{SOC}}$). Finally, dFC is converted to fuel consumption per distance traveled during the AE (L/100km). (Calculating dFC^{-1} and converting units would theoretically result in a measure of FE, but in practice results in extremely large numbers due to rounding error and near-zero division.)

$$dFC_{\text{normalized}} = \frac{dFC_{\text{corrected}}}{\text{distance}} \tag{5.4}$$
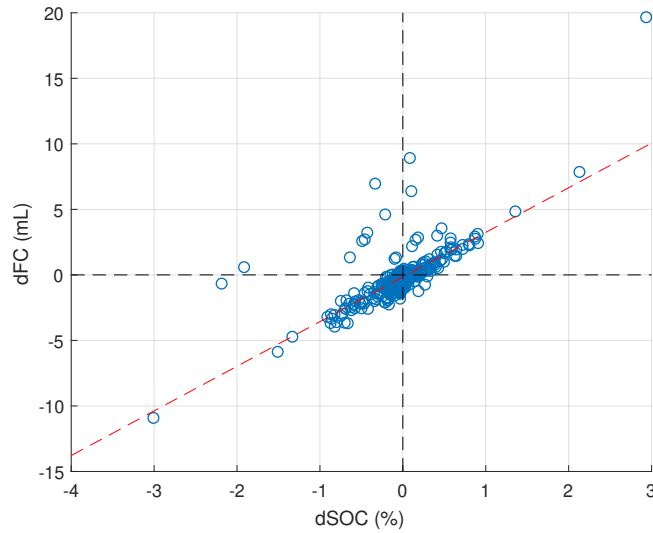

Figure 5.1: Linear fit of dFC and $dSOC$ for all cycle AEs

5.2 Individual Cycle Results

5.2.1 City Driving Cycle: NYCC

In simulations of city driving, FE improvement potential is high for both Optimal Cycle and Optimal AE control, and Approximate AE FE is nearly as high as Optimal AE FE. Most likely as a

result of the low-aggression driving common to these cycles, effective fuel consumption reduction is achieved in the vast majority of AEs, leading to high FE gains.

The New York City Cycle (NYCC) is a standard EPA test schedule meant to simulate low speed urban driving. It includes many low-aggression AEs, frequent stops, and almost no cruising. With an average speed of 11.4 kph, it is more than twice as slow as the next-slowest cycle studied. In previous sections, it was found that significant and reliable FE improvements are achieved for low-aggression AEs, which is true here: the greatest Approximate AE and Optimal AE FE improvements of all the cycles are achieved for the NYCC.

A variety of characteristics and results for the NYCC are listed in Table 5.3; the simulated FE results are plotted in Figure 5.2; selected simulation outputs are plotted in Figure 5.3; and results for individual AEs are given in Table 5.4.

Table 5.3: Characteristics of the NYCC cycle

Drive Cycle	Duration (sec)	Distance (km)	Average Speed (kph)	Max Speed (kph)	#AE	Time %AE	Baseline FE (mpg)	Approximate AE FE (mpg)	Optimal AE FE (mpg)	Optimal Cycle FE (mpg)
NYCC	598	1.9	11.4	44.6	13	24.8%	37.90	39.38	39.81	42.10
								3.92%	5.06%	11.10%
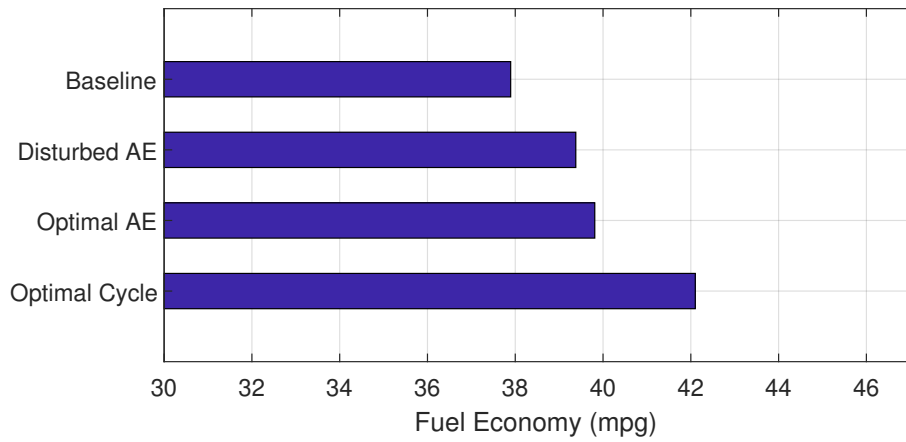
(a) NYCC cycle FE results
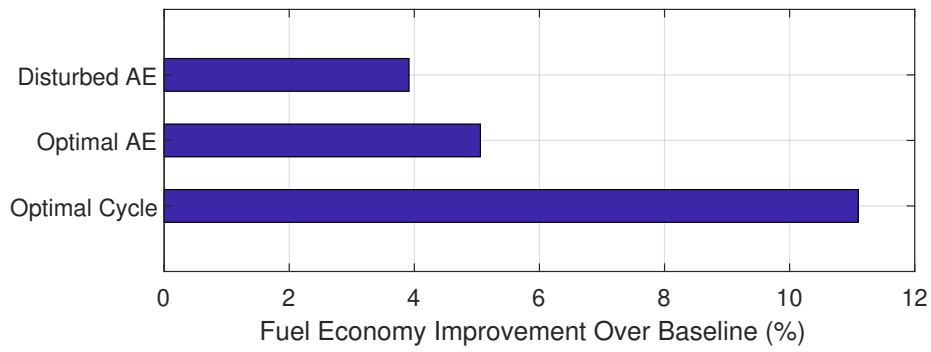
(b) NYCC cycle FE improvement results

Figure 5.2: FE results for NYCC cycle

Figure 5.3: Simulation outputs for the NYCC cycle

Table 5.4: Characteristics of AEs in the NYCC cycle

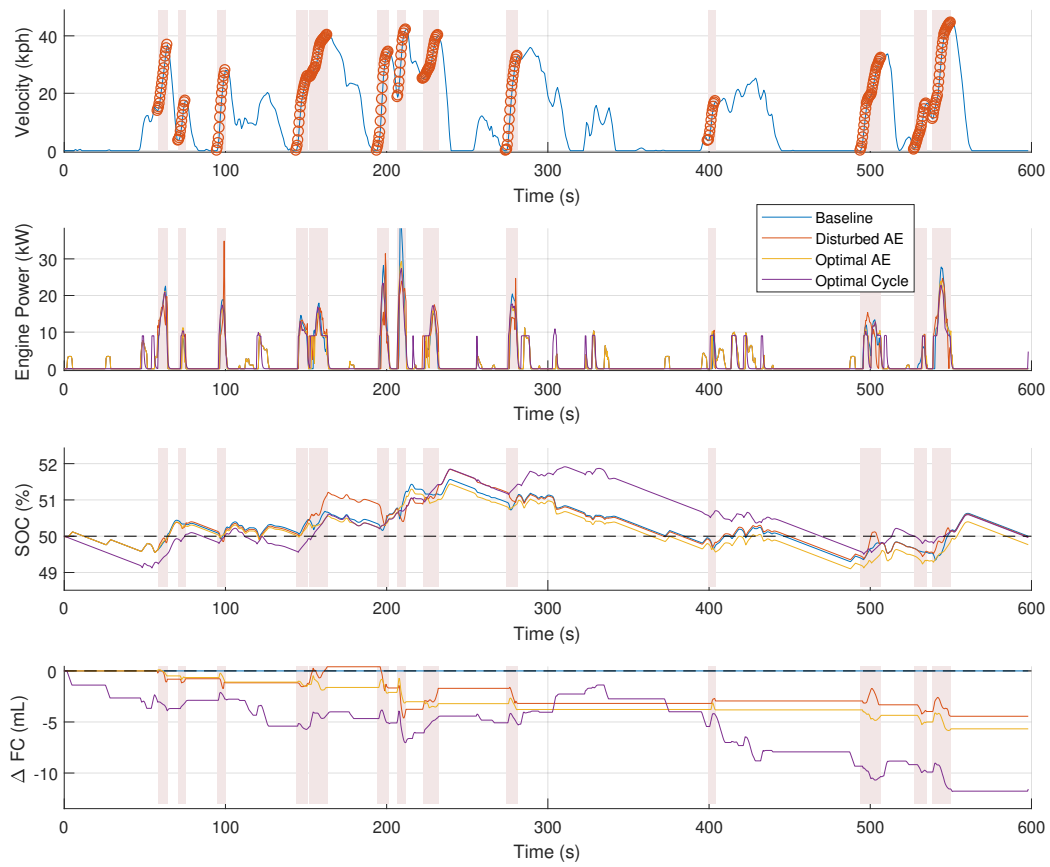|		Initial Speed (kph)	Final Speed (kph)	Duration (s)	# AE in Category	Optimal Control	Disturbed Control	dFC (mL)	dSOC (%)	dFC corrected (mL)	dFC normalized (mL/100km)
						NYCC					
AE #	1	13.8	36.9	6.4	32	Advance	Advance	-0.60	-0.12	-0.18	-41.61
	2	3.5	17.4	4.8	107	Delay	Delay	0.04	0.03	-0.07	-54.64
	3	0.0	28.0	5.6	178	Delay	Delay	-0.40	-0.09	-0.10	-45.35
	4	0.0	26.0	7.6	178	Delay	Advance	-0.05	0.02	-0.13	-39.23
	5	25.6	40.3	11.6	65	Delay	Advance	1.62	0.51	-0.13	-12.08
	6	0.0	34.4	7.6	138	Delay	Delay	-2.08	-0.57	-0.15	-37.35
	7	18.6	42.2	5.6	43	Advance	Advance	-2.09	-0.48	-0.47	-96.27
	8	25.1	40.2	10.0	65	Delay	Advance	2.05	0.59	0.06	6.89
	9	0.0	33.0	7.6	138	Delay	Delay	-1.48	-0.31	-0.43	-117.31
	10	3.4	17.2	5.2	107	Delay	Delay	0.24	0.13	-0.19	-132.35
	11	0.0	32.3	13.2	138	Delay	Advance	-0.38	-0.06	-0.16	-22.64
	12	0.4	16.4	8.0	230	Delay	Delay	-0.66	0.04	-0.79	-471.84
	13	11.0	44.6	11.6	25	Advance	Advance	-0.46	-0.04	-0.32	-32.61

The Disturbed Optimal EMS achieves a significant portion (77%) of the FE improvement achieved by Optimal AE control and 35% of the FE improvement achieved by Optimal Cycle control. With the exception of some instances of high engine power for SOC correction, the Disturbed engine power trace appears to follow the Optimal AE engine power trace closely, indicating that the categorization scheme sufficiently limits prediction error to provide a close match between the Expected and Actual Optimal EMS.

The results for this cycle illustrate how apparent increases to fuel consumption, like in AEs #5 and #8, can result in increases to SOC that allow significant fuel consumption reductions later in the cycle. From Table 5.4, four AEs have positive dFC, which might seem to apply that prediction error is causing a reduction to cycle FE during those AEs. However, only one (AE #8) has a positive SOC-corrected dFC, so the net result of Disturbed Optimal EMS is a significant improvement to cycle FE.

5.2.2 Other City Driving Cycles

Two other cycles with city driving are simulated. The Denver Downtown and Fort Collins Downtown drive cycles were measured from real-world driving. The simulation results are in

Appendix D. Although FE improvements achieved by Disturbed EMS along the other city driving cycles are smaller than for the NYCC cycle, they are the next two greatest among all cycles studied.

5.2.3   Highway Driving Cycle: HWFET

FE improvement potential via AE Optimal EMS in highway driving is typically much lower than in city driving, since AEs reach higher speeds and are less frequent, with cruising dominating the cycle. Despite the low improvement potential, positive FE improvement is achieved in all highway cycles.

The HWFET (Highway Fuel Economy Test) cycle is the standard EPA highway test schedule. It is mostly high-speed cruising and involves only 4 AEs which account for only 10% of driving time. Room for FE improvement is therefore small when EMS are confined to AE windows, but a significant portion of the potential FE improvement is still achieved via Disturbed EMS control. A variety of characteristics of the HWFET cycle are listed in Table 5.5; the simulated FE results are plotted in Figure 5.4; selected simulation outputs are plotted in Figure 5.5; and results for individual AEs are given in Table 5.6.

Table 5.5: Characteristics of the HWFET cycle

Drive Cycle	Duration (sec)	Distance (km)	Average Speed (kph)	Max Speed (kph)	#AE	Time %AE	Baseline FE (mpg)	Approximate AE FE (mpg)	Optimal AE FE (mpg)	Optimal Cycle FE (mpg)
HWFET	764	16.5	77.8	96.4	4	10.0%	61.08	61.39	61.60	64.15
								0.50%	0.84%	5.01%
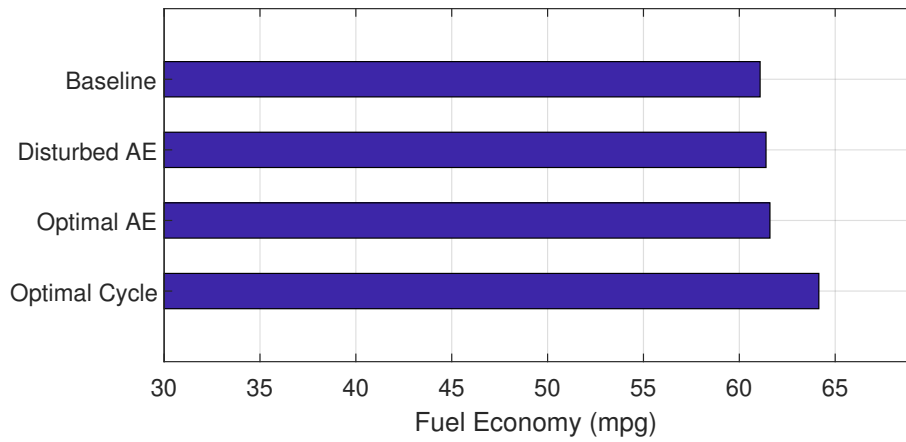
(a) HWFET cycle FE results
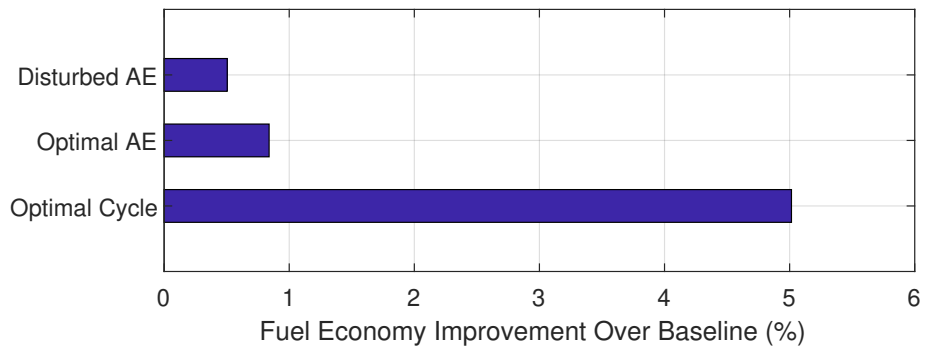
(b) HWFET cycle FE improvement results

Figure 5.4: FE results for HWFET cycle
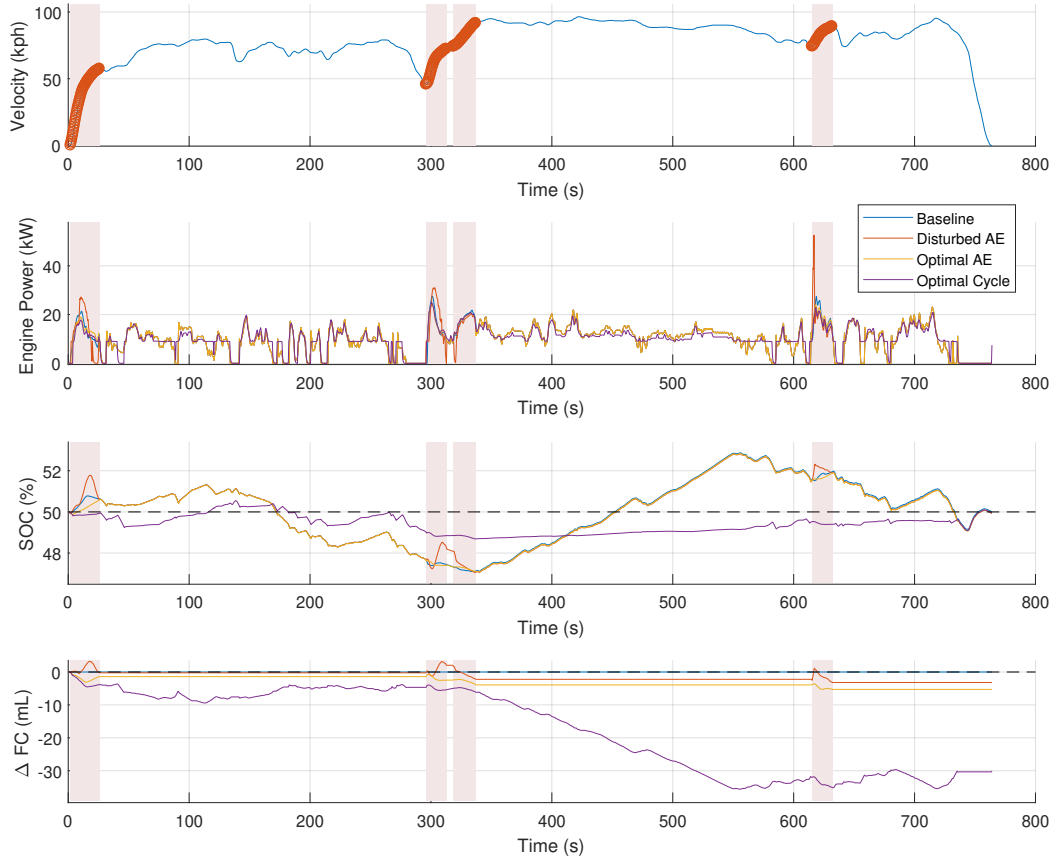
Figure 5.5: Simulation outputs for the HWFET cycle

Table 5.6: Characteristics of AEs in the HWFET cycle

		Initial Speed (kph)	Final Speed (kph)	Duration (s)	# AE in Category	Optimal Control	Disturbed Control	dFC (mL)	dSOC (%)	dFC corrected (mL)	dFC normalized (mL/100km)
		HWFET									
AE #	1	0.0	57.5	24.4	231	Delay	Advance	-0.08	-0.03	0.00	0.07
	2	45.7	72.3	17.2	23	Advance	Advance	2.29	0.80	-0.45	-15.46
	3	74.1	91.6	19.2	18	Advance	Delay	-4.00	-0.81	-1.23	-28.55
	4	74.2	89.2	17.2	18	Advance	Advance	-0.65	0.00	-0.65	-16.64

The Disturbed EMS achieves 60% of the FE improvement achieved by Optimal AE control and 10% of the FE improvement achieved by Optimal Cycle control. The Disturbed EMS engine

power trace deviates visibly from the Optimal EMS engine power trace, running at higher power earlier in each AE than any other control strategy.

5.2.4   Other Highway Driving Cycles

Two other cycles with highway driving are simulated. The Denver Highway and Fort Collins Highway drive cycles were measured from real-world driving. The simulation results are in Appendix D. The results for the Fort Collins Highway cycle are similar to the results for the HWFET cycle, where the AE Optimal EMS achieves a small FE improvement (less than 1%), of which the Disturbed EMS achieves a portion. The Denver Highway cycle has greater FE improvement potential than the other highway cycles because it includes both highway and city driving.

5.2.5   Aggressive Driving Cycle: US06

The US06 cycle is the aggressive EPA test schedule, characterized by high-speed driving, fast accelerations, and an extended high-speed cruising period in the middle. More than half of the AEs have final velocities greater than the highest-speed v_f category, so the expected AE is often of significantly lower speed than the actual cycle AE. With so much driving beyond the boundaries of the dataset and a great deal of cruising, the US06 cycle has the least room for improvement of any cycle, during AEs or otherwise, and is the only cycle for which FE improvement is not achieved with Disturbed Optimal EMS control. A variety of characteristics of the US06 cycle are listed in Table 5.7; the simulated FE results are given in Figure 5.6; selected simulation outputs are plotted in Figure 5.7; and results for individual AEs are given in Table 5.8.

Table 5.7: Characteristics of the US06 cycle

Drive Cycle	Duration (sec)	Distance (km)	Average Speed (kph)	Max Speed (kph)	#AE	Time %AE	Baseline FE (mpg)	Approximate AE FE (mpg)	Optimal AE FE (mpg)	Optimal Cycle FE (mpg)
US06	600	12.9	77.3	129.2	12	26.6%	40.60	40.13	40.82	42.19
								-1.16%	0.54%	3.91%

(a) US06 cycle FE results

(b) US06 cycle FE improvement results

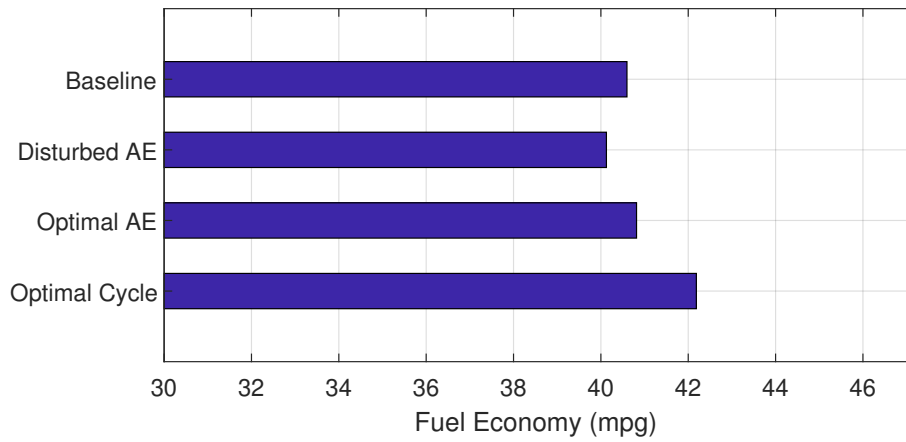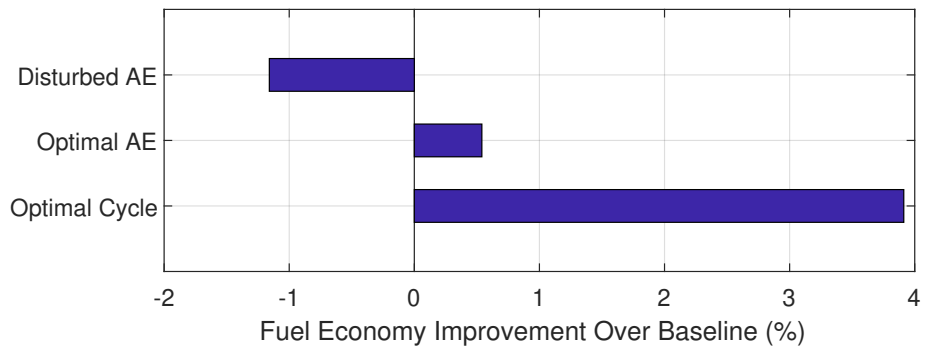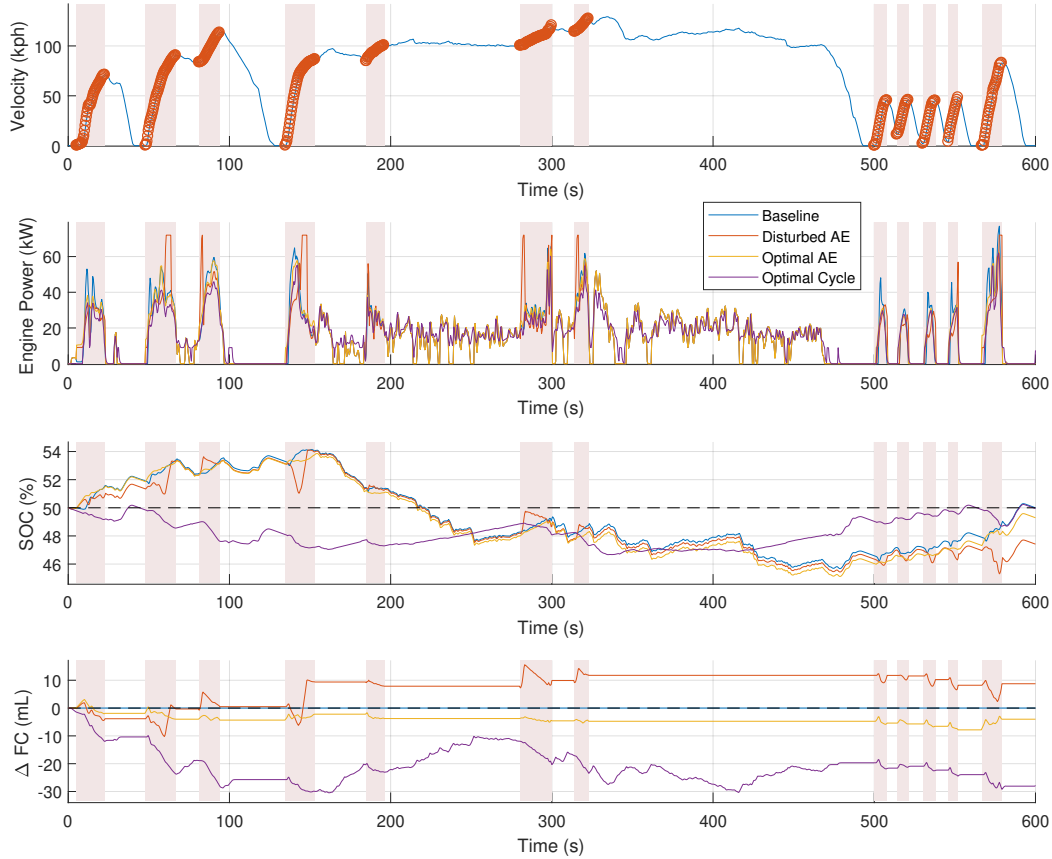**Figure 5.6:** FE results for US06 cycle

Figure 5.7: Simulation outputs for the US06 cycle

Table 5.8: Characteristics of AEs in the US06 cycle

		Initial Speed (kph)	Final Speed (kph)	Duration (s)	# AE in Category	Optimal Control	Disturbed Control	dFC (mL)	dSOC (%)	dFC corrected (mL)	dFC normalized (mL/100km)
						US06					
	1	0.1	71.0	18.0	110	Advance	Advance	-3.74	-0.66	-1.50	-81.44
	2	0.0	90.5	19.2	54	Advance	Advance	3.50	0.47	1.89	63.39
	3	83.6	113.3	13.2	18	Advance	Advance	1.28	-0.07	1.53	44.35
	4	0.0	86.6	18.8	54	Advance	Advance	8.87	0.09	8.55	275.87
	5	84.8	100.6	11.6	18	Advance	Advance	-1.28	-0.04	-1.15	-39.31
AE #	6	100.2	120.5	20.0	18	Advance	Advance	2.66	-0.45	4.19	71.42
	7	114.3	127.3	9.2	18	Advance	Advance	2.63	0.16	2.08	70.74
	8	0.0	45.4	8.4	166	Delay	Delay	-0.02	-0.11	0.37	66.30
	9	11.1	45.8	7.6	27	Advance	Delay	-0.20	-0.19	0.46	76.76
	10	1.9	45.1	8.4	85	Delay	Delay	-1.29	-0.42	0.14	22.86
	11	3.9	48.3	6.4	85	Advance	Advance	-2.04	-0.74	0.48	97.28
	12	0.0	82.9	12.8	54	Advance	Advance	0.54	-1.91	7.03	456.56

59

Disturbed EMS control achieves a lower FE than the Baseline EMS. dFC improvement is achieved in only 2 of 12 AE, indicating that the Disturbed EMS is poorly equipped to control AE this aggressive.

AE #4 is the most unsuccessful application of Disturbed EMS control for any AE in any cycle simulated. Simulation outputs for this AE are given in Figure 5.8. The Disturbed EMS underestimates the required engine power and discharges the battery during the first half of the AE, likely because it "expects" the AE to end soon and at a speed lower than 80 kph. Since the second half of the AE is a gradual acceleration at high speed, the AE effectively lasts about 10 seconds longer than the Disturbed EMS expects it to, and since it must make up for the large SOC deficit from the first half, it runs the engine at maximum power for 3 full seconds. As a result, a significant amount of fuel is consumed at low engine efficiency and is clearly a worst-case example for Disturbed control.
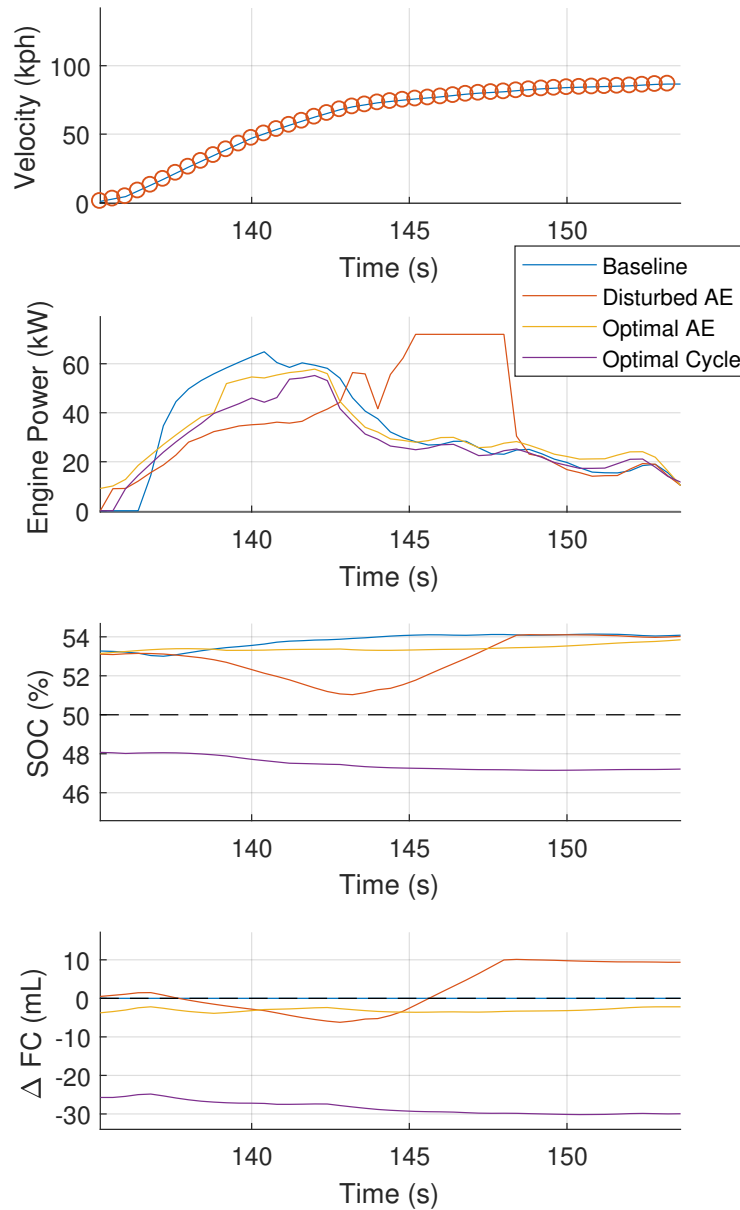
Figure 5.8: AE #4 from the US06 cycle, the worst-performing AE of any cycle

Since AEs in the US06 cycle are faster than the fastest AEs in the dataset, the US06 cycle is a poor example for Disturbed Optimal EMS application. In practice, the Disturbed Optimal EMS may be turned off by default during high-speed and high-aggression driving. To simulate this, both

the cruising section and the outlier AEs were removed from the US06 cycle and the simulation was repeated. The FE results are shown in Figure 5.9 and outputs of the simulation are plotted in Figure 5.10. With this truncation, the Disturbed EMS achieves 72% of Optimal AE FE improvement and 61% of Optimal Cycle FE improvement.
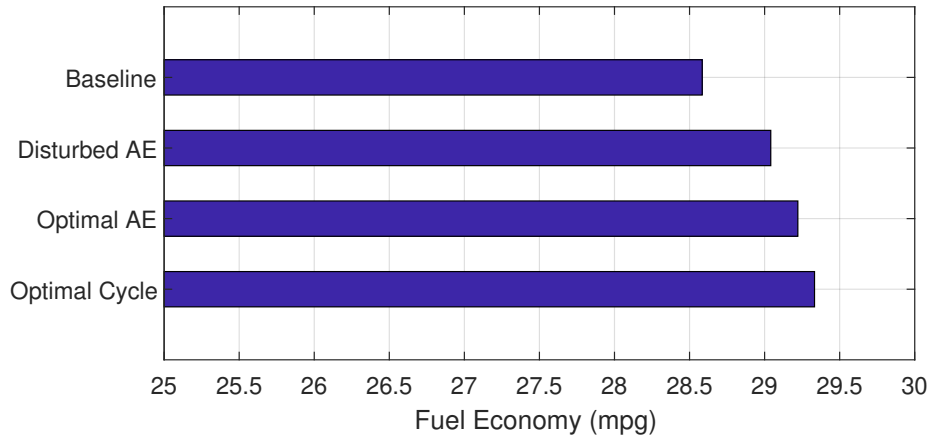
(a) Truncated US06 cycle FE results
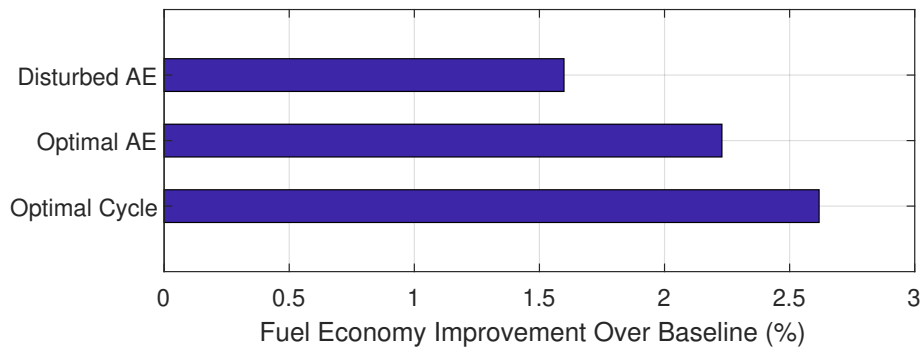
(b) Truncated US06 cycle FE improvement results

Figure 5.9: FE results for truncated US06 cycle
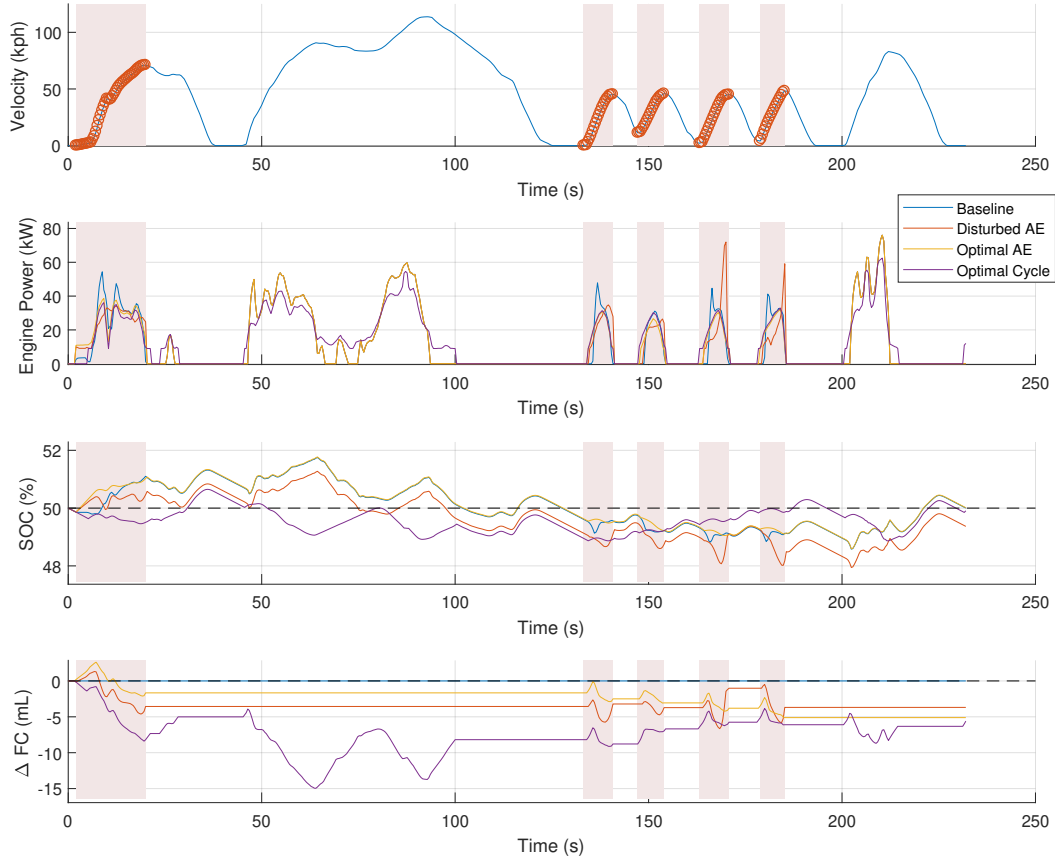
Figure 5.10: Simulation outputs for the truncated US06 cycle

5.3 General Results

The FE results for all seven cycles, sorted in order of increasing Disturbed EMS FE improvement are given in Figure 5.11. The cycle on which the Disturbed EMS is least successful is US06, the aggressive cycle; the next three are the highway cycles; and the cycles with the greatest Disturbed EMS performance are the city cycles. This is one indication that Disturbed EMS control is most successful in city driving and less successful with increasing aggressiveness.
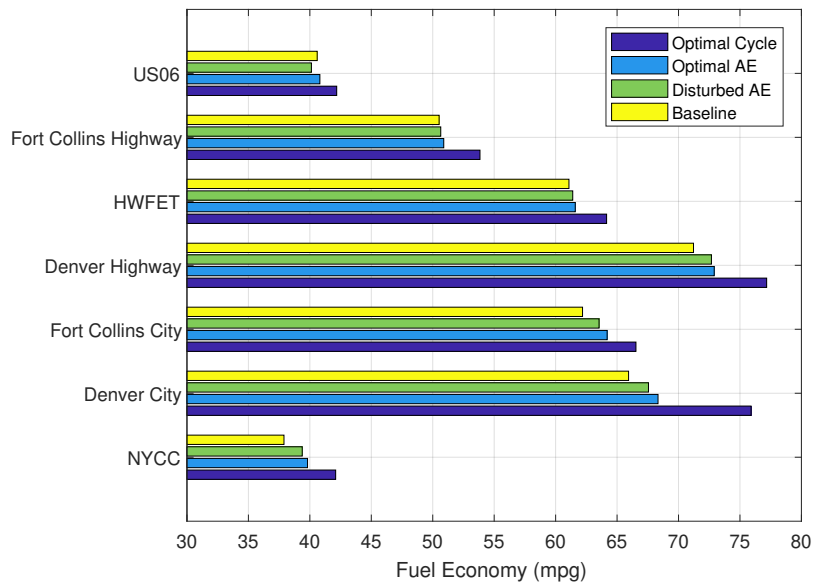
(a) FE for all cycles for all control strategies
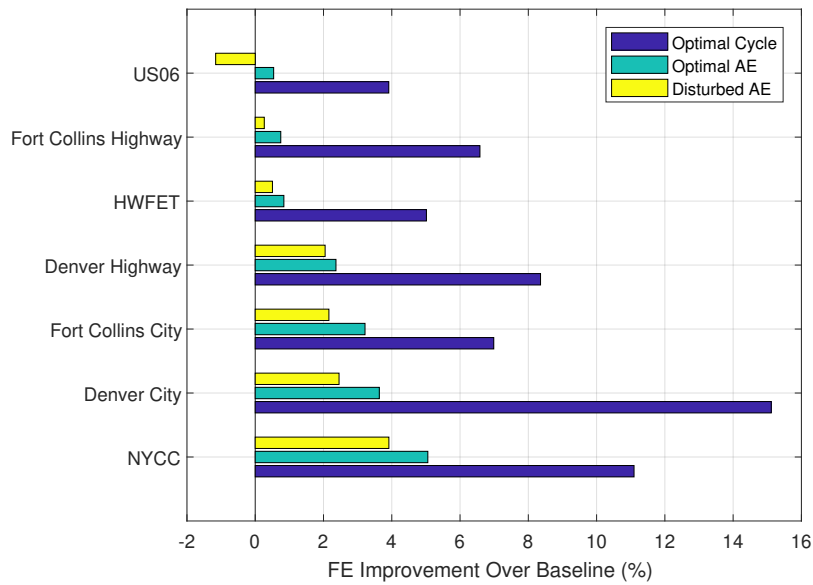
(b) Improvement over baseline for each control strategy

Figure 5.11: FE results for all seven cycles

5.3.1 AE Factors Influencing FE Results

To understand how AE attributes correlate with FE results, initial and final velocity (Figure 5.12) and speed increase and average acceleration (Figure 5.13) are plotted against normalized dFC.
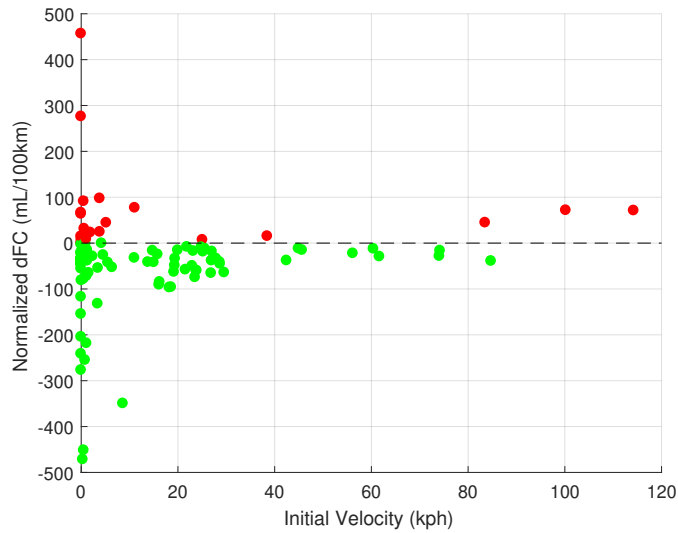
(a) Initial velocity versus dFC for all cycle AEs
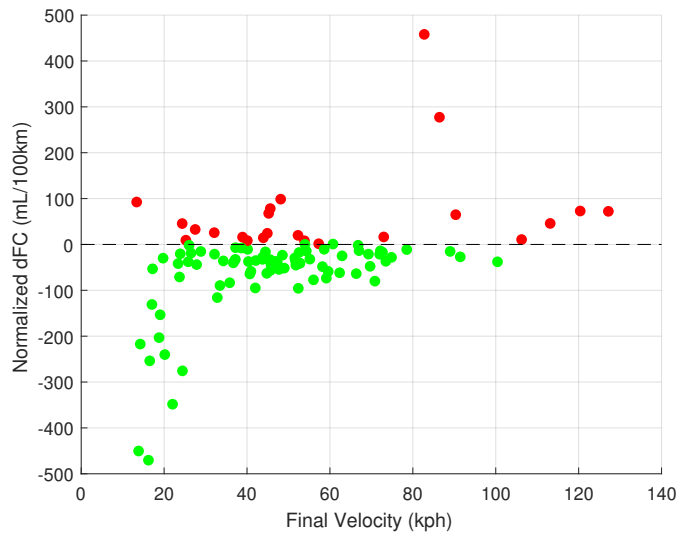
(b) Final velocity versus dFC for all cycle AEs

Figure 5.12: v_i and v_f versus dFC for all cycle AEs

The plots in Figure 5.12 reinforce that disturbed control is not well suited to AEs with high v_f. The greatest increases to normalized dFC all occur when v_i is near zero and v_f is greater than 80 kph, while the greatest and most frequent reductions to dFC occur when v_i and v_f are both low. dFC is never negative above a starting speed of 90 kph or an ending speed of 100 kph.

High aggression driving implies high speeds as well as fast accelerations. To understand how this affects FE, increase in velocity $v_f - v_i$ and average acceleration $\frac{v_f - v_i}{t_f - t_i}$ are plotted against normalized dFC (Figure 5.13).
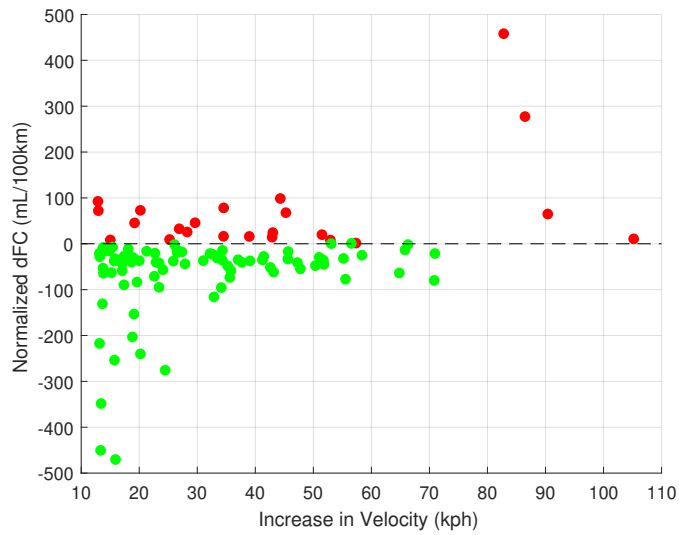
(a) Velocity increase versus *d*FC for all cycle AEs
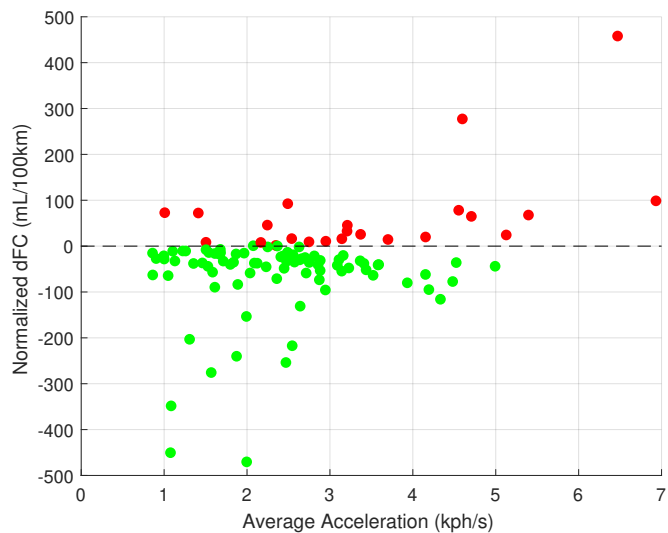
(b) Average acceleration versus *d*FC for all cycle AEs

Figure 5.13: Velocity increase and average acceleration versus *d*FC for all cycle AEs

Smaller velocity increases enable the greatest reductions to FC, while the greatest increases to FC occur for AEs during which velocity increases by the greatest amounts. This trend can also be seen when duration is taken into account: FC is never reduced when acceleration rate is greater than 5 kph/s, and almost never increased when acceleration rate is less than 2 kph/s.

As concluded in Chapter 4, FE performance is often poor for sparsely populated categories. In Figure 5.14 the number of AE in the category is plotted against dFC. As shown, the greatest FC reductions occur for the most populated categories, but increases to dFC occur for sparsely and densely populated categories alike.
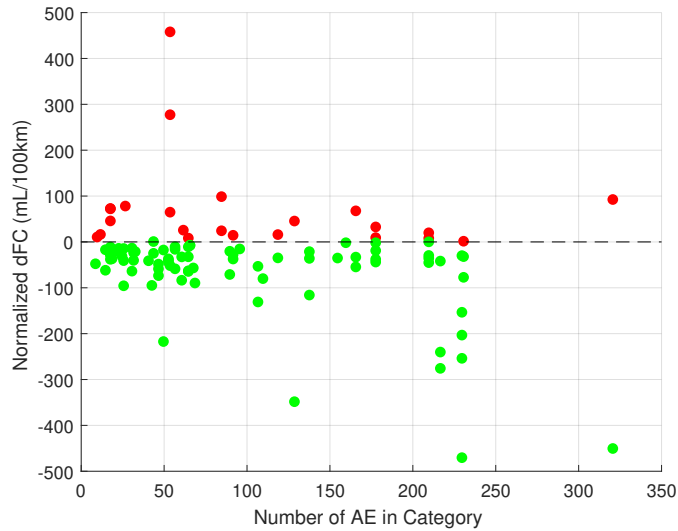
Figure 5.14: Category population versus dFC for all cycle AEs

In agreement with the conclusions of Chapter 4, FE improvements occur in cycles and locally among AE when the driving style is low-aggression. This may be explained in part because potential FE benefits are smaller for higher-aggression drive cycles. For the NYCC, the maximum FE improvement that can be achieved via AE control (i.e., by the Optimal AE EMS) is 5.06%, whereas for the US06 cycle it is 0.54%. This may also be because the AE dataset is not representative of the highest-aggression AEs seen in the drive cycles. A greater portion of the potential FE benefits may be achievable using a dataset that represents a wider variety of driving styles.

Control Type Mismatch

Chapter 3 introduced the hypothesis that applying the wrong control type (Delayed or Advanced) to AEs via Disturbed Optimal EMS causes reductions to FE. This misapplication is termed

"mismatch." In Chapter 4, it was found that none of the cases of mismatch occurred in any of the worst-performing categories.

To understand the effect of mismatch in cycles, every AE in every cycle was examined manually to identify the control types applied by the Optimal AE EMS and Disturbed AE EMS. Of 315 AEs, there were 67 occurrences of positive dFC (i.e., FE reduction) and 54 occurrences of mismatch, but only 7 occurrences of both, which may suggest that mismatch is not correlated with FE loss. The results of the mismatch characterization are shown in Table 5.9.

Table 5.9: Contingency table relating AE FC results to mismatch condition

		FC Reduced?		
		Yes	No	
Mismatch Condition?	No	201	60	261
	Yes	47	7	54
		248	67	315

Using the data in Table 5.9, Fisher's exact test of independence was performed. The null hypothesis for this test is that there are no nonrandom associations between the two categories (negative dFC and mismatch), so the null hypothesis must be rejected (p-value < 0.05) to be able to claim a significant association between mismatch and FE. The test results in a p-value of 0.1425, meaning the null hypothesis cannot be rejected. Therefore, control type mismatch is not significantly correlated with positive or negative FE effects.

5.4 Conclusions

In this chapter, the FE results of applying Disturbed Optimal EMS control to AEs in cycles were obtained and analyzed. The results of this chapter primarily concern Research Questions #2 and #3.

5.4.1 Research Question #2

2. *What FE tradeoffs occur when prediction accuracy is reduced from exact velocity trace prediction to prediction of basic AE attributes?*

The results in this chapter support conclusions from Chapter 4:

- (From Chapter 4): The greatest and most reliable FE improvements are achieved for low speed, long duration, and low acceleration rate AEs, regardless of category scheme. FE reductions tend to occur during high-aggression AEs, which are characterized by high speeds, short durations, and high acceleration rates.

  - The greatest cycle FE improvements are achieved for the city cycles, which are characterized by low-aggression driving.

  - As shown in Figures 5.12-5.13, with increasing final velocity, velocity increase, and average acceleration, the magnitude of FE loss increases.

- (From Chapter 4): Mismatch of control type between the expected and actual AE does not correlate with losses to FE.

  - This is further evidenced by the results of the Fisher test on the cycle AE set (Section 5.3.1)

- (From Chapter 4): The poorest average FE improvement occurs in sparsely populated categories.

  - As shown in Figure 5.14, the greatest FE losses occur during AEs in sparsely populated categories.

5.4.2 Research Question #3

3. *How can low-accuracy-prediction enabled EMS be applied to achieve consistent FE benefits in real driving contexts?*

- The methods introduced in Chapter 3 are used in this chapter to apply Disturbed AE EMS in cycles and evaluate the results. By accounting for the effects of over- and under-charging the battery on fuel consumption, it was shown that FE improvement can be achieved via Disturbed AE EMS despite local increases to FC during an AE.

- Following from the conclusions addressing RQ#2, Disturbed AE EMS are best applied to low-aggression AEs, which are common in city driving.

- Overall cycle FE improvement potential is limited in highway driving, since AEs are rare and, if they occur, are of high speed.

- The dataset containing expected AEs can limit the FE improvement potential of Disturbed AE Optimal EMS, as evidenced by the poor performance on the US06 cycle. Choosing not to apply the Disturbed AE Optimal EMS to AEs that are poorly represented by the dataset may be one way to enable robust FE improvements, as shown by the application to the truncated US06 cycle.

Chapter 6

Summary

This thesis presents an approach for applying Optimal EMS during AEs to improve FE that is implementable using hardware common on current production vehicles. Simulation methods were used to characterize the FE improvement potential with the approach and evaluate a variety of methods of EMS application.

In Chapter 2, the simulation tools required to investigate AE Optimal EMS, including a vehicle model and four Optimal EMS application methods, were defined.

In Chapter 3, attributes of AE velocity traces and corresponding Optimal EMS were analyzed via PCA and neural network classification. A variety of evidence was presented to support the hypothesis that initial and final velocity are significant attributes accounting for variation in the Optimal EMS. This improved confidence that AE prediction on the basis of initial and final velocity could enable near-optimal EMS.

In Chapter 4, a categorization approach for selecting EMS based on predictions of AE attributes was presented and evaluated. FE improvements averaging between 1 and 2% were demonstrated to be achievable for categorization schemes that include final AE velocity as one of the defining attributes and 10 or more bins of each defining attribute. The greatest FE improvements were demonstrated to occur during AEs with low speeds and accelerations, whereas FE reductions were more likely to occur during AEs with high speeds and accelerations.

In Chapter 5, EMS were applied to AEs in seven drive cycles via a categorization scheme from Chapter 4 based on initial and final AE velocity. FE improvement was achieved for all but the most aggressive drive cycle, with the greatest FE improvements being achieved in city driving. If the categorization method of application is applied only during low-aggression AEs, FE improvement is predicted to be significant and robust.

Efforts are well underway to implement this Optimal EMS approach in a physical HEV to demonstrate real-world FE improvements during AEs. This has involved design and fabrication of

a test HEV platform, and will require developing methods for predicting AE attributes, translating the simulated control strategies into actual HEV control software, and a whole lot of testing.

Bibliography

[1] U.S. Environmental Protection Agency. Fast facts on transportation greenhouse gas emissions. https://www.epa.gov/greenvehicles/fast-facts-transportation-greenhouse-gas-emissions, 2016. Accessed: 2019-1-23.

[2] U.S. Environmental Protection Agency. Smog, soot, and other air pollution from transportation. https://www.epa.gov/air-pollution-transportation/smog-soot-and-local-air-pollution, September 2015. Accessed: 2017-10-16.

[3] CO2 emissions from fuel combustion highlights 2016. Technical report, International Energy Agency, 2016.

[4] World health statistics 2016: Monitoring health for the SDGs. Technical report, World Health Organization, 2016.

[5] A E Atabani, Irfan Anjum Badruddin, S Mekhilef, and A S Silitonga. A review on global fuel economy standards, labels and technologies in the transportation sector. *Renewable Sustainable Energy Rev.*, 15(9):4586–4610, December 2011.

[6] Zachary D. Asher, David A. Trinko, and Thomas H. Bradley. *Increasing the Fuel Economy of Connected and Autonomous Lithium-Ion Electrified Vehicles*, pages 129–151. Springer International Publishing, Cham, 2018.

[7] Zachary D. Asher, Van Wifvat, Anthony Navarro, Scott Samuelsen, and Thomas Bradley. The importance of HEV fuel economy and two research gaps preventing real world implementation of optimal energy management. In *SAE Technical Paper*. SAE International, 01 2017.

[8] Koichiro Muta, Makoto Yamazaki, and Junji Tokieda. Development of new-generation hybrid system ths ii - drastic improvement of power performance and fuel economy. In *SAE Technical Paper*. SAE International, 03 2004.

[9] Chan-Chiao Lin, Huei Peng, Jessy W. Grizzle, Jason Liu, and Matt Busdiecker. Control system development for an advanced-technology medium-duty hybrid electric truck. In *SAE Technical Paper*. SAE International, 11 2003.

[10] Daniel J. Fagnant and Kara Kockelman. Preparing a nation for autonomous vehicles: opportunities, barriers and policy recommendations. *Transportation Research Part A: Policy and Practice*, 77(C):167–181, 2015.

[11] Chan-Chiao Lin, Jun-Mo Kang, J W Grizzle, and Huei Peng. Energy management strategy for a parallel hybrid electric truck. In *Proceedings of the 2001 American Control Conference*, volume 4, pages 2878–2883 vol.4, 2001.

[12] N Kim, S Cha, and H Peng. Optimal control of hybrid electric vehicles based on pontryagin's minimum principle. *IEEE Trans. Control Syst. Technol.*, 19(5):1279–1287, 2011.

[13] Pei Zhang, Fuwu Yan, and Changqing Du. A comprehensive analysis of energy management strategies for hybrid electric vehicles based on bibliometrics. *Renewable Sustainable Energy Rev.*, 48(Supplement C):88–104, August 2015.

[14] X Y Zhou. Maximum principle, dynamic programming, and their connection in deterministic control. *J. Optim. Theory Appl.*, 65(2):363–373, May 1990.

[15] Jinming Liu, Jonathan Hagena, Huei Peng, and Zoran S Filipi. Engine-in-the-loop study of the stochastic dynamic programming optimal control design for a hybrid electric HMMWV. *Int. J. Heavy Veh. Syst.*, 15(2-4):309–326, January 2008.

[16] Daniel F Opila, Xiaoyong Wang, Ryan McGee, and J W Grizzle. Real-Time implementation and hardware testing of a hybrid vehicle energy management controller based on stochastic dynamic programming. *J. Dyn. Syst. Meas. Control*, 135(2):021002, March 2013.

[17] Dominik Lang, Roman Schmied, and Luigi Del Re. Prediction of preceding driver behavior for fuel efficient cooperative adaptive cruise control. *SAE Int. J. Engines*, 7:14–20, 04 2014.

[18] Rahmi Akçelik and Mark Besley. Acceleration and deceleration models. *23rd Conference of Australian Institutes of Transport Research*, January 2001.

[19] David A. Trinko, Zachary D. Asher, and Thomas H. Bradley. Application of pre-computed acceleration event control to improve fuel economy in hybrid electric vehicles. In *WCX World Congress Experience*. SAE International, Apr 2018.

[20] U.S. Environmental Protection Agency. 2017 best and worst fuel economy vehicles. https://www.fueleconomy.gov/feg/best-worst.shtml. Accessed: 2017-10-16.

[21] Namwook Kim, Aymeric Rousseau, and Eric Rask. Autonomie model validation with test data for 2010 toyota prius. In *SAE Technical Paper*. SAE International, 04 2012.

[22] Nobuki Kawamoto, Kiyoshi Naiki, Toshihiro Kawai, Takasuke Shikida, and Mamoru Tomatsuri. Development of new 1.8-liter engine for hybrid vehicles. In *SAE Technical Paper*. SAE International, 04 2009.

[23] Z D Asher, D A Baker, and T H Bradley. Prediction error applied to hybrid electric vehicle optimal fuel economy. *IEEE Trans. Control Syst. Technol.*, PP(99):1–14, 2017.

[24] Rajesh Rajamani. *Vehicle Dynamics and Control*. Springer Science & Business Media, December 2011.

[25] John Paul Arata, III. *Simulation and control strategy development of power-split hybrid-electric vehicles*. PhD thesis, Georgia Institute of Technology, 2011.

[26] Timothy A Burress, Steven L Campbell, Chester Coomer, Curtis William Ayers, Andrew A Wereszczak, Joseph Philip Cunningham, Laura D Marlino, Larry Eugene Seiber, and Hua-Tay Lin. Evaluation of the 2010 toyota prius hybrid synergy drive system.

[27] Richard F Gunst. Response surface methodology: Process and product optimization using designed experiments. *Technometrics*, 38(3):284–286, 1996.

[28] Andrew A Frank. Control method and apparatus for internal combustion engine electric hybrid vehicles, April 2000. US Patent 6054844.

[29] Recommended practice for measuring the exhaust emissions and fuel economy of Hybrid-Electric vehicles. Technical Report J1711, SAE International, 2002.

[30] Downloadable dynamometer database | argonne national laboratory. https://www.anl.gov/energy-systems/group/downloadable-dynamometer-database. Accessed: 2017-10-16.

[31] Dimitri P Bertsekas. *Dynamic Programming and Optimal Control*, volume I. Athena Scientific, 1995.

[32] R Bellman. Dynamic programming and lagrange multipliers. *National Acad Sciences*, 42(10):767–769, 1956.

Appendix A

List of Acronyms

Table A.1: Acronyms used in this document

Acronym	Meaning
AE	Acceleration Event
ANN	Artificial Neural Network
BSFC	Brake Specific Fuel Consumption
DP	Dynamic Programming
EPA	Environmental Protection Agency
FC	Fuel Consumption
FE	Fuel Economy
HEV	Hybrid Electric Vehicle
ICE	Internal Combustion Engine
PCA	Principal Components Analysis
SOC	State of Charge

Appendix B

AE Attribute Terminology

"During Acceleration"

Many of the attributes are calculated "during acceleration," meaning only during timesteps of changing vehicle velocity. This is often different from the time during which the variable itself is changing in value, because steady speed does not necessitate steady engine state. An example of this is shown in Figure B.1.
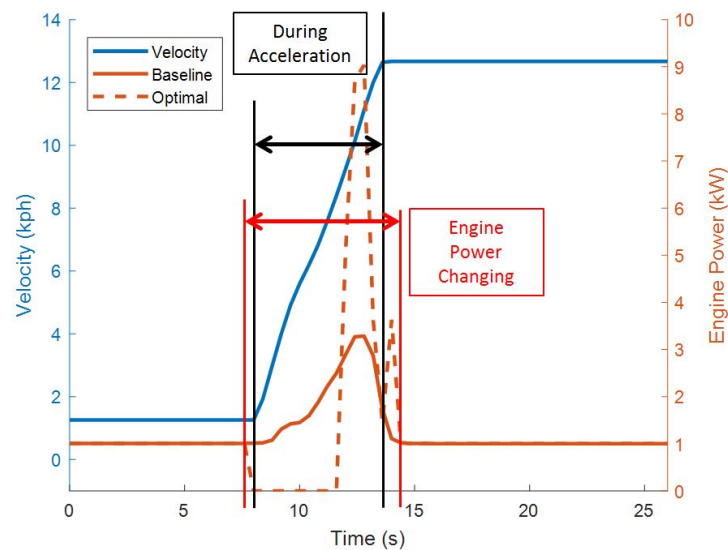

Figure B.1: Example of engine state changing outside of "acceleration"

Modality

Accelerator pedal signal, engine power, and total vehicle power often display multiple modes, or peaks. "Modality" is expressed as the number of modes. One mode has occurred when the signal exceeds and drops below its mean "during acceleration" value. An engine power signal with two modes is shown in Figure B.2.
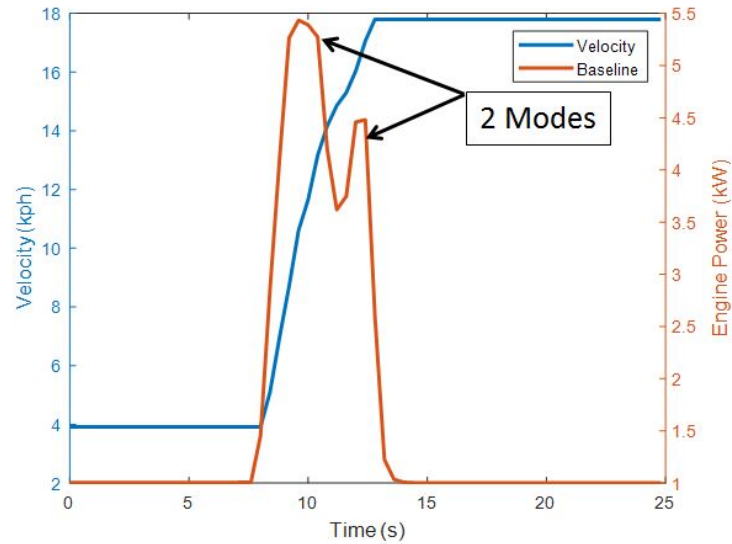
Figure B.2: Example engine power trace with a modality of 2

Ramp-Up / Ramp-Down / Stabilization

All of the signals are at a steady state value for several timesteps at the beginning and end of each AE. Ramp-up is the time at which the signal first begins to change from its initial steady state value, whereas ramp-down or stabilization are the time at which the signal first reaches its final steady state value. Stabilization applies to the velocity trace, since velocity never decreases during an AE, while ramp-down applies to all other traces, whose magnitudes begin and end at low values relative to their values during acceleration. These are illustrated in Figure B.3.
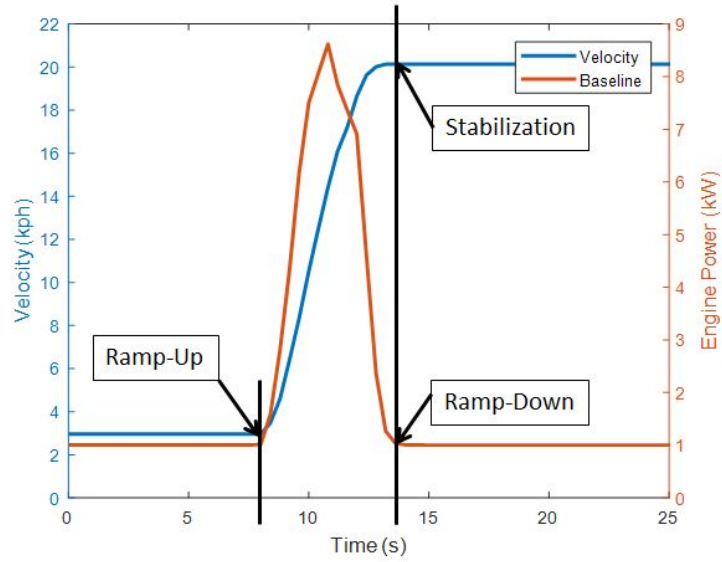
Figure B.3: Illustration of ramp-up, ramp-down, and stabilization

Ramp-Up Rate

Ramp-up rate R is the average rate of change of a signal between the time of ramp-up and the time the variable reaches its maximum:

$$R = \frac{X_{max} - X_{ss}}{t_{max} - t_{ramp-up}} \tag{B.1}$$

where X_{max} is the signal's maximum value, $X_{ss-init}$ is the signal's initial steady state value, t_{max} is the time at which the signal assumes its maximum value, and $t_{ramp-up}$ is the time at which ramp-up begins for the signal. This is illustrated for an engine power trace in Figure B.4.
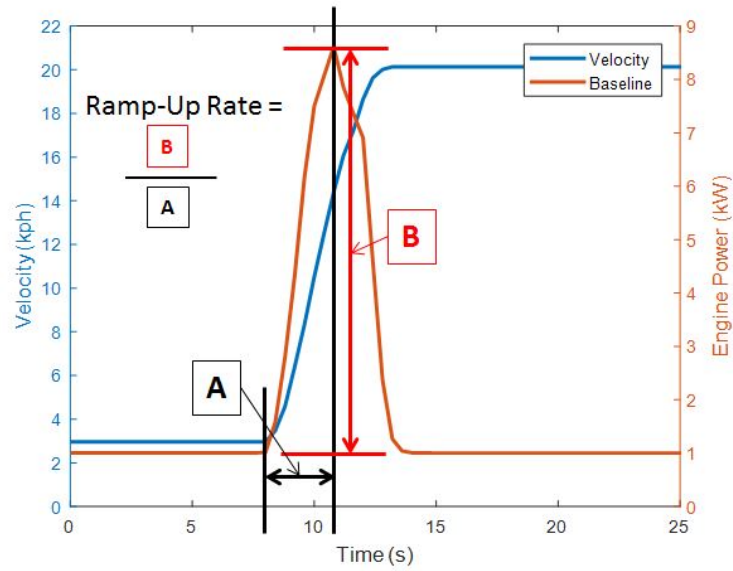
Figure B.4: Illustration of ramp-up rate

Dip

Engine power and battery SOC sometimes drop below their steady-state values for a short time before increasing during acceleration. "Dip" is the difference between the initial steady-state value of the signal and the minimum value of the signal during acceleration. This is illustrated in Figure B.5 for an engine power trace.
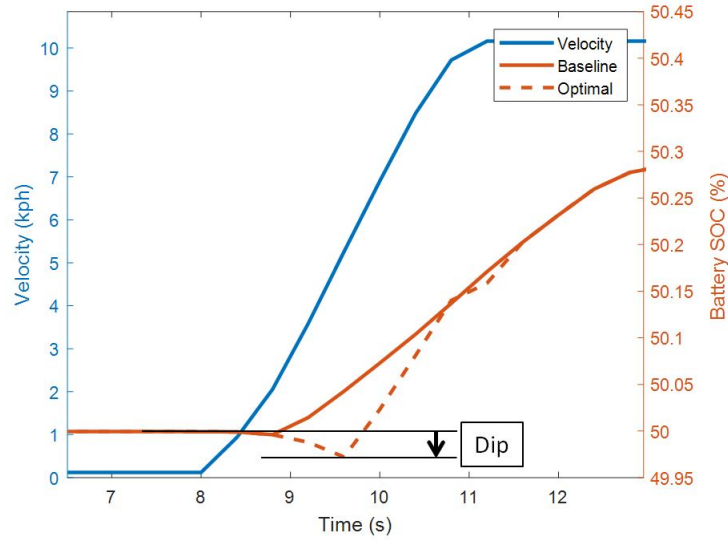
Figure B.5: Illustration of dip.

Note on Accelerator Pedal Signal

Accelerator pedal signal is obtained from the drive cycle dataset from which the AE velocity traces were originally obtained. AE are analyzed as occurring at steady state, where the vehicle is simulated as moving at constant velocity before and after acceleration. Thus, accelerator pedal signal is unavailable before and after acceleration, so its value during those times cannot be used in AE classification. However, its modality during acceleration is a useful statistic for filtering AE for control type analysis (discussed in the next section), so post-processing statistics on accelerator pedal signal are still calculated.

Appendix C

Additional Categorization Investigations

C.1   Categorize Using Final Velocity and Duration

The analysis applied in Section 4.2 is applied to a category scheme based on final velocity and AE duration (referred to here as the "duration" category scheme), as shown in Table C.1. All figures are analogous to the figures in Section 4.2.

Attributes Used	Duration	Final Velocity
Number of Bins	10	10
Expected AE Selection	Initial Velocity	

Table C.1: Summary of duration category scheme

Duration category bins are approximately 3 seconds wide and velocity category bins are approximately 7 kph wide. AEs are constrained to a duration range of 0-30 seconds and an end velocity range of 0-80 kph. Of the $10 \times 10 = 100$ categories, 86 are occupied by AEs. The numbers of AEs in each category are illustrated in Figure C.1.
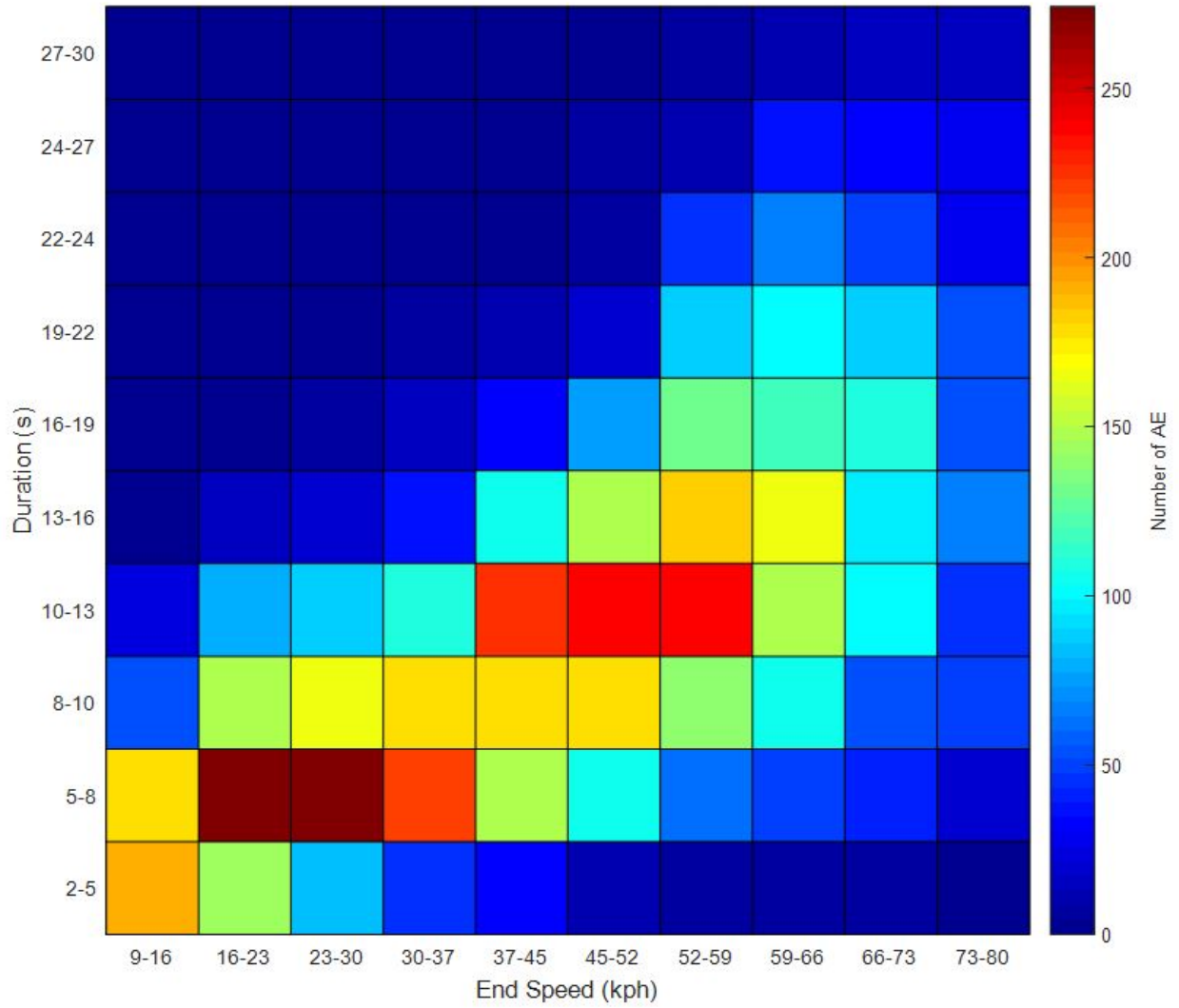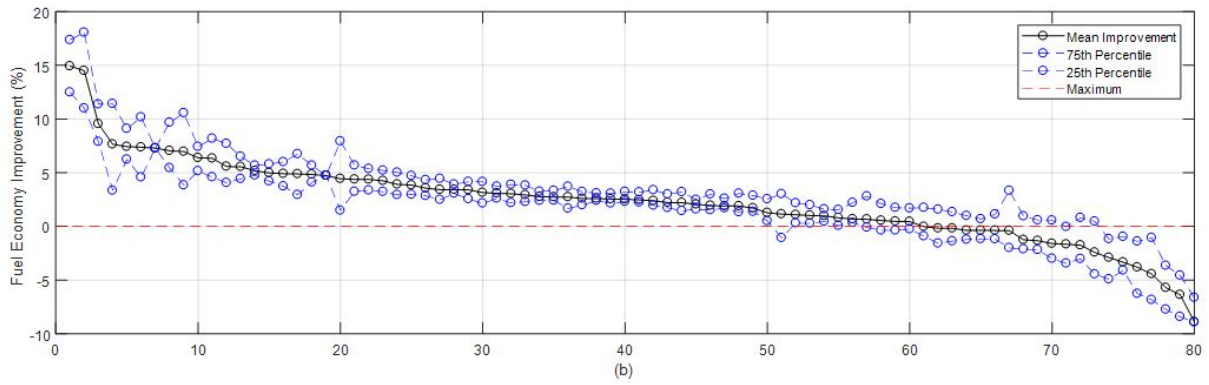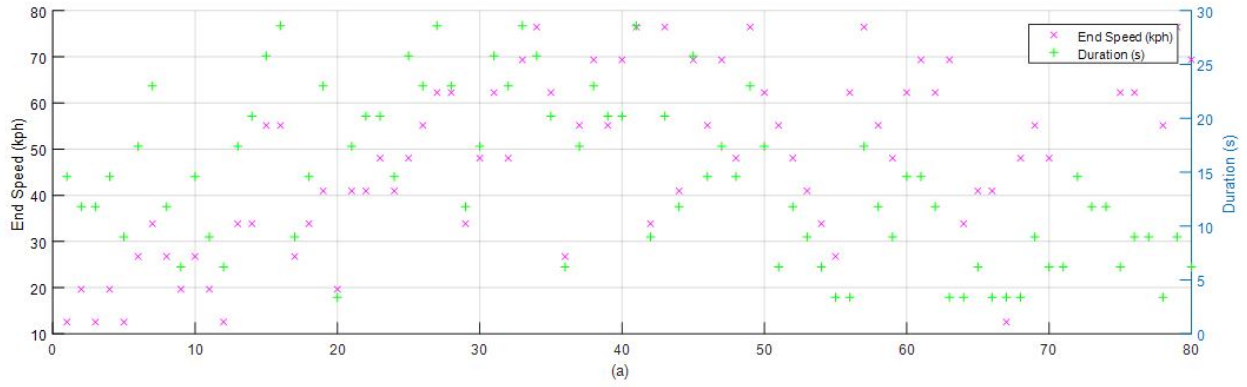
Figure C.1: Population of duration categories

Figure C.2: FE improvement results by duration category in order of decreasing mean FE improvement
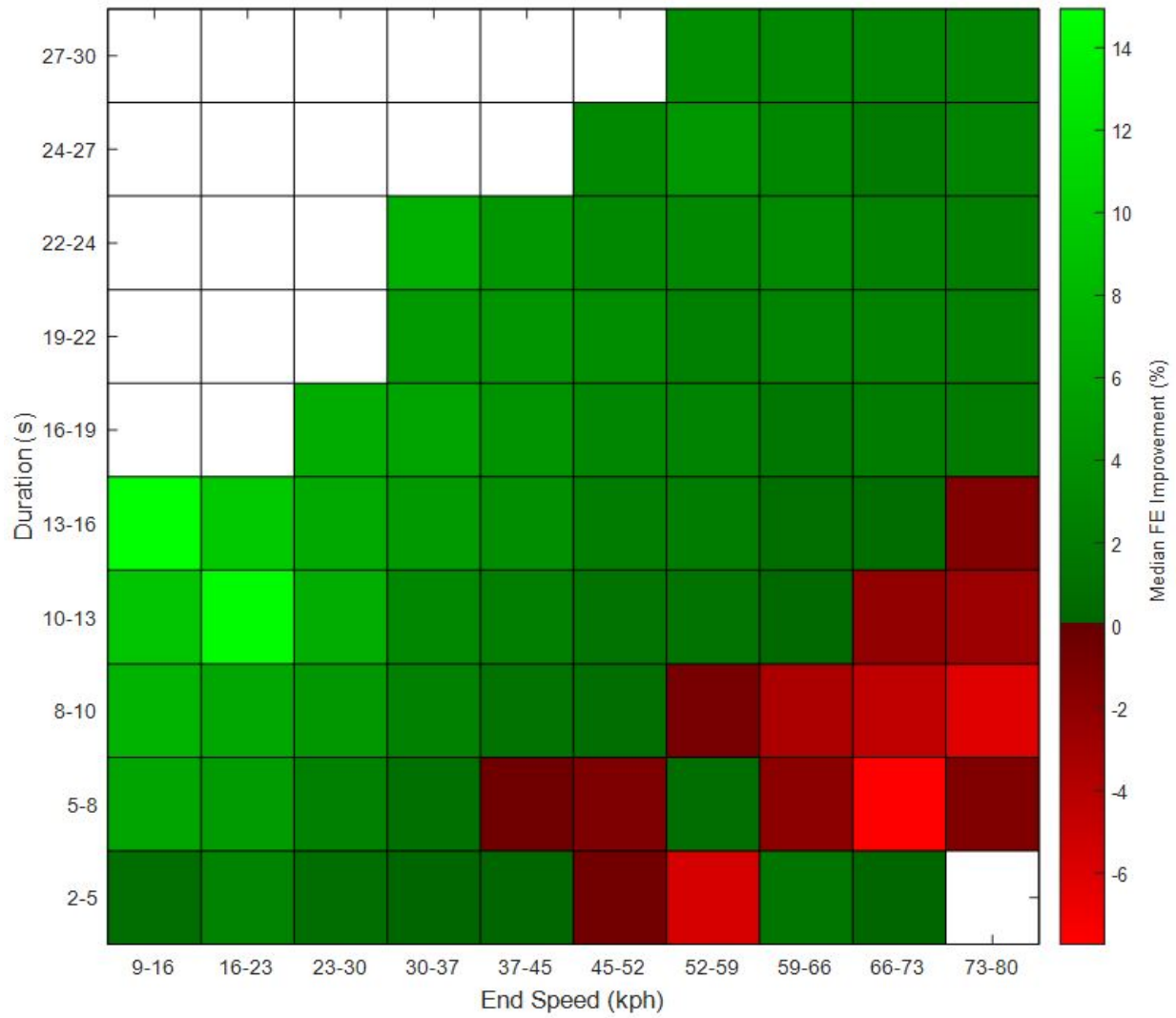
Figure C.3: Median FE improvement results organized by duration category

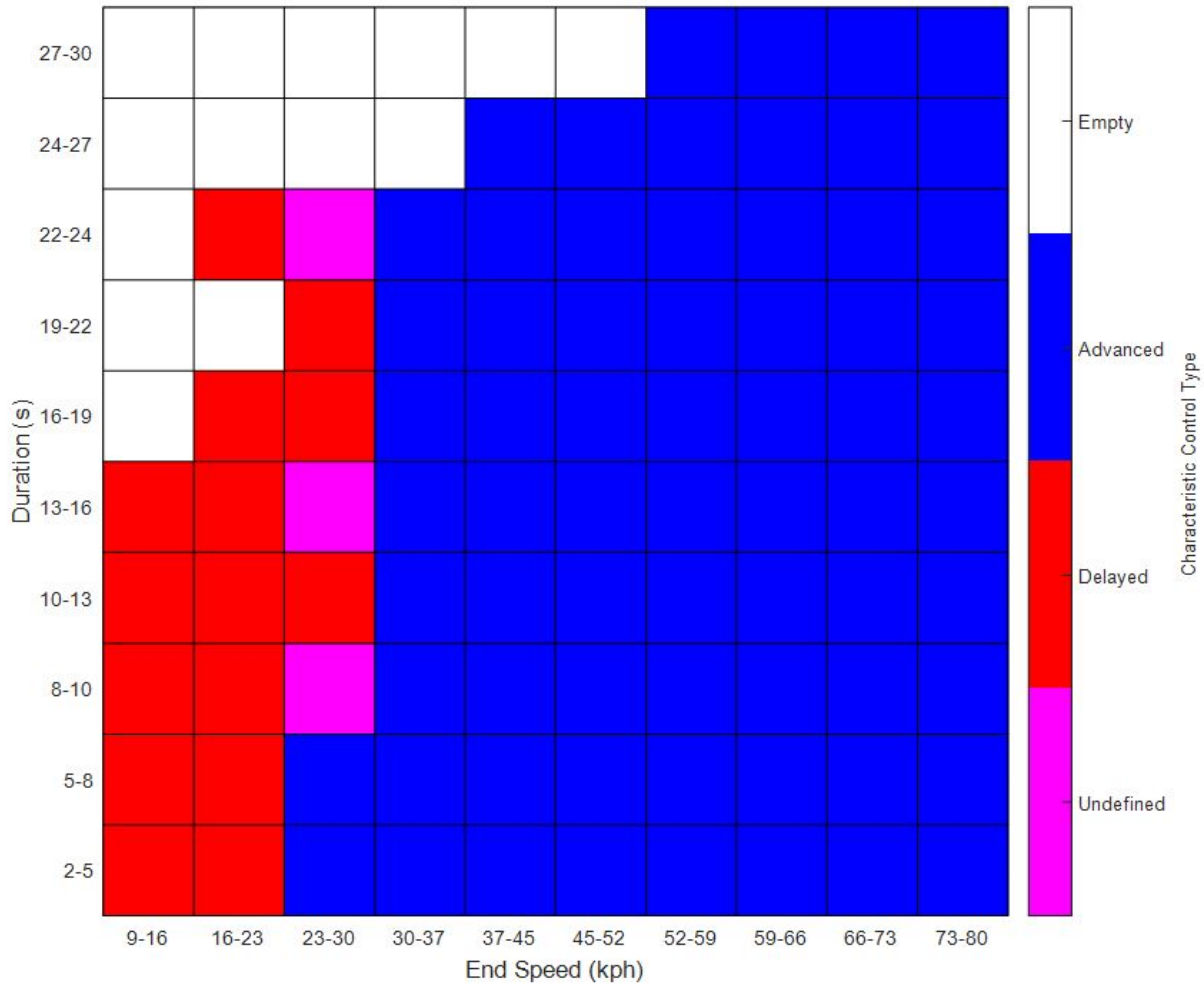## C.1.1   Investigate Control Type Mismatch

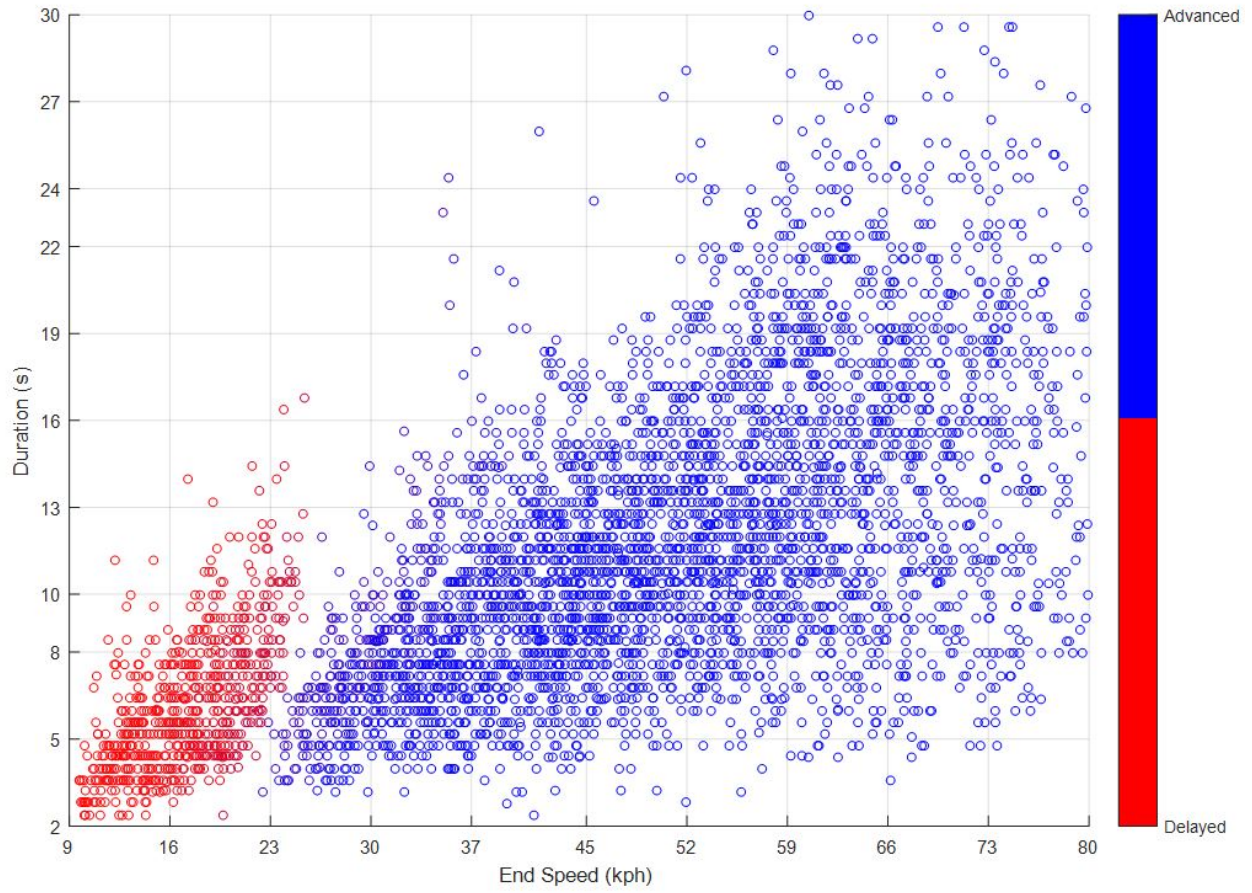**Figure C.4:** Expected AE control type organized by duration category

Figure C.5: Actual AE control types on grid corresponding to duration categories
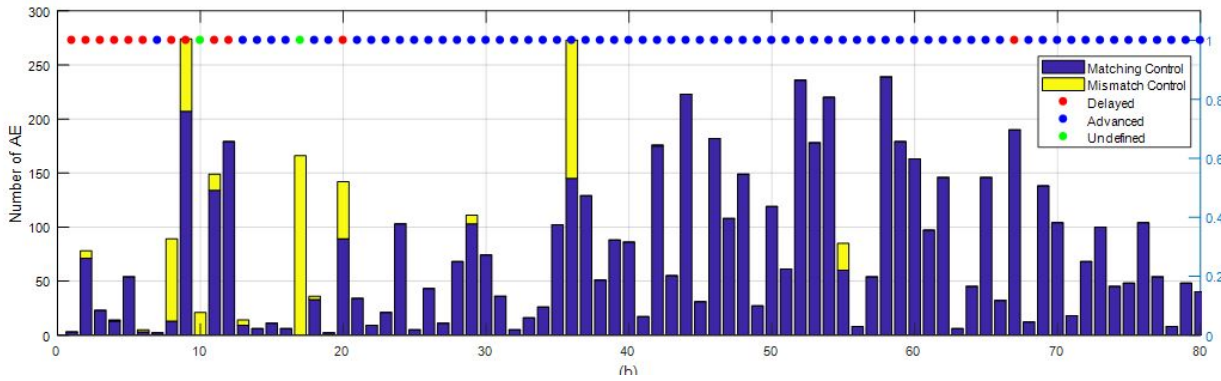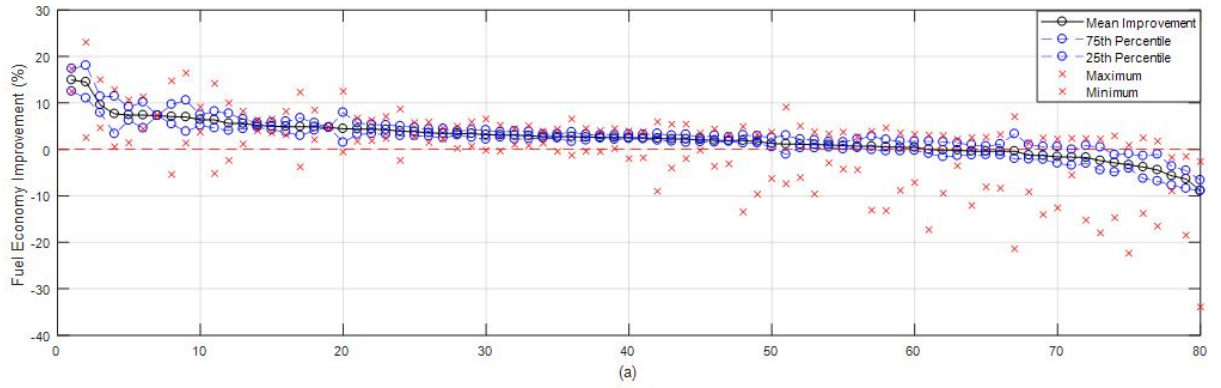
Figure C.6: Control type mismatch and FE improvement for duration categories

C.1.2 Investigate Prediction Error

For this scheme, prediction error is expressed as the difference between actual and expected initial velocity. Figure C.7 compares prediction error to FE improvement and SOC_f error.
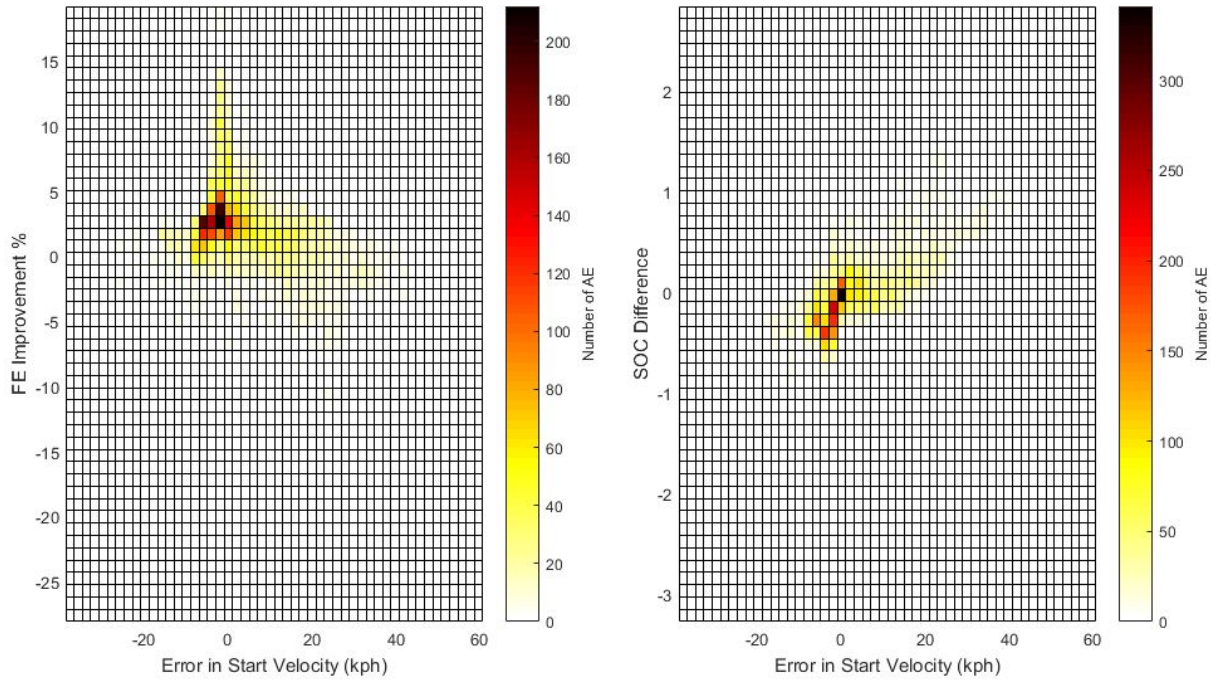
Figure C.7: Prediction error, FE improvement, and SOC error for duration categories

C.1.3 Adjust Category Sizes

Attributes Used	Duration	Final Velocity
Number of Bins	1-10	1-10
Expected AE Selection	Initial Velocity	

Table C.2: Finer and coarser categorizations by duration
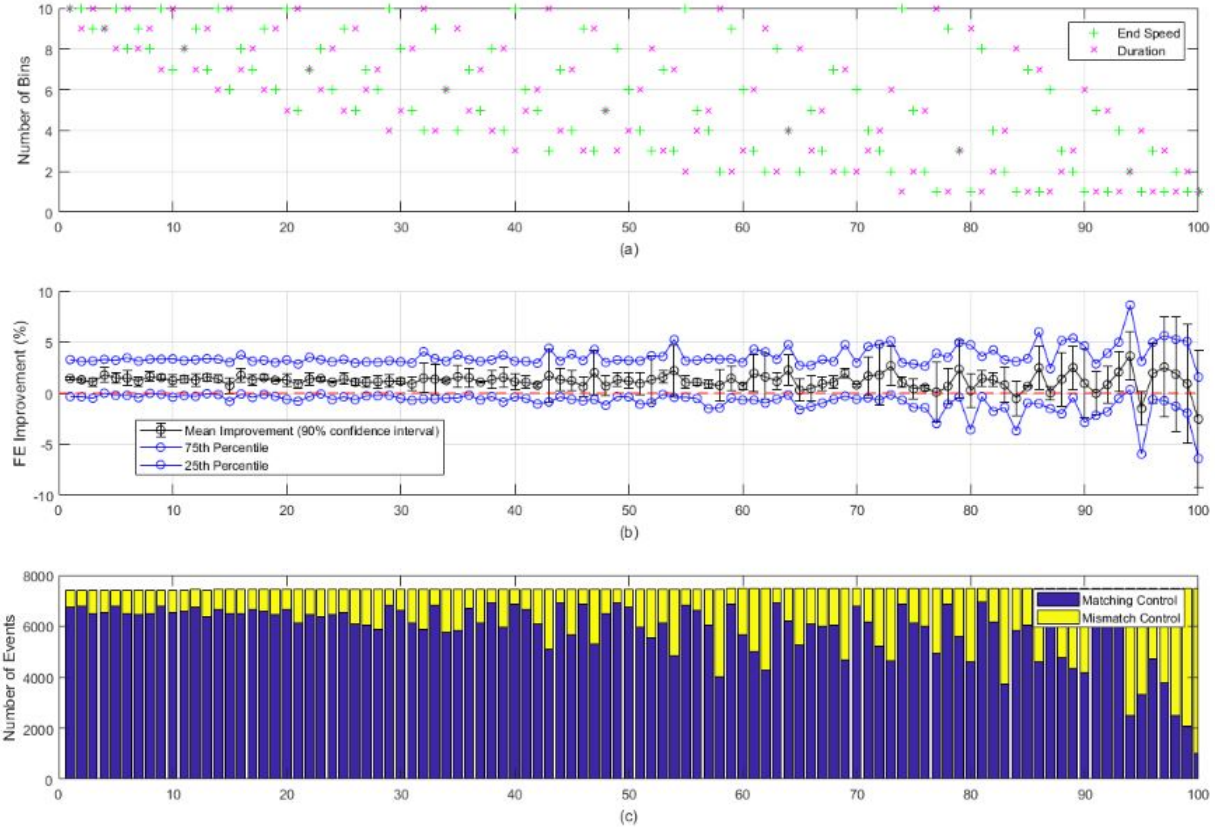
Figure C.8: FE results for finer and coarser duration categorizations

C.2 Categorize Using Average Acceleration and Final Velocity

The analysis applied in Sections 4.2 and C.1 is applied to a category scheme based on final velocity and average acceleration (referred to here as the "acceleration" category scheme), as shown in Table C.1. All figures are analogous to the figures in Section 4.2. Average acceleration is defined as

$$a_{avg} = \frac{v_f - v_i}{t_f - t_i} \tag{C.1}$$

Attributes Used	Acceleration Magnitude	Final Velocity
Number of Bins	10	10
Expected AE Selection	Initial Velocity	

Table C.3: Summary of acceleration category scheme

Acceleration category bins are approximately 0.6 kph/s wide, with maximum acceleration constrained to 6 kph/s. Final velocity category bins are approximately 7 kph wide. Of a total of $10 \times 10 = 100$ categories, 95 are occupied. The numbers of AEs in each category are illustrated in Figure C.9.

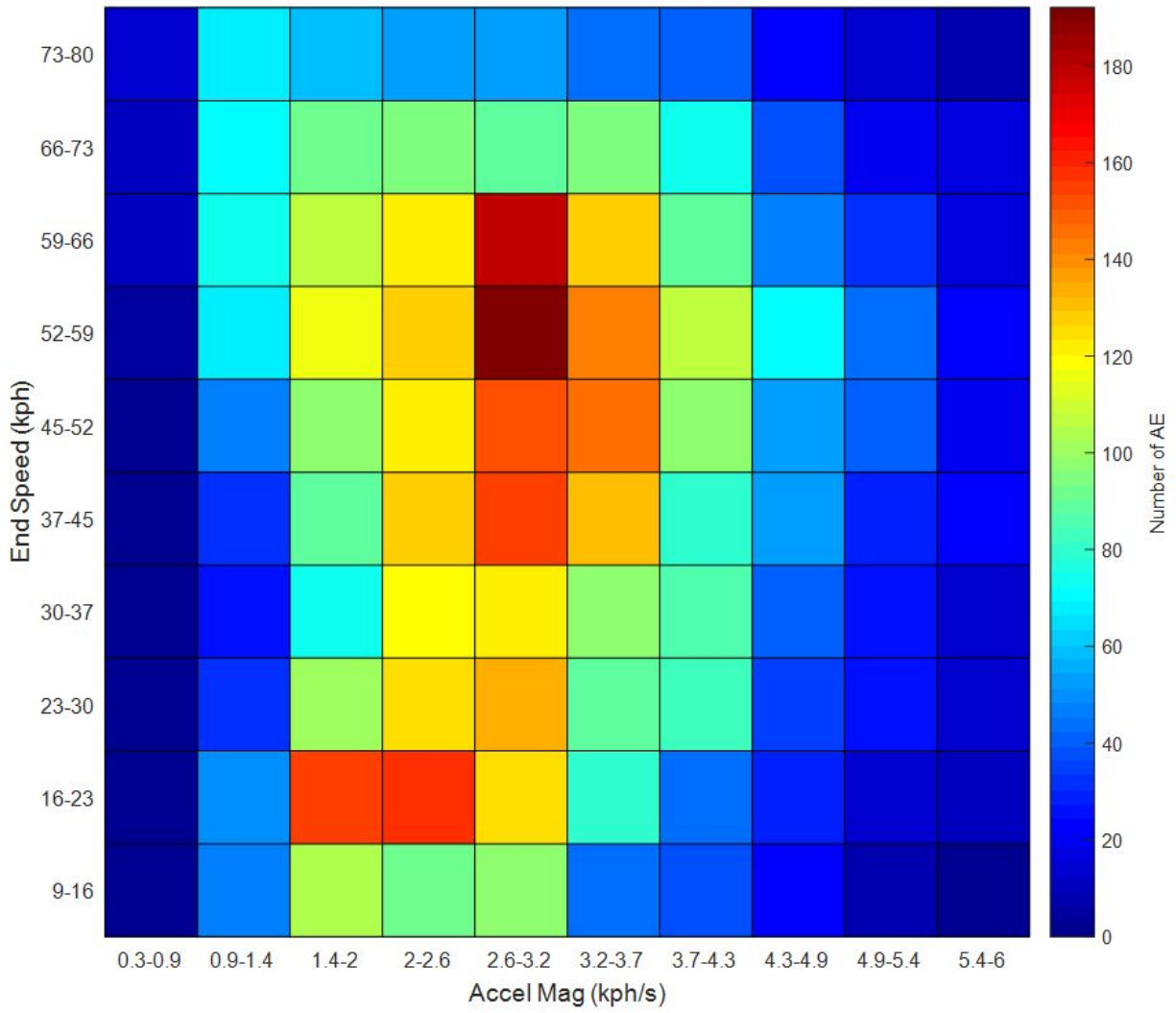**Figure C.9:** Population of acceleration categories
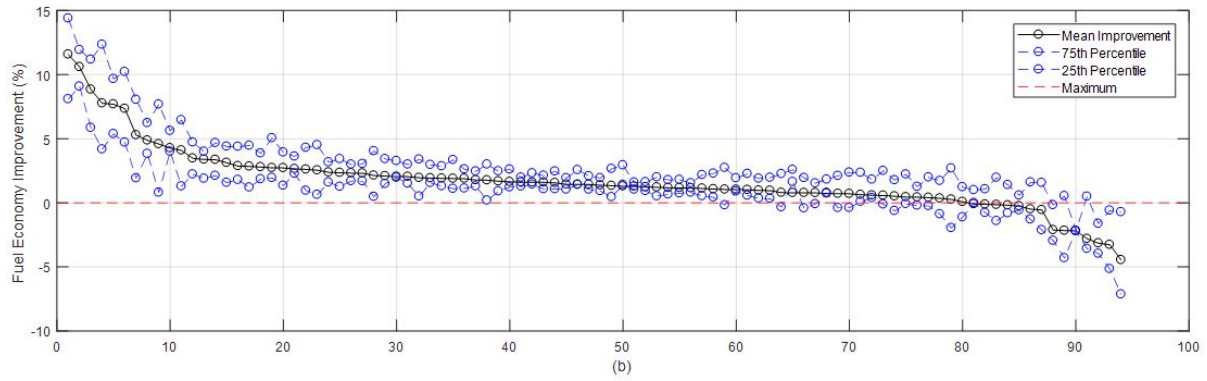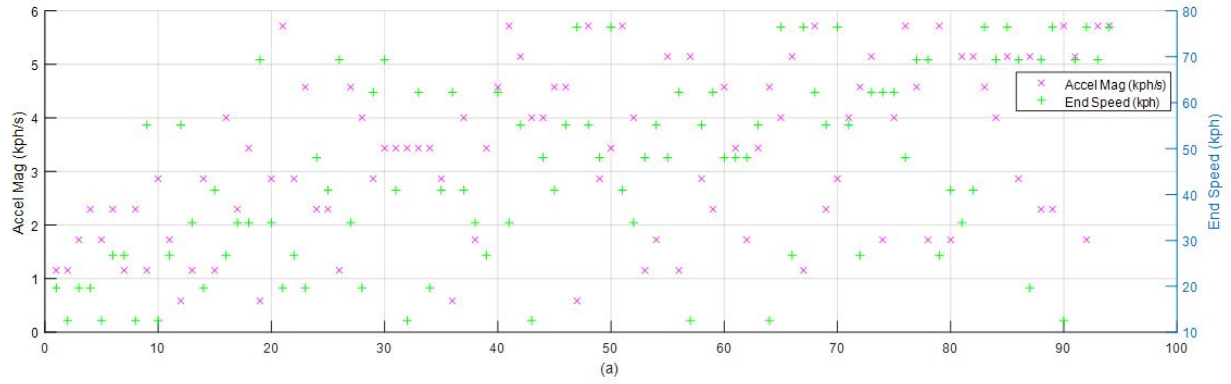
Figure C.10: FE improvement results by acceleration category
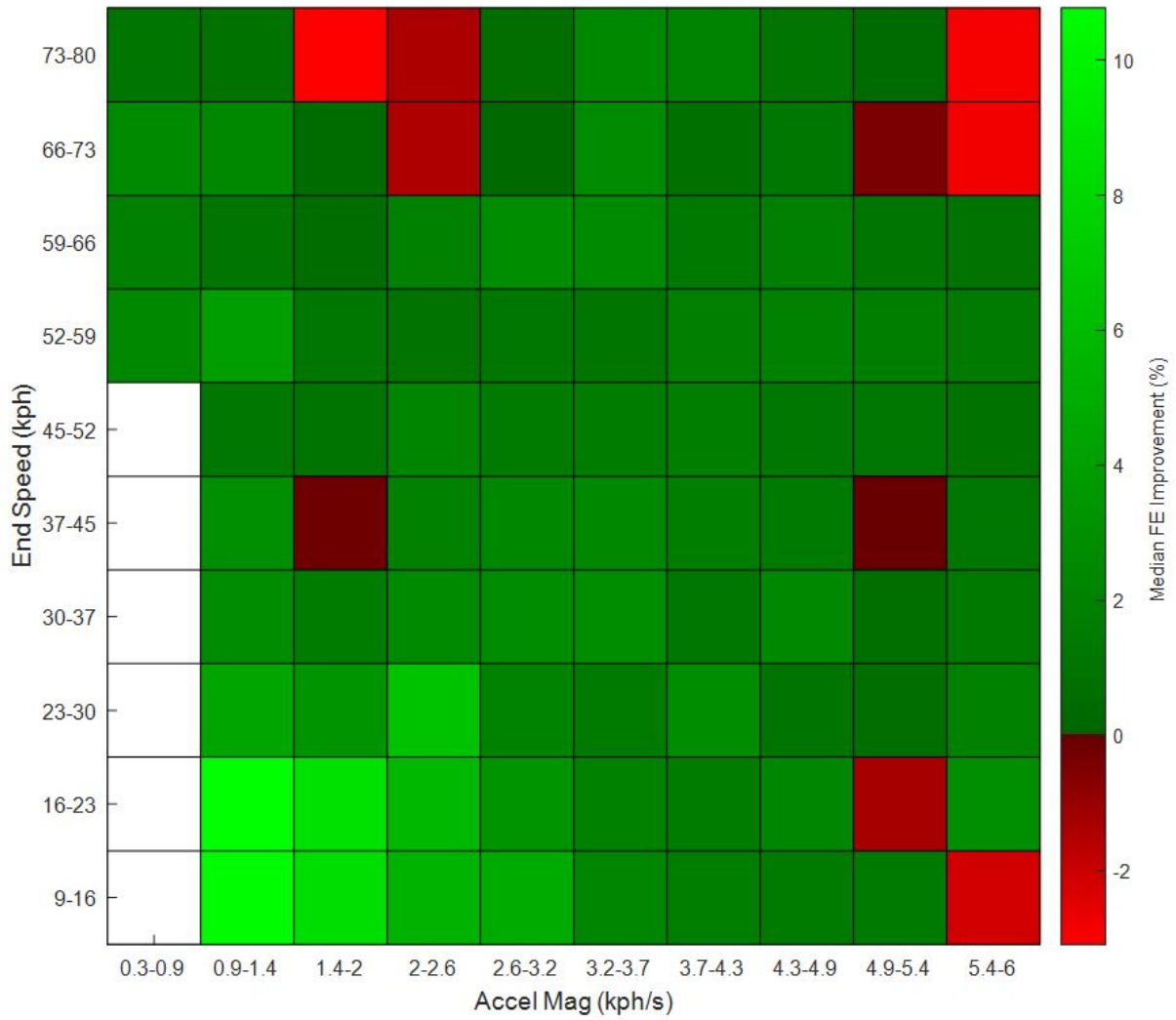
Figure C.11: Median FE improvement results organized by acceleration category

C.2.1 Investigate Control Type Mismatch
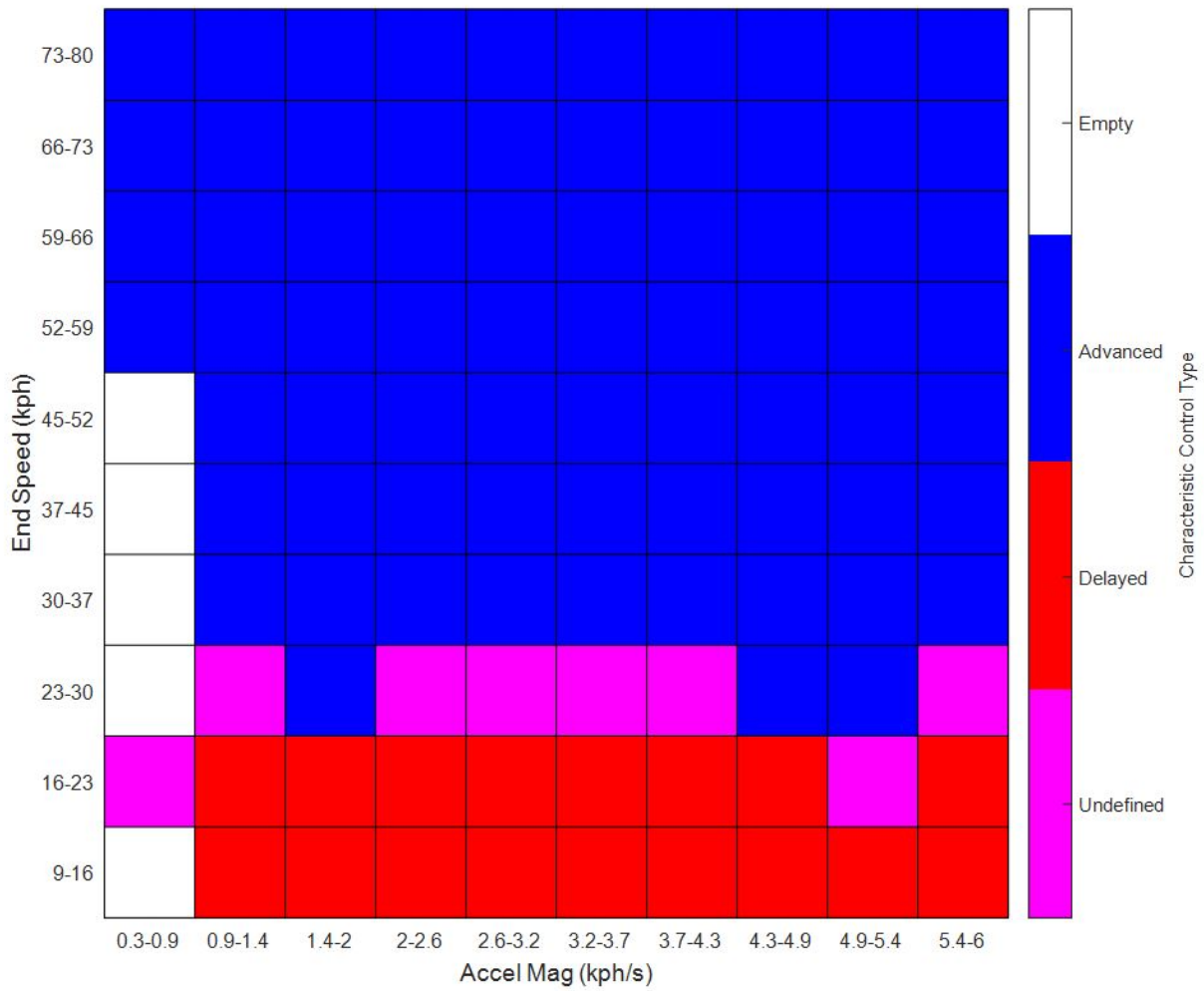
Figure C.12: Expected AE control type organized by acceleration category
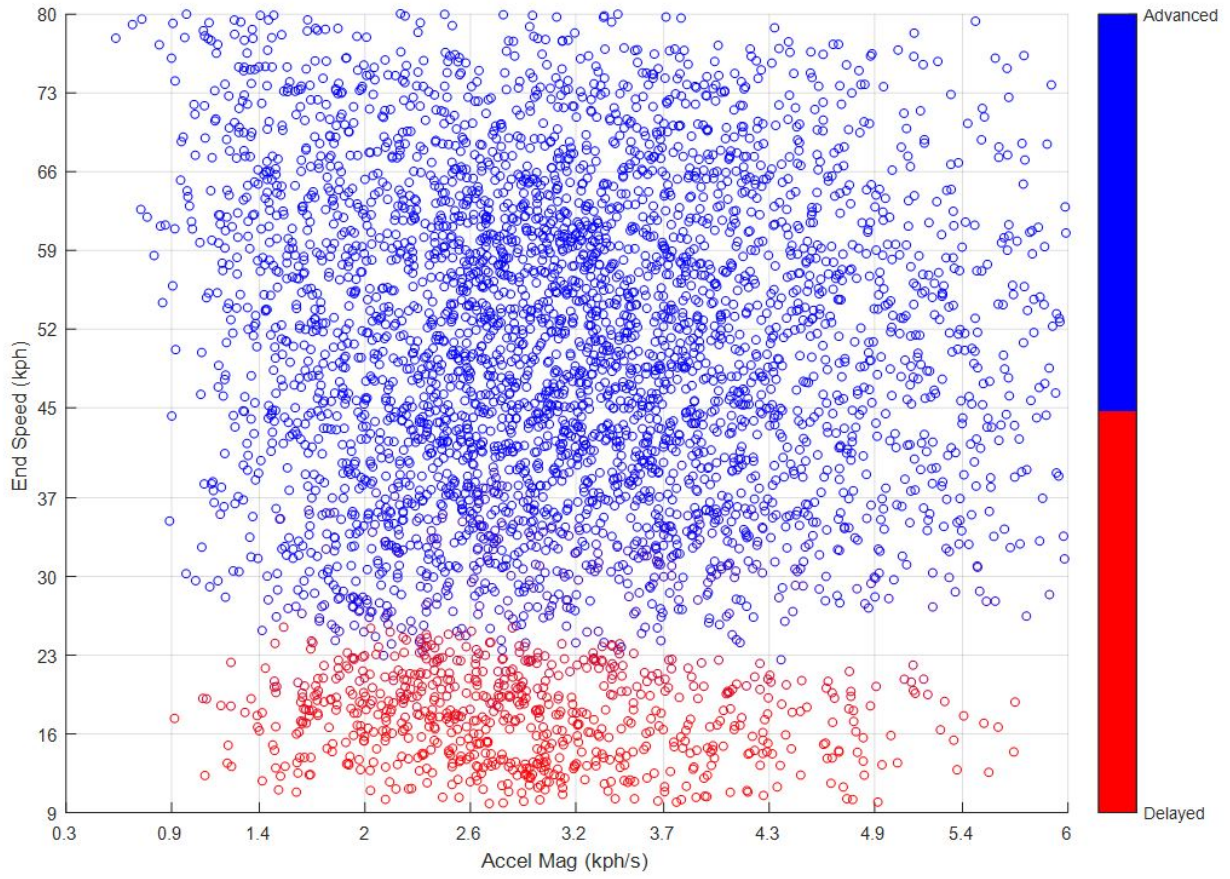
Figure C.13: Actual AE control types on grid corresponding to acceleration categories
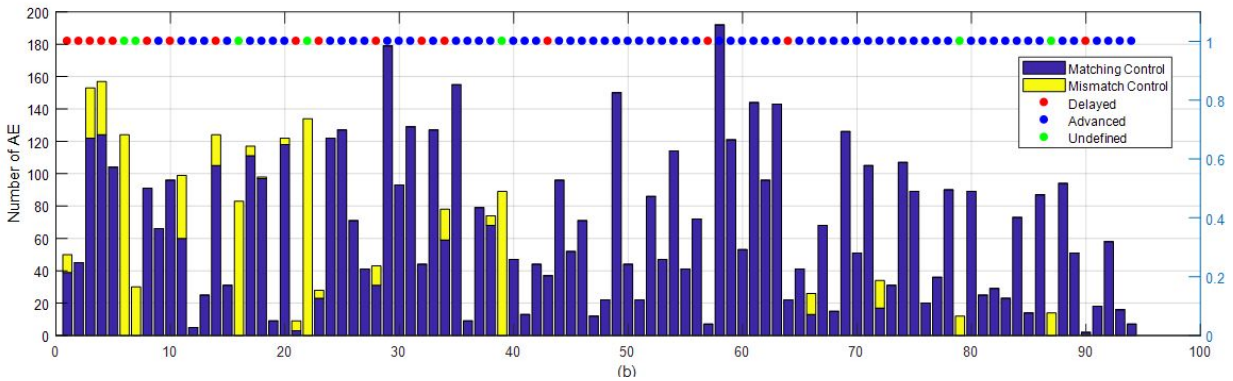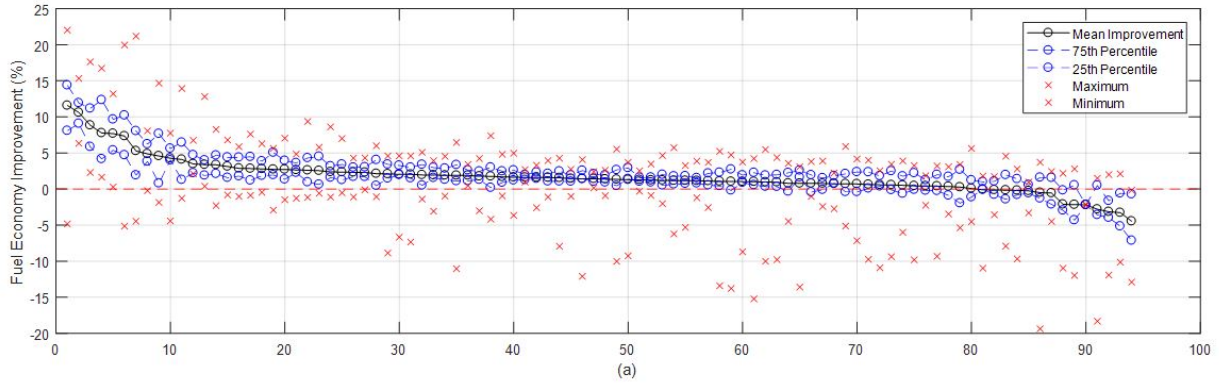
Figure C.14: Control type mismatch and FE improvement for acceleration categories

C.2.2 Investigate Prediction Error

For this scheme, prediction errors in duration and initial velocity are more or less unconstrained, but since average acceleration is linearly related to duration, initial velocity, and final velocity, duration and initial velocity errors are approximately proportional to each other. Prediction error is chosen as error in duration.
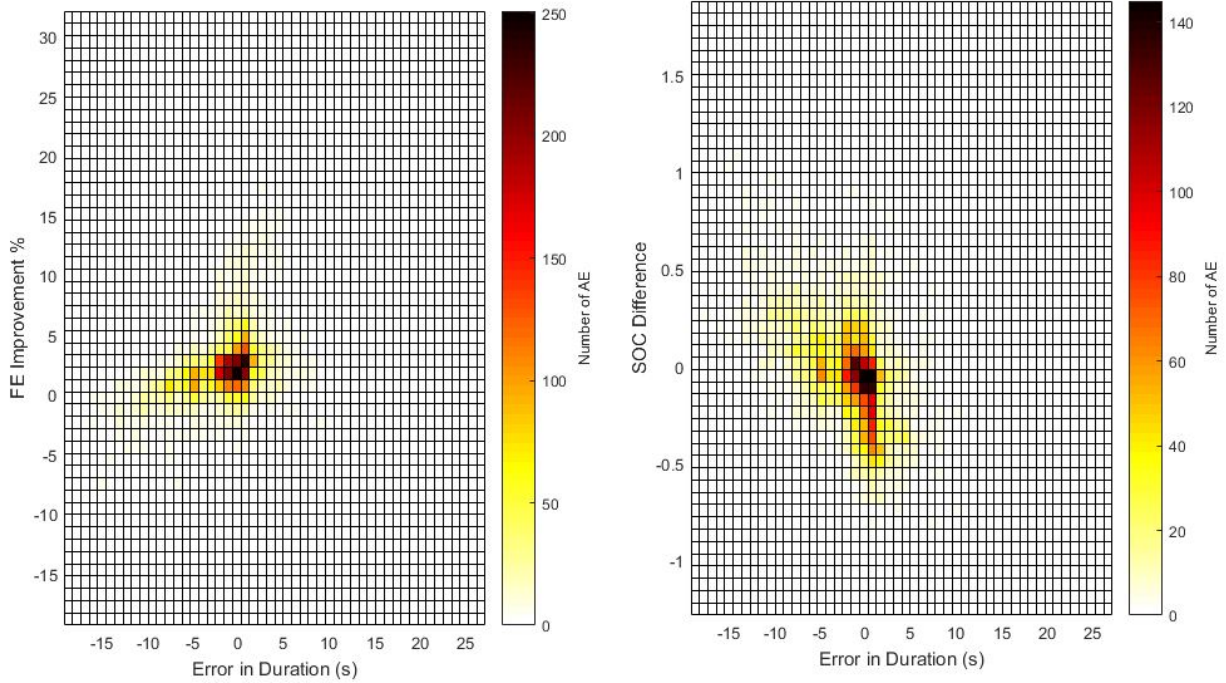
Figure C.15: Prediction error, FE improvement, and SOC error for acceleration categories

C.2.3   Adjust Category Sizes

Attributes Used	Accel Mag	Final Velocity
Number of Bins	1-10	1-10
Expected AE Selection	Initial Velocity	

Table C.4: Finer and coarser categorizations by duration

Figure C.16a, b, and c are all sorted by decreasing total number of categories left to right.
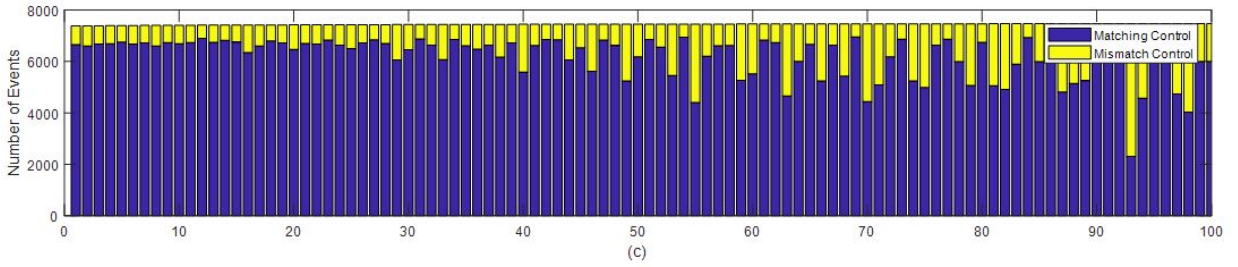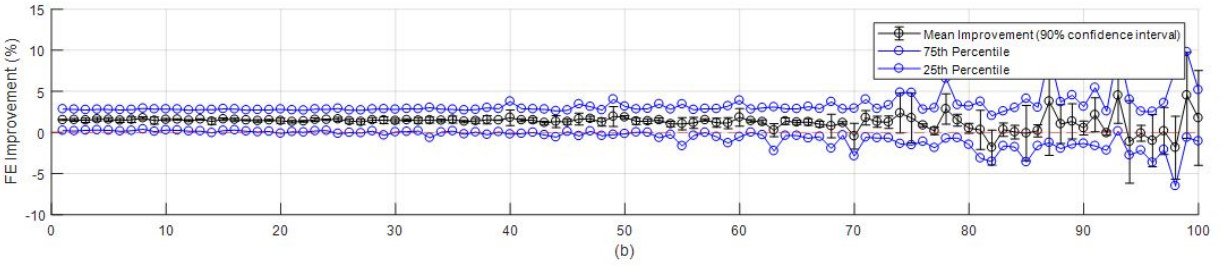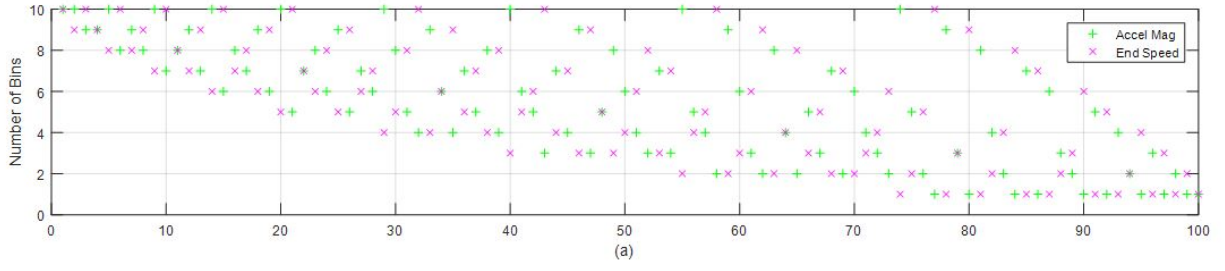
Figure C.16: FE results for finer and coarser acceleration categorizations

Appendix D

Additional Drive Cycle Investigations

D.1 City Driving Cycle 2: Denver Downtown

The Denver Downtown cycle is a real world, urban cycle. It has a higher top speed, a much longer distance and duration, more AEs, and a higher baseline FE than the NYCC. A variety of characteristics of the Denver Downtown cycle are listed in Table D.1, and the simulated FE results are given in Figure D.1.

Table D.1: Characteristics of the Denver Downtown cycle

Drive Cycle	Duration (sec)	Distance (km)	Average Speed (kph)	Max Speed (kph)	#AE	Time %AE	Baseline FE (mpg)	Approximate AE FE (mpg)	Optimal AE FE (mpg)	Optimal Cycle FE (mpg)
Denver Downtown	2202.8	15.9	26.1	71.6	28	21.7%	65.94	67.56	68.33	75.90
								2.46%	3.63%	15.12%
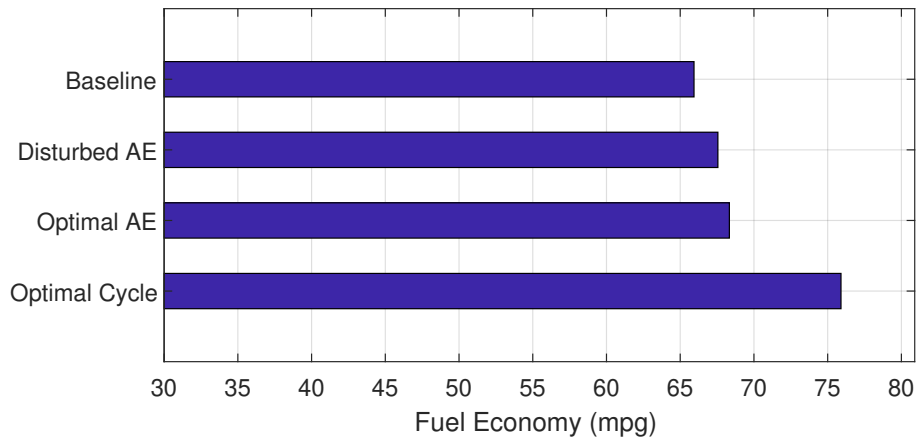
(a) Denver Downtown cycle FE results
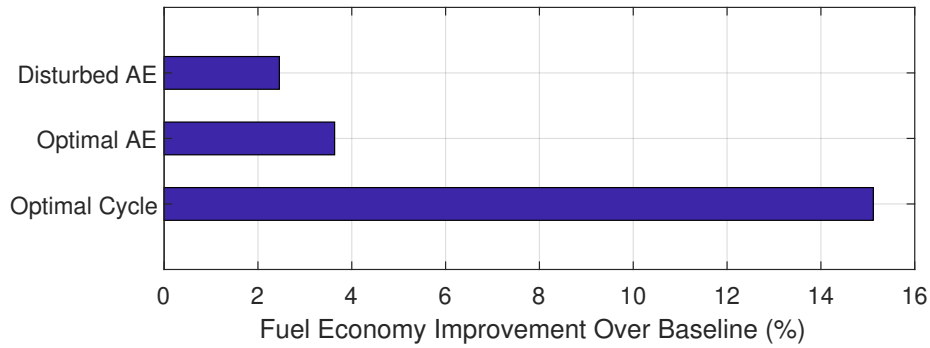
(b) Denver Downtown cycle FE improvement results

Figure D.1: FE results for Denver Downtown cycle

Disturbed control achieves 68% of the FE improvement achieved by Optimal AE control and 16% of the FE improvement achieved by Optimal Cycle control. Again, the disturbed dFC trace follows closely behind the Optimal AE trace. The length of the cycle gives the Optimal Cycle strategy plenty of room to maneuver, so it stores battery energy early in the cycle to permit almost full-EV operation from approximately t = 800 seconds to t = 1200 seconds when power demands are low. This results in huge FE improvement over baseline, which disturbed control does not approach.

This cycle also illustrates the need for SOC correction of dFC. From Table D.2, of the 9 AE with positive dFC, only two remain positive after SOC correction, but two with negative

uncorrected dFC have positive dFC after correction. Regardless, the losses to FE are again easily recouped by the contributions of the other cycle AE.

Figure D.2: Simulation outputs for the Denver Downtown cycle

Table D.2: Characteristics of AEs in the Denver Downtown cycle

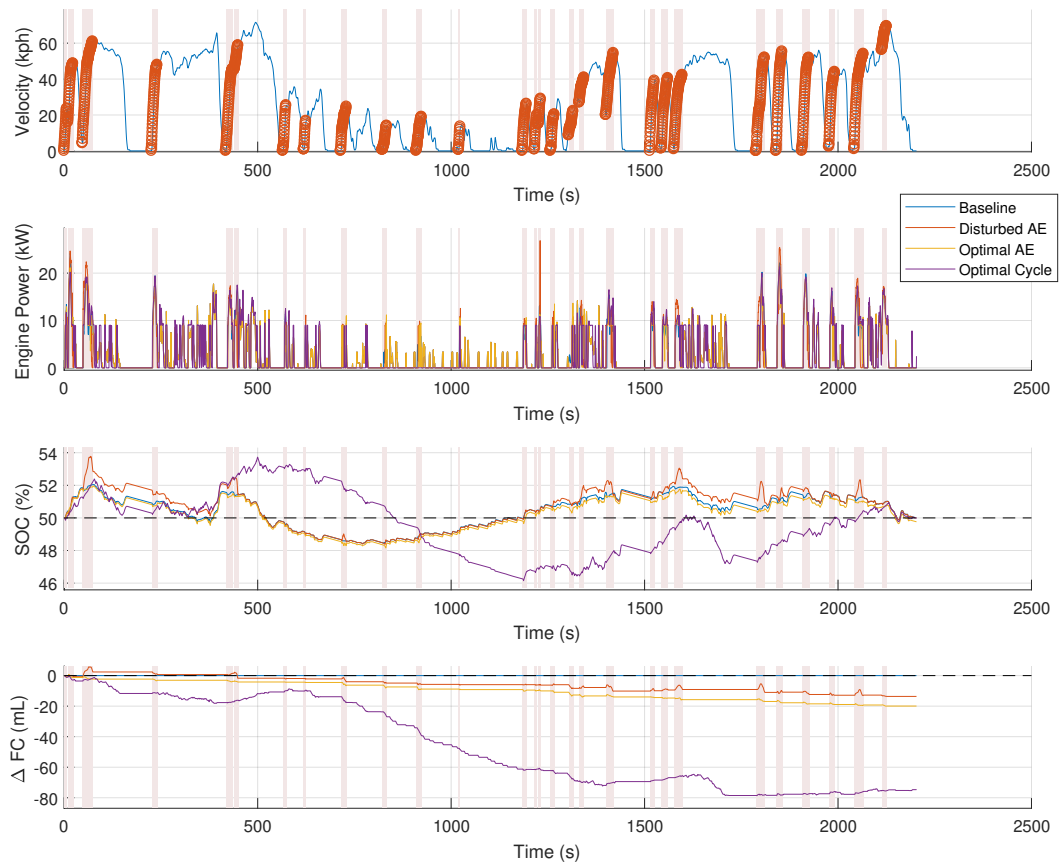|		Initial Speed (kph)	Final Speed (kph)	Duration (s)	# AE in Category	Optimal Control	Disturbed Control	dFC (mL)	dSOC (%)	dFC corrected (mL)	dFC normalized (mL/100km)
	1	0.0	23.5	7.6	217	Delay	Delay	-0.37	-0.08	-0.11	-43.23
	2	15.8	48.7	13.6	32	Advance	Delay	-0.33	0.00	-0.34	-24.88
	3	4.2	60.9	27.2	44	Delay	Advance	3.08	0.91	-0.02	-0.62
	4	0.0	47.9	15.2	166	Delay	Delay	-1.70	-0.29	-0.69	-55.99
	5	0.0	45.7	18.4	166	Delay	Delay	0.86	0.39	-0.46	-34.58
	6	45.0	58.8	11.2	57	Advance	Advance	-3.26	-0.90	-0.19	-12.00
	7	0.1	25.4	9.2	178	Delay	Delay	-0.19	-0.06	0.02	7.84
	8	0.8	16.7	6.4	230	Delay	Delay	-0.26	0.02	-0.34	-255.23
	9	0.0	24.6	15.6	217	Delay	Delay	-1.86	-0.02	-1.78	-277.10
	10	0.6	14.0	12.4	321	Delay	Delay	-0.87	0.01	-0.89	-451.84
	11	0.0	18.9	14.4	230	Delay	Delay	-0.85	-0.02	-0.79	-204.60
	12	0.5	13.5	5.2	321	Delay	Delay	-0.18	-0.07	0.08	91.02
	13	0.0	26.2	11.6	178	Delay	Delay	0.00	0.00	-0.01	-3.19
AE #	14	0.9	19.9	7.2	230	Delay	Delay	-0.17	-0.03	-0.06	-31.36
	15	14.8	29.0	7.2	96	Delay	Delay	-0.12	-0.01	-0.07	-16.75
	16	0.0	20.3	10.8	217	Delay	Delay	0.26	0.30	-0.76	-241.59
	17	8.7	22.2	12.4	129	Delay	Delay	-2.31	-0.16	-1.77	-349.79
	18	26.9	40.8	13.2	65	Advance	Advance	0.56	0.41	-0.82	-65.78
	19	20.0	54.5	20.4	26	Advance	Advance	-2.34	-0.59	-0.34	-15.83
	20	0.0	39.1	12.4	119	Delay	Delay	0.21	0.03	0.12	14.57
	21	1.3	40.5	18.4	92	Delay	Delay	0.48	0.28	-0.47	-38.70
	22	0.9	42.3	22.4	155	Delay	Delay	0.34	0.28	-0.62	-36.58
	23	0.0	51.9	23.2	210	Delay	Delay	-1.90	-0.32	-0.83	-46.54
	24	0.0	55.3	16.4	231	Delay	Delay	0.16	0.19	-0.48	-33.46
	25	0.0	51.9	18.8	210	Delay	Delay	-1.52	-0.27	-0.59	-37.05
	26	2.4	43.9	15.6	92	Delay	Delay	-0.49	-0.04	-0.35	-28.98
	27	1.0	54.0	24.4	210	Delay	Delay	0.08	-0.02	0.16	6.57
	28	56.2	69.5	13.2	33	Advance	Advance	-0.62	-0.03	-0.51	-22.58

D.2   City Driving Cycle 3: Fort Collins Downtown

The Fort Collins Downtown cycle is another real world city cycle, with many similar characteristics to the Denver Downtown cycle but a shorter duration, which leads to lower Optimal Cycle FE improvement potential. A variety of characteristics of the Fort Collins Downtown cycle are listed in Table D.3, and the simulated FE results are given in Figure D.3.

Table D.3: Characteristics of the Fort Collins Downtown cycle

Drive Cycle	Duration (sec)	Distance (km)	Average Speed (kph)	Max Speed (kph)	#AE	Time %AE	Baseline FE (mpg)	Approximate AE FE (mpg)	Optimal AE FE (mpg)	Optimal Cycle FE (mpg)
Fort Collins Downtown	1074	12.1	40.5	77.6	19	22.7%	62.19	63.53	64.19	66.54
								2.16%	3.22%	6.99%
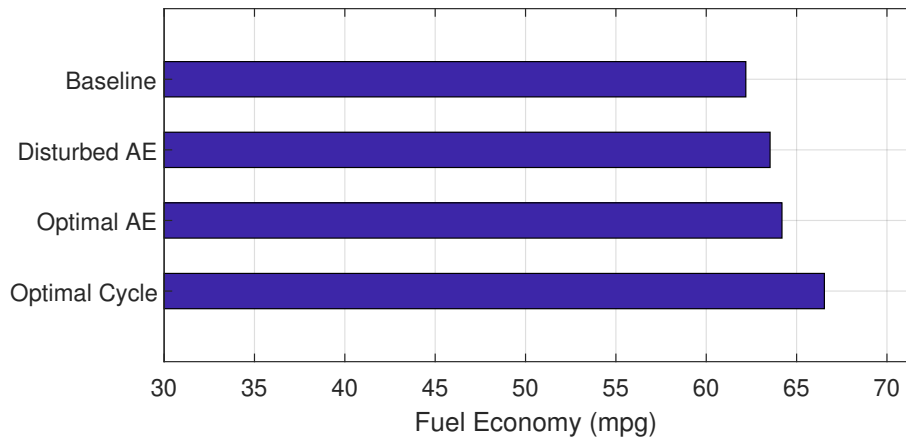
(a) Fort Collins Downtown cycle FE results
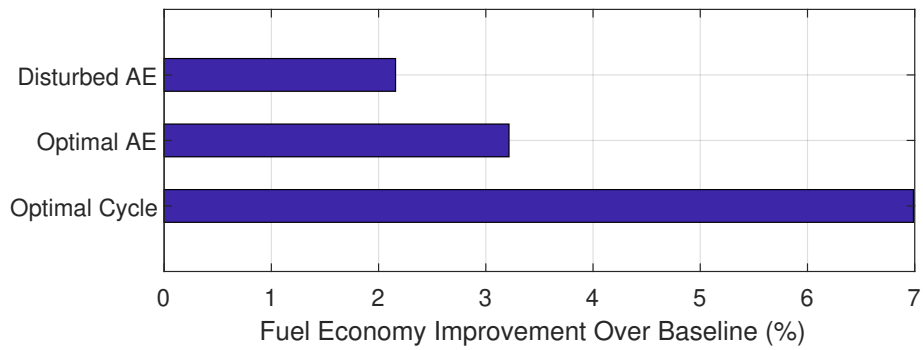
(b) Fort Collins Downtown cycle FE improvement results

Figure D.3: FE results for Fort Collins Downtown cycle

Disturbed control achieves 67% of the FE improvement achieved by Optimal AE control and 31% of the FE improvement achieved by Optimal Cycle control. Though it lacks the low-speed driving section in the middle of the Denver Downtown cycle, the Optimal AE FE is approached just as closely.

Figure D.4: Simulation outputs for the Fort Collins Downtown cycle

Table D.4: Characteristics of AEs in the Fort Collins Downtown cycle

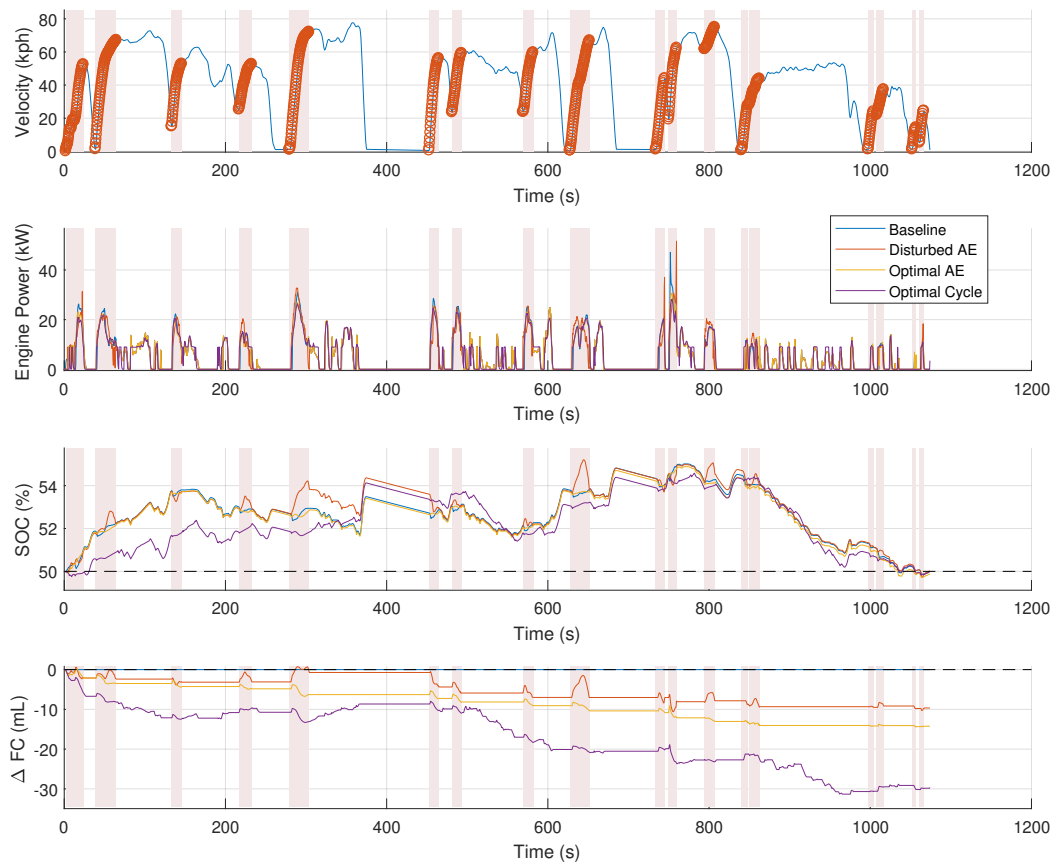|		Initial Speed (kph)	Final Speed (kph)	Duration (s)	# AE in Category	Optimal Control	Disturbed Control	dFC (mL)	dSOC (%)	dFC corrected (mL)	dFC normalized (mL/100km)
	1	0.0	19.2	9.6	230	Delay	Delay	-0.49	-0.02	-0.41	-154.82
	2	18.3	52.5	11.6	26	Advance	Advance	-1.46	-0.10	-1.12	-97.07
	3	1.3	67.2	26.4	31	Advance	Advance	-0.27	0.07	-0.52	-14.92
	4	15.0	52.9	13.2	26	Advance	Delay	-0.78	-0.06	-0.59	-42.17
	5	25.2	52.7	16.4	50	Advance	Advance	0.07	0.13	-0.36	-19.08
	6	1.1	72.2	25.2	23	Delay	Delay	2.37	0.92	-0.74	-22.77
	7	0.5	56.2	12.4	231	Advance	Delay	-3.65	-0.79	-0.95	-78.65
	8	23.6	59.3	12.4	47	Advance	Advance	-1.52	-0.13	-1.09	-74.93
	9	23.8	59.7	13.2	47	Delay	Advance	-1.11	-0.05	-0.94	-60.16
AE #	10	0.5	67.0	25.2	160	Delay	Delay	-0.02	0.02	-0.09	-3.21
	11	1.1	44.1	11.6	92	Delay	Delay	-0.01	-0.03	0.09	13.01
	12	19.2	62.5	10.4	15	Advance	Advance	-1.05	-0.07	-0.80	-63.21
	13	61.7	75.0	13.2	18	Advance	Advance	0.39	0.32	-0.71	-29.56
	14	0.7	27.7	8.4	178	Delay	Delay	-0.87	-0.28	0.09	31.23
	15	27.9	43.9	14.0	65	Delay	Advance	-0.49	0.00	-0.47	-33.86
	16	1.2	24.1	7.2	90	Delay	Delay	-0.16	-0.03	-0.05	-21.84
	17	21.9	37.4	9.2	66	Delay	Delay	0.33	0.12	-0.06	-8.56
	18	1.1	14.4	5.2	50	Delay	Delay	-0.61	-0.10	-0.27	-218.65
	19	5.2	24.5	6.0	129	Delay	Delay	0.12	0.00	0.11	44.06

D.3   Highway Driving Cycle 2: Denver Highway

The Denver Highway cycle is a real-world cycle characterized by high-speed highway driving in the first third, high-traffic highway driving in the middle third, and urban driving in the final third. Since much of the cycle is not high-speed cruising, the room for FE improvement is greater than for the other highway cycles. A variety of characteristics of the Denver Highway cycle are listed in Table D.5, and the simulated FE results are given in Figure D.5.

Table D.5: Characteristics of the Denver Highway cycle

Drive Cycle	Duration (sec)	Distance (km)	Average Speed (kph)	Max Speed (kph)	#AE	Time %AE	Baseline FE (mpg)	Approximate AE FE (mpg)	Optimal AE FE (mpg)	Optimal Cycle FE (mpg)
Denver Highway	1256.8	16.0	45.8	90.5	18	19.8%	71.22	72.68	72.90	77.17
								2.05%	2.37%	8.36%
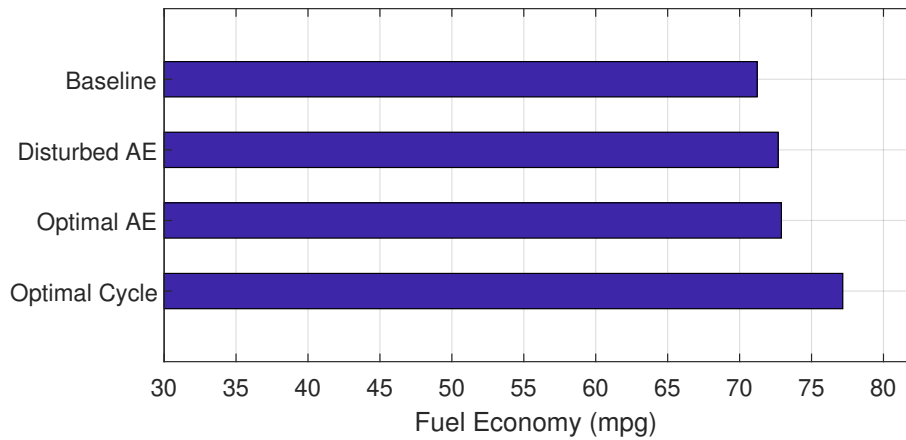
(a) Denver Highway cycle FE results
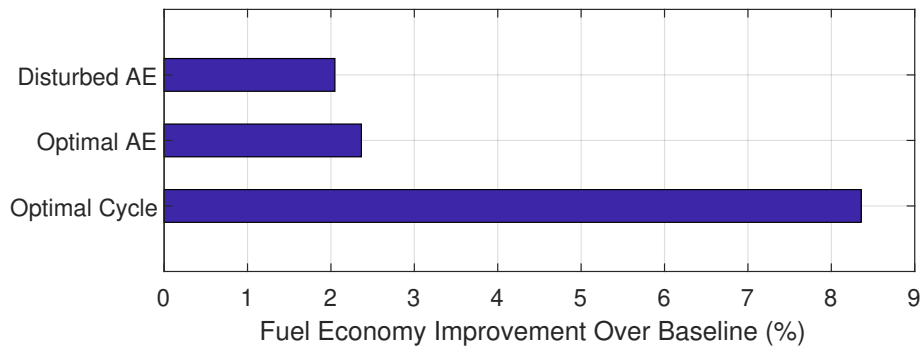
(b) Denver Highway cycle FE improvement results

Figure D.5: FE results for Denver Highway cycle

Disturbed control achieves 87% of the FE improvement achieved by Optimal AE control and 25% of the FE improvement achieved by Optimal Cycle control. In all but the second AE, which is the only AE during which FE is lost, disturbed engine power matches the optimal engine power traces closely.
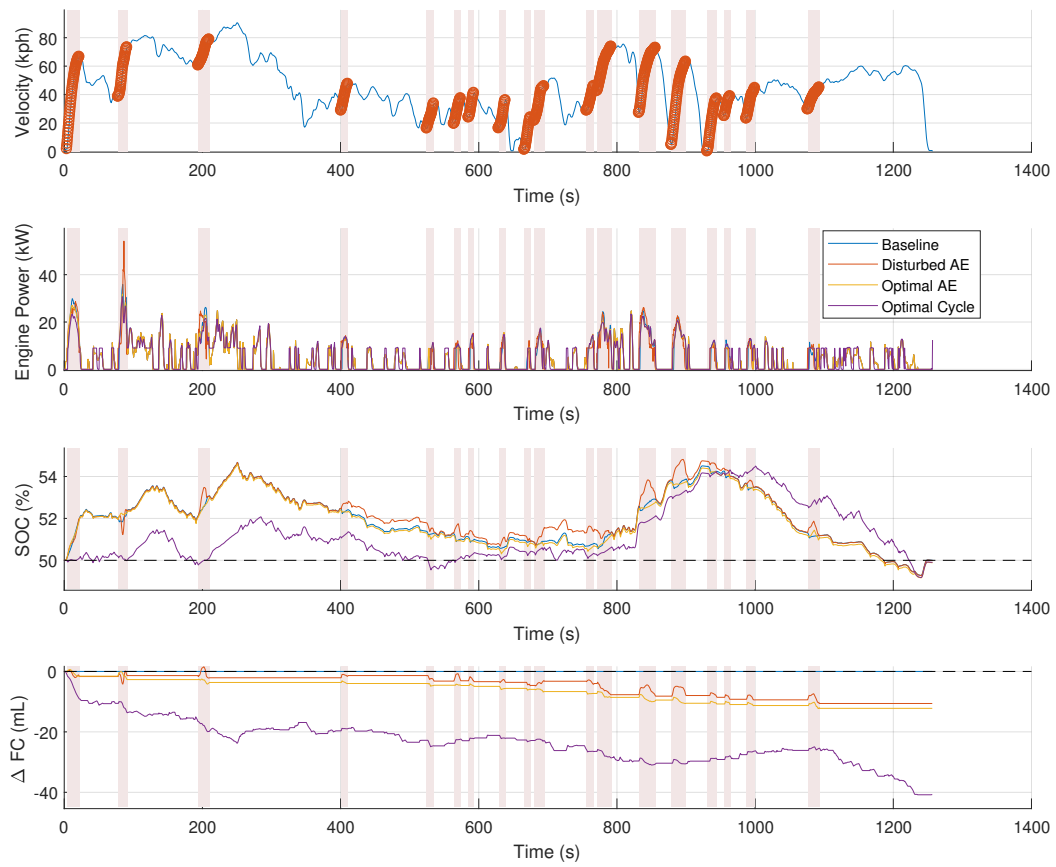
Figure D.6: Simulation outputs for the Denver Highway cycle

**Table D.6:** Characteristics of AEs in the Denver Highway cycle

		Initial Speed (kph)	Final Speed (kph)	Duration (s)	# AE in Category	Optimal Control	Disturbed Control	dFC (mL)	dSOC (%)	dFC corrected (mL)	dFC normalized (mL/100km)
							Denver Highway				
AE #	1	1.6	66.5	18.4	31	Advance	Advance	-1.48	-0.02	-1.41	-65.13
	2	38.5	73.1	13.6	12	Advance	Advance	0.31	0.00	0.31	14.90
	3	60.5	78.7	16.4	18	Advance	Advance	-0.43	-0.01	-0.39	-12.58
	4	28.7	47.5	10.4	53	Advance	Advance	0.73	0.35	-0.45	-41.37
	5	16.1	33.6	10.8	69	Delay	Delay	-1.83	-0.35	-0.64	-91.02
	6	19.4	37.3	10.4	61	Delay	Advance	0.11	0.11	-0.27	-34.08
	7	23.9	41.1	8.4	57	Delay	Advance	-0.30	0.04	-0.43	-60.07
	8	16.3	36.0	10.4	61	Delay	Delay	-0.23	0.10	-0.58	-84.99
	9	1.1	23.9	9.6	90	Delay	Delay	-1.02	-0.23	-0.22	-72.39
	10	21.6	45.8	15.2	68	Delay	Delay	1.39	0.65	-0.83	-58.20
	11	28.7	45.9	11.2	53	Delay	Advance	-0.61	-0.03	-0.50	-45.49
	12	42.5	73.6	21.2	19	Advance	Advance	-3.70	-0.69	-1.34	-38.18
	13	27.1	72.8	24.4	15	Advance	Advance	-0.48	0.07	-0.70	-18.50
	14	4.6	63.1	21.6	44	Delay	Advance	0.21	0.25	-0.63	-26.35
	15	0.0	37.2	14.4	119	Delay	Delay	-0.59	-0.09	-0.30	-36.26
	16	24.9	38.8	9.2	66	Delay	Delay	-0.65	-0.17	-0.07	-9.26
	17	23.2	44.6	13.2	57	Delay	Advance	-0.19	0.01	-0.22	-17.60
	18	29.6	44.9	17.6	65	Delay	Advance	-1.20	-0.01	-1.18	-64.36

# D.4   Highway Driving Cycle 3: Fort Collins Highway

The Fort Collins Highway cycle is a real-world cycle characterized by high-speed urban driving in the first half and high-speed highway driving in the second half. Since most of the cycle involves cruising, the room for FE improvement during AE is smaller than for the other highway cycles. A variety of characteristics of the Fort Collins Highway cycle are listed in Table D.7, and the simulated FE results are given in Figure D.7.

Table D.7: Characteristics of the Fort Collins Highway cycle

Drive Cycle	Duration (sec)	Distance (km)	Average Speed (kph)	Max Speed (kph)	#AE	Time %AE	Baseline FE (mpg)	Approximate AE FE (mpg)	Optimal AE FE (mpg)	Optimal Cycle FE (mpg)
Fort Collins Highway	1310.8	25.9	71.0	136.2	11	12.9%	50.52	50.65	50.90	53.84
								0.26%	0.75%	6.58%
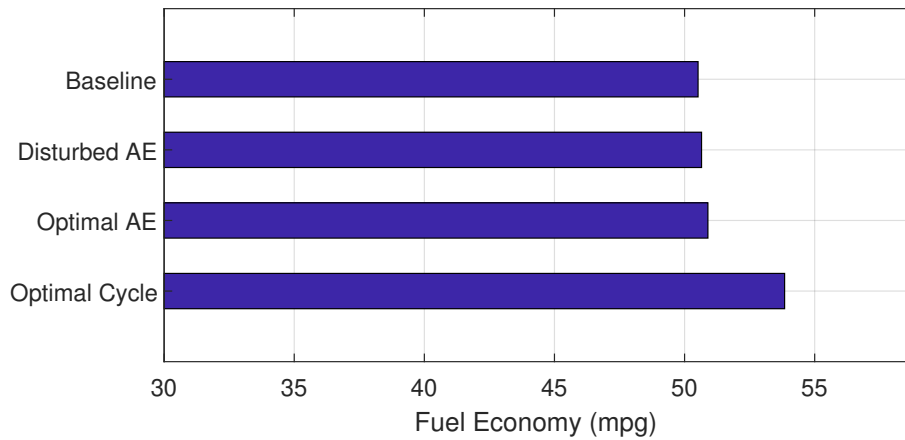
(a) Fort Collins Highway cycle FE results
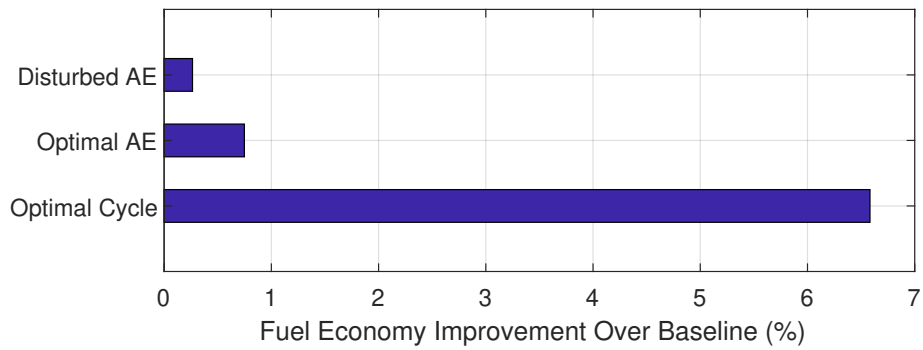
(b) Fort Collins Highway cycle FE improvement results

Figure D.7: FE results for Fort Collins Highway cycle

Disturbed control achieves 35% of the FE improvement achieved by Optimal AE control and 4% of the FE improvement achieved by Optimal Cycle control, which is the worst performance relative to the Optimal control strategies for any cycle other than US06. Since Optimal Cycle control can operate during cruising, its FE improvement is high. To achieve significant FE benefits in this type of drive cycle, expanding the control window beyond AE may be necessary.
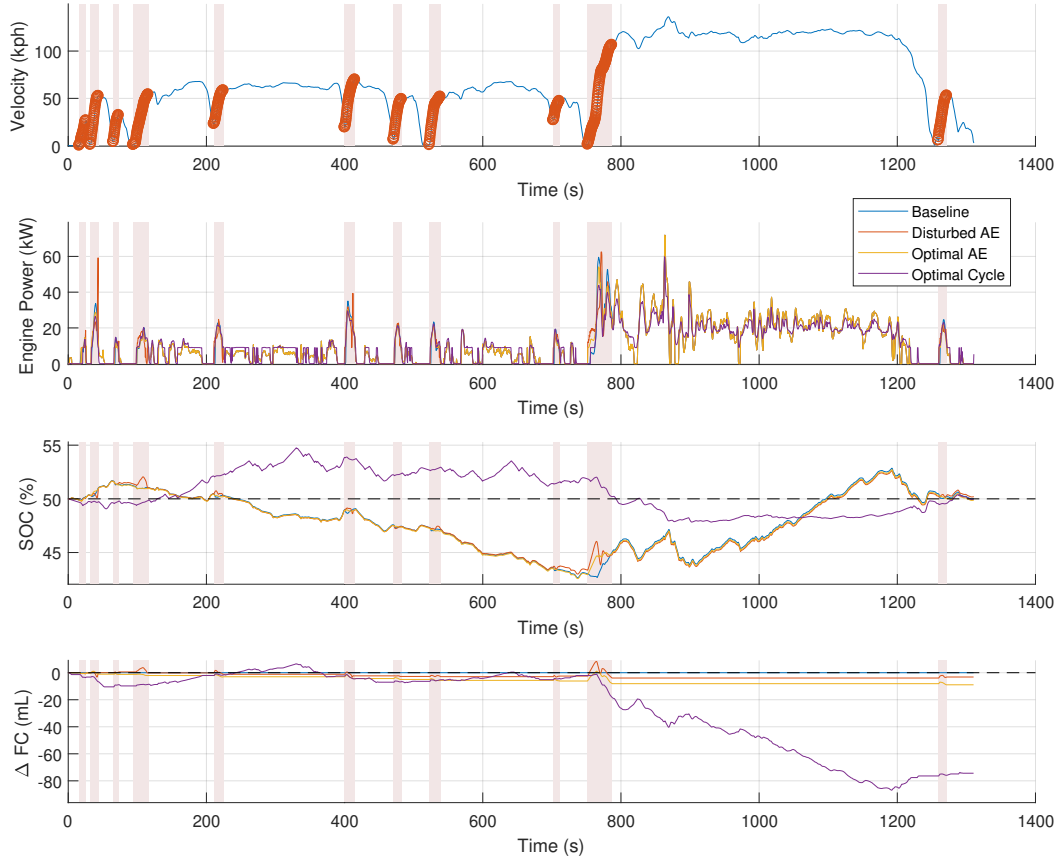
Figure D.8: Simulation outputs for the Fort Collins Highway cycle

Table D.8: Characteristics of AEs in the Fort Collins Highway cycle

		Initial Speed (kph)	Final Speed (kph)	Duration (s)	# AE in Category	Optimal Control	Disturbed Control	dFC (mL)	dSOC (%)	dFC corrected (mL)	dFC normalized (mL/100km)
							Fort Collins Highway				
	1	0.0	26.7	10.4	178	Delay	Delay	-0.17	-0.03	-0.07	-20.33
	2	0.9	52.5	12.4	210	Advance	Advance	0.21	0.01	0.19	18.43
	3	3.9	32.3	8.4	62	Delay	Delay	0.55	0.13	0.11	24.22
	4	0.9	54.1	22.4	210	Delay	Delay	-0.73	-0.21	-0.02	-1.23
	5	23.0	58.4	14.4	47	Delay	Advance	-1.01	-0.05	-0.84	-49.83
AE #	6	19.4	69.9	15.6	9	Advance	Advance	-1.17	-0.04	-1.03	-49.11
	7	6.4	49.1	12.4	54	Delay	Delay	-0.43	0.04	-0.58	-53.13
	8	0.6	51.7	16.4	210	Delay	Delay	-0.17	0.10	-0.49	-30.98
	9	27.0	47.1	9.6	53	Advance	Advance	0.44	0.24	-0.38	-38.39
	10	1.1	106.4	35.6	10	Advance	Advance	-1.45	-0.58	0.53	9.23
	11	5.6	52.9	13.2	41	Advance	Advance	0.75	0.37	-0.50	-42.50